Daphne Wojciechowski Rocha

Licenciada em Ciências de Engenharia Civil

FLEXURAL STRENGTHENING BY MEANS OF A RC OVERLAY IN THE TENSION ZONE

Dissertação para obtenção do Grau de Mestre em Engenharia Civil – Perfil de Estruturas

Orientador: Prof. Doutor Válter José da Guia Lúcio

Júri:

Presidente: Prof. Doutor Nuno Manuel da Costa Guerra
Arguente: Prof. Doutor Duarte Miguel Viúla Faria
Vogal: Prof. Doutor Válter José da Guia Lúcio

FACULDADE DE CIÊNCIAS E TECNOLOGIA
UNIVERSIDADE NOVA DE LISBOA

Setembro 2012

Acknowledgments

First and foremost, I would like to thank the person who most contributed to the elaboration of this dissertation, with his guidance and advice, Professor Válter Lúcio.

I would also like to thank Hugo Fernandes, for all his help and companionship during the laboratory work, and Professor Duarte Faria, for the interest in the subject.

The company Concremat, that cooperated and assisted with the production of experimental models, in particular Eng. Romeu Reguengo and Eng. José Figueiredo.

Leonel Silva, from Instituto Superior Técnico, and Eng. Ana Martins, from Escola Superior de Tecnologia do Barreiro, for the willingness to assist with the concrete characterization tests.

Jorge Silvério and José Gaspar, laboratory technicians, also had a vital role in the elaboration of the experimental program.

Finally, I would also like to acknowledge the help of my family and friends, who have been by my side during all this process, and whose support was vital for the accomplishment of this dissertation.

Resumo

O reforço à flexão, em estruturas em betão armado, pode ser realizado através da adição de uma nova camada de betão na zona tracionada. No entanto, a ligação entre o betão inicial e o betão do reforço é uma zona mais fraca, que pode causar modos de rotura para cargas inferiores às que seriam previsíveis, caso se tratasse de uma estrutura monolítica. Assim, o sucesso desta técnica depende da capacidade da interface de transmitir tensões.

Tanto a limpeza da superfície, como o tratamento da mesma são dois factores estudados que podem afetar bastante a aderência entre as duas camadas de betão. No entanto, um factor que pode sobrepor-se ao efeito da aderência da interface é a quantidade e disposição da armadura a cruzar a mesma. Nos últimos anos, têm-se realizado diversos estudos sobre a ligação entre betões de idades diferentes, que têm interesse não apenas para o reforço estrutural, mas também para o caso de elementos pré-fabricados que são ligados ao betão betonado *in situ*.

Na presente dissertação elabora-se um estudo experimental, no qual avalia-se o desempenho da interface, de modo a caracterizar a sua resistência e modos de rotura quando sujeita a um estado de tensão de corte e de tração. Para o efeito, foram testadas vigas simplesmente apoiadas, reforçadas com uma nova camada de betão na zona traccionada sujeitas a uma carga concentrada a meio-vão. Analisaram-se três ligações diferentes, das quais a primeira é assegurada apenas por aderência, enquanto que as restantes ligações foram desenvolvidas com o intuito de avaliar a contribuição de armadura a cruzar a interface, tanto para o modo de rotura como para a resistência. Relativamente às soluções de reforço com armadura a cruzar a interface, estuda-se o efeito da armadura concentrada nos bordos da camada de reforço, ou distribuída ao longo da área da interface.

Durante os ensaios foram registados: a carga de rotura, deformação da peça, a extensão da armadura longitudinal, a evolução da fendilhação e o modo de rotura. Os valores obtidos são comparados com os previstos no EC2 e MC2010.

PALAVRAS-CHAVE: Betão Armado; Acção de Reforço; Interface; Aderência; Conetores

Abstract

Reinforced concrete structures may be flexurally strengthened in the tension zone by the addition of a new concrete layer with embedded steel reinforcement. However, the interface between the new and old concrete creates a weak area that may cause failure to occur for loads inferior to the designed. Therefore the success of this technique relies on the interface capacity to transmit stress.

Surface treatments and cleanliness are the two main aspects that affect adhesion between different age concretes cast against each other. Nevertheless, the amount of steel reinforcement crossing the interface is a factor that may overcome adhesion and improve shear resistance. In the last years, several studies have been elaborated on this theme.

In the present dissertation, an experimental study was conducted in order to evaluate the performance of this strengthening solution, characterize failure modes and shear resistance at the interface. Simply supported beams with a bonded concrete overlay in the tension zone were subjected to a three point bending test, and interfacial failure was forced. Three different solutions for stress transmission across the interface are analyzed. In the first solution, shear transmission relies solely on adherence, whereas the two remaining solutions were developed with the aim of evaluating the contribution of reinforcement crossing the interface. Regarding the strengthening solutions with reinforcement crossing the interface, the difference between the effect of reinforcement concentrated near the borders of the new concrete layer or equally distributed along the interface is studied.

During the tests, ultimate load, deflections, steel strains, cracking and rupture modes were analyzed. The obtained values were compared among each other and with the provisions of EC2 and MC2010.

KEY WORDS: Reinforced Concrete; Structural Strengthening; Interface; Adherence; Connectors

Contents

Figures

Tables

Notations

Meaning of Roman capital letters:

A	area
A_i	area of the interface
A_s	area of reinforcement
$A_{s,i}$	area of reinforcement crossing the interface
E	elasticity modulus
F	applied load
F_s	steel force
I	moment of inertia
M	moment
N	normal force
R	reaction, roughness
R_a	average roughness
$R_{z(DIN)}$	mean to peak valley height
V	shear force

Meaning of roman lower case letters:

b	width
b_i	width of the interface
c	cohesion
d	effective depth to main tension reinforcement or the diameter of the hole
f	shear flow
f_c	cylinder compressive strength of concrete
f_{ctm}	mean axial tensile strength
$f_{c,ci}$	cubic compressive strength of concrete
$f_{c,cm}$	mean value of compressive strength $f_{c,ci}$
f_{cd}	design value of f_c
f_{ck}	characteristic value of f_c
f_y	yield stress of non-prestressing reinforcement
f_{yd}	design value of yield stress of non-prestressing reinforcement

f_{yk} characteristic value of tension yield stress of non-prestressing reinforcement

l length

l_i length of the interface

s slip

$v_{ed,i}$ design value for shear stress in the interface

v_i interface shear stress

$v_{rd,i}$ design limit value for interface shear

w crack width

x height of the compression zone

z internal lever arm

Meaning of Greek lower case letters:

α angle or coefficient for dowel action

β ratio of the longitudinal force in the new concrete and the total longitudinal force

γ safety factor

γ_c safety factor for concrete

γ_M homogeneity coefficient

γ_s safety factor for steel

ε strain

ε_c concrete strain

ε_s steel strain

κ coefficient for tensile force activated in the reinforcement or dowel

μ friction coefficient

ρ_i ratio of reinforcement crossing the interface

σ normal stress

τ shear stress

$\emptyset$ nominal diameter of steel bar

Chapter 1

Introduction

1.1 Background

Over the last century, with the continuous proliferation of concrete in construction, the need to repair, strengthen and adapt structures to new loads is increasing (Clímaco & Regan, 2001). Repair actions involve re-establishing the strength and function of damaged elements whereas strengthening consists of upgrading the strength or stiffness of structural elements.

Structural problems can be the result of several factors, such as: project or execution errors; structure's misuse (when elements are subjected to loads different from the designed); quality of materials and deterioration agents. These factors can ultimately lead to structural failure. However, before failure, usually some symptoms are displayed, for instance large deformations or excessive cracking. At this point retrofitting actions may be considered. It is important to make an assessment of the actual condition of the structure and the eventual damage or degradation causes.

Most procedures involved in rehabilitation require expert materials, techniques and knowledge, making rehabilitation a complex task (Garcia & Clímaco, 2001). To reduce the cost of an intervention, it is possible to use traditional materials and methods (Pires, 2003).

A widely used strengthening technique that uses traditional materials consists of placing a new concrete layer at the top or the underside of an existing RC element. The most usual procedure is to increase the compression zone. Reinforcement may, or not, be embedded in the new concrete layer. This technique implies either an increase in the elements dimensions and weight or, if the goal is to maintain the geometry of the section, the surface must be partially demolished.

When strengthening a slab or beam with a new concrete layer, flexural strength can be improved either by an increase in the compression zone (and the inner lever arm), or by an increase in the tension zone with addition of steel reinforcement.

However, the bond between the differently aged concretes presents a weak link in the composite structure, and the success of the intervention relies on the interface capacity to transmit stresses and ensure monolithic behavior. Shear stresses and strength along the interface has been the object of studies by numerous authors, and the subject has continuously been revised over the years (Beushausen & Alexander, 2007; Moyamez et al. 2002; Santos & Julio, 2010). Even MC2010 presents a much more thorough approach than provisions in MC90 and EC2. Some of the new aspects present in MC2010 are a quantitative evaluation of roughness, differential shrinkage and edge reinforcement.

This dissertation focuses on flexural strengthening by means of a bonded concrete layer with the particularity that the element's flexural strength is improved by the

addition of tensioned steel reinforcement embedded in the new concrete layer. The element may need a thickness enlargement, or the substrate concrete might be partially demolished and the new concrete poured to the previous height. The latter technique was recently used in building *Visconde de Alvalade,* Lisbon. The structural strengthening was designed by VERSOR, Lda.

Figure 1.1: Cracking pattern around the columns (Building *Visconde de Alvalade*)

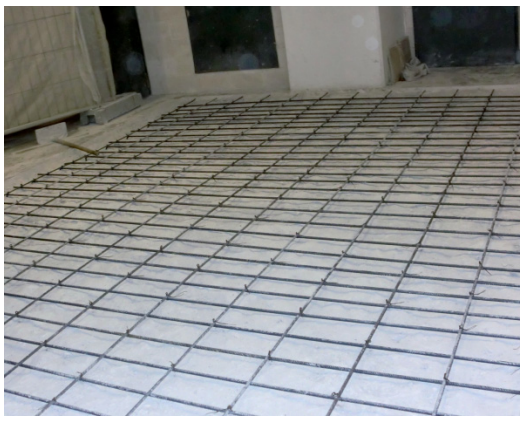

Figure 1.2: Reinforced concrete overlay (Building *Visconde de Alvalade*)

This technique is suitable for large intervention areas, such as buildings slabs or bridge decks, where increasing the compression zone is not possible (Keesom et al., 2008). One of the shortcomings inherent to this type of strengthening intervention is the difficulty in respecting the anchorage lengths of the new reinforcement.

The design methodology adopted when repairing a structure with a new concrete layer might be relate to a precast element which receives in situ topping, as both should consider stress transfer across the interface (MC2010).

1.2 Developed work

This dissertation presents a study about RC overlays in the tension zone as a strengthening solution that is expected to increase the flexural capacity of RC slabs or beams. As mentioned, the success of this technique relies on the interface capacity to transmit stresses between the new and old concrete layers. Stress transfer is dependent on a number of factors, in particular, adhesion between concretes, roughness, the amount of reinforcement crossing the interface and the location of the same reinforcement.

In this dissertation, an experimental research was conducted on large scale strengthened beams. Specifically for this purpose, nine beams were created and later strengthened at a precast plant. The beams were subjected to three point bending tests. Cores were also drilled to perform pull-off tests, which would allow for knowledge of the bond's behavior under both tensile and field stresses.

The development of such beams was related to the fact that the problem would be easier to understand if it was isolated in only one direction. The beams had enough transversal reinforcement, therefore forcing a failure mode related to the interface capacity to transmit stress and, also, related to how much of the flexural resistance of an equivalent monolithic cross-section is activated.

The experimental tests were conducted at the Civil Engineering Department of *Universidade Nova de Lisboa.*

The substrate beams were designed with interrupted longitudinal reinforcement at midspan, which created a deficit in flexural resistance. To correct this situation, the beams were then strengthened by means of a RC overlay in the tension zone. Prior to the overlay placement, the substrate surface was roughened with jackhammers.

The strengthened beams were designed to resist high bending and shear loads, in such a way that the interface shear stress, necessary to mobilize all flexural resistance, would be very high. Therefore, as mentioned, interfacial failure was expected, when the composite specimens were subjected to bending tests, allowing for a quantification of ultimate shear stress.

Three different situations were considered regarding stress transmission across the interface (described in Table 1.1). The first solution (SMI) was developed to quantify bond strength between the two concrete layers. Strengthening models with solutions II and III were used to analyze contribution of reinforcement crossing the interface for shear resistance and the influence of the location of the same reinforcement. Each of the mentioned strengthening solution consisted on three specimens.

Table 1.1: Strengthening models (SM)

SMI	Shear transmission between concrete layers relies only on the concrete-to-concrete capacity to transmit stresses. For an interfacial failure, bond strength in a combined state of shear and tension can be determined.
SMII	Dowels anchored in the substrate cross the interface with the intent of increasing ultimate shear strength. For a failure in the interface plane, ultimate shear strength can be determined.
SMIII	The length of the new reinforcement bars is higher than in the previous models, and the rebars are bent into an *L* shape, crossing the interface and anchored in the substrate, near the end of the overlay. In case of failure across the interface, ultimate shear strength can be determined.

Structural behavior is reported in terms of: steel strains, deflections, cracking behavior, ultimate load, failure modes. Adhesive strength was to be determined by the pull-off test.

This study is a part of the investigation project, funded by the "*Fundação para a Ciência e Tecnologia",* PTDC/ECM/114492/2009 – FLAT – Behavior or flat slabs under cyclic and seismic loads.

1.3 Objectives

The objective of this dissertation is to increase knowledge about RC overlays in the tension zone, as a flexural strengthening solution. Moreover, this dissertation intends to characterize the load bearing behavior of strengthened beams, the resistance of the interface and help to understand specifically the contribution of reinforcement crossing the interface.

Regarding the contribution of reinforcement crossing the interface, the location and amount of steel reinforcement differ for each of the three beam models. The overall resistance and its relation with the location of the mentioned reinforcement is also investigated in the present dissertation.

Failure mechanisms and the ultimate load resisted by the strengthened elements are determined. Ultimate shear strength and bond strength are to be quantified, compared and related to the amount and location of the steel reinforcement crossing the interface and the increase in the overall flexural resistance.

Analyzing the different cracking behaviors, the evolution in vertical deflections of each specimen and relating the obtained results with the properties or pre-existing conditions of each beam is also a goal for this dissertation.

From the obtained results it is possible to evaluate the effectiveness of each solution.

Furthermore, results obtained in the different tests are compared among each other, with the provisions from MC2010 and EC2, and other predictions encountered in literature about this subject.

Another goal for this dissertation was to determine bond strength under tensile stress, and compare it with the results obtained from the beam tests. However, due to difficulties regarding the execution of the pull-off tests, it was not possible to advance with this objective.

1.4 Organization

This dissertation is organized in six chapters and two appendixes, comprising an introduction and a conclusion, a contextualization about different strengthening solutions, state of the art about interfaces between differently aged concretes, experimental program, test results and discussion.

Chapter two provides an overview of different strengthening solutions, emphasizing the problematics of interfaces between different materials used in concrete rehabilitation. In chapter three, the actual state of knowledge on RC overlays, particularly in the case where the strengthening provides an increase in steel force (by adding additional reinforcement) is briefly described. Stress state at the interface is explained, as well as approaches to shear resistance. Research conducted on the theme allowed for an identification of the main factors that can influence adhesion and ultimate shear stress.

Chapters four and five cover the experimental research, the first provides a characterization of the tested specimens and laboratory test setup, as well as the behavior expected for each model. In Chapter five test results are displayed and the different behaviors of the composite beams are analyzed.

Chapter six presents final remarks and a brief summary, regarding test results and their analysis, as well as suggestions for future research.

Appendix A provides a description of roughness measurements and parameters. In Appendix B, some results from the pull-off test are demonstrated.

Chapter 2

Repair and strengthening of RC elements

2.1 Introduction

Rehabilitation of RC structures is an issue that has been addressed worldwide. A rehabilitation project should begin with an assessment of structural conditions, the choice of materials and the development of a strengthening solution. For each condition encountered in the field, one strengthening solution may be preferred to another, and as always, engineering judgment is required.

In this chapter concrete rehabilitation is outlined, and particular emphasis is given to flexural strengthening of horizontal elements. The performance of the bond between substrate and repair materials is also given special attention.

2.2 Materials

An important concern associated with strengthening and repair actions is the careful selection of materials. Although technological developments have introduced innovative materials, which are increasing importance in the rehabilitation field (Rodrigues, 2005), traditional construction materials are still viable options.

These materials should have as characteristics: low permeability, durability, good adherence to concrete and steel, good structural resistance, low shrinkage and workability, easiness of application and compatible properties with concrete and steel (Santos, Shehata & Shehata, 2007).

Most common repair and strengthening solutions involve the utilization of:

- cementitous materials
- (polymer) modified cementitous materials
- composite materials
- epoxy resins
- addition of steel plates/rebars
- introduction of prestress

2.2.1 Cementitious materials

A mortar or concrete used in structural rehabilitation should have as properties high compressive resistance, workability, low retraction and compatible properties with the existing concrete. The concrete placement may present some difficulties, because of specifications inherent to each circumstance, and, therefore, in some cases, different processes might be used.

Projecting concrete (shotcrete) is a common method used when placing a new concrete layer in the underside of a slab. Using a cast and pouring the concrete, not to mention the vibration of the same concrete, would be otherwise too complicated to execute in this case. Self-compacting concrete is also usually employed in places where concrete vibration is complicated, or when it is necessary to pour concrete into a large area with small thickness.

2.2.1.1 Shotcrete

Shotcrete is defined as “mortar or concrete pneumatically projected at high speed onto a surface”. There are two basic types of shotcrete – dry mix and wet mix. In dry mix shotcrete, the dry cement, sand and coarse aggregate, if used, are premixed only with sufficient water to reduce dusting. This mixture is then forced through a delivery line to the nozzle by compressed air. At the nozzle, sufficient water is added to the moving stream to meet the requirement of cement hydration. For wet mix shotcrete, the cement, sand and coarse aggregate are first mixed in water and the resulting concrete is then pumped to the nozzle with compressed air (Smoak, 2004).

2.2.1.2 Self-compacting concrete

Self-compacting concrete is able to flow when placed in a cast, covering and passing through the reinforcement (Pereira & Barros, 2004). The cast is filled by the effect of the concrete’s self-weight, requiring little or no vibration. This type of concrete is particularly suitable for regions of difficult vibration, which is often the case with strengthening procedures.

Technological evolution in chemical admixtures, especially in what concerns super plasticizers, have endowed a fluid behavior to concrete in the fresh state.

The highly flowable nature is also the result of a careful mix proportion with continuously graded powder; much of the coarse aggregate is replaced by fine aggregate, cement and chemical admixtures (Figure 2.1). Concrete in the fresh state can be divided into a solid (aggregate) and fluid component (cement paste/binder), which combines cement, admixtures and water. The suspension particles in the fluid component have the tendency to form flakes that have larger equivalent diameters than the particles that compose them, reducing the fluidity of the paste and requiring more water to achieve the same fluidity. Super plasticizers disperse these particles, avoiding the segregation which favors the interaction and results in higher stability and better rheological performance. This allows concrete’s water cement ratio to be kept at low value and still provides fluidity and workability.

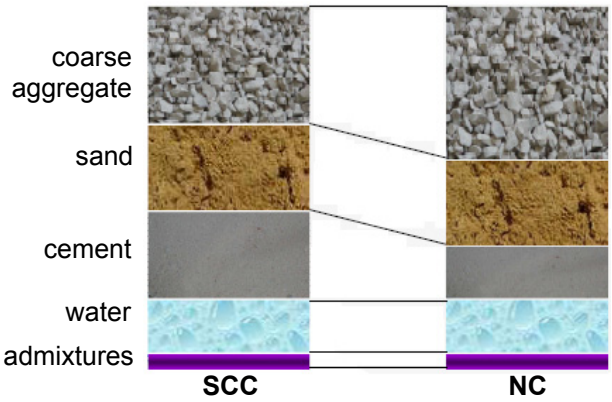

Figure 2.1: Self-compacting concrete (SCC) and normal concrete (NC) mix proportion, adapted from Gonçalves (2007)

2.3 Strengthening Techniques

2.3.1 Addition of new concrete layers

This technique involves adding a bonded concrete layer to an existing RC element. It is appropriate to strengthen columns, slabs and beams. As an outcome of this strengthening solution, the element's cross-section might be enlarged, so when it is necessary to increase the concrete compressive strength, or control deformations this solution can be especially appropriate.

One of the shortcomings of applying new reinforced concrete layers is that it might introduce new weight to the structure, and require the adaptation of other structural elements (such as beams and columns).

The procedures related to this technique require lowering the structural element loads to a minimum and reducing stresses in the intervened elements. Part of the load and the weight of the elements should be directed to shoring in order to proceed with the strengthening intervention (Rodrigues, 2005).

After shoring is installed, the concrete surface must be prepared to ensure good bond with the new layer. Then, if necessary, new reinforcement and formwork may be positioned. Provided that the surface is cleaned, the new concrete can be cast or projected onto the surface. To avoid possible cracking due to shrinkage, it is necessary to ensure a moist environment during the curing process (Rodrigues, 2005).

2.3.1.1 Horizontal elements

Bonded concrete layers may be applied onto the element's top or lower surface. If the layer is to be applied to the top surface, then concrete may be simply poured on top, whereas for the underside, shotcrete is usually preferred. As mentioned in section 1.1, this can be done by an enlargement in the element's cross-section. However, in some cases it is possible to maintain the previous thickness by demolishing a layer in the substrate concrete. Decisions about increasing the element dimensions or introducing extra reinforcement, as all decisions regarding strengthening procedures, are determined by many variables that differ with each case. Reasons for choosing one over the other may be:

- The geometry of the RC member. A small thickness may lead to high deflections, and in this case it would be most suitable to increase the cross section, probably with an increase the compression zone (if it's demonstrated that enough longitudinal reinforcement is present).
- Eventual corrosion, lack of reinforcement, or misplaced reinforcement may require the introduction of new reinforcement. In this case the element's thickness may be maintained.
- Interventions may only be performed on one of the surfaces of the slab. For instance, if the goal is to increase flexural strength for negative bending moments, an increase on the slab's height (applying the new layer to the underside), would be a possible solution. But in some cases, it might not be possible to act on this side, so a reinforced concrete overlay onto the top surface may present a valid alternative.

This method is very effective when increasing the resistance, stiffness and ductility of the element is desired. It's also most indicated when the concrete element is severely damaged (Rodrigues, 2005).

Figure 2.2 illustrates two examples of flexural strengthening for negative bending moments in the tension, and compression zone. In both cases, punching shear resistance also increases, either because there is an increase in the elements thickness, or in the reinforcement ratio.

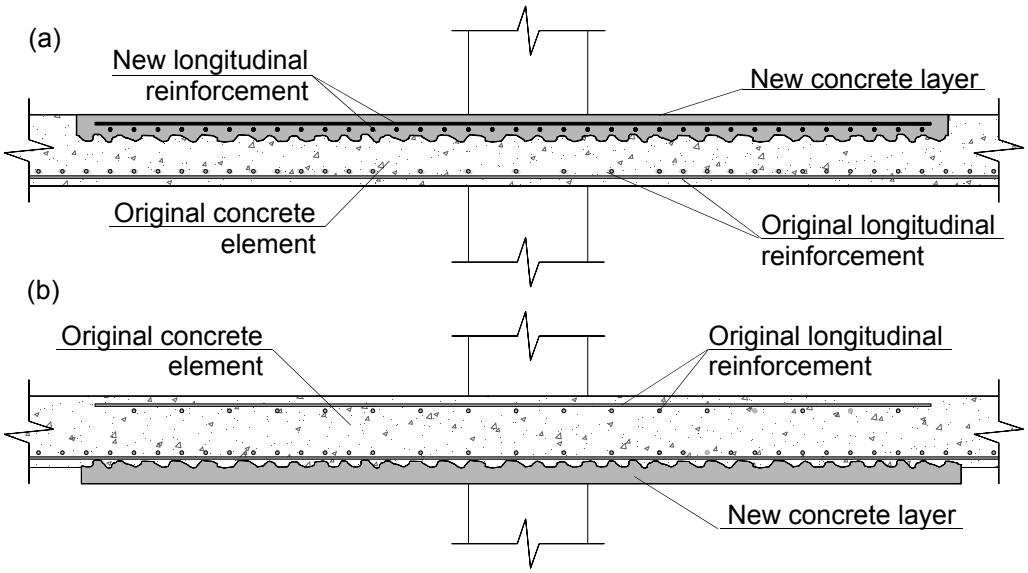

Figure 2.2: Flexural strengthening of a RC flat slab for negative bending moments in the tension (a) and compression (b) zone

If the goal is to increase positive bending moments, a RC overlay in the compression side might be a possibility. Strengthening the tension side is also an option. Both this strengthening solutions are schematized in Figure 2.3.

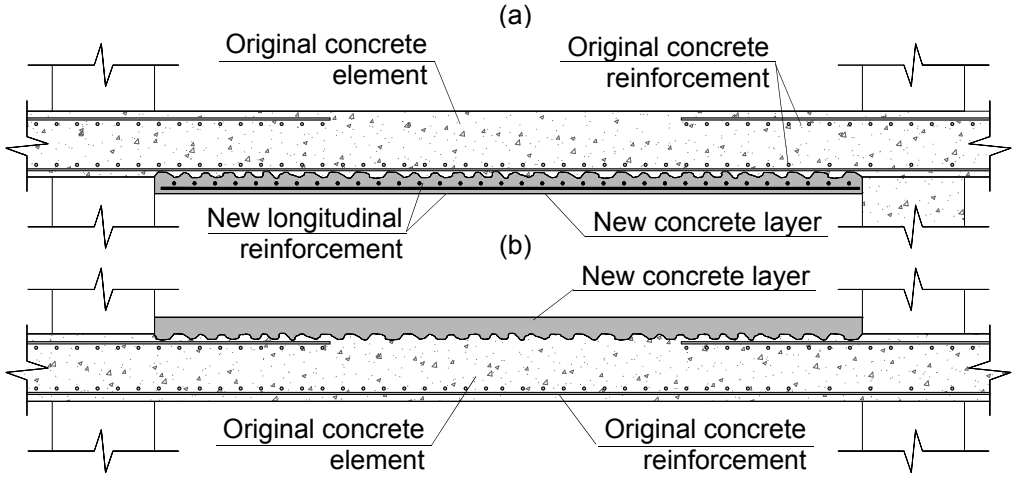

Figure 2.3: Flexural strengthening of a RC flat slab for positive bending moments in the tension (a) and compression (b) zone

2.3.2 Addition of steel plates

A common technique for increasing the flexural capacity of a reinforced concrete element is to add steel plates glued with an epoxy resin, with the eventual help of bolts or post-installed anchors.

The steel plate installation is rather easy. However overlapping plates may present some difficulties, therefore this method works best when strengthening is required in only one direction. Another disadvantage of this system is that when applied to the top of a slab, it might interfere with the flooring system (Banu & Taranu, 2010).

This technique is most suitable to increase flexural strength in the situation of insufficient reinforcement. The quality of concrete and cross-section dimensions must ensure the necessary resistance, avoiding excessive deformation.

The interface between the steel plate and the concrete element may also experience debonding. To increase shear strength, connectors are usually placed.

2.3.3 Addition of carbon fibers

FRP sheets and glass fibers are commonly used to strengthen structures because of their high resistance to tensile stress. The fibers work as reinforcement attached to the concrete element, providing extra tensile resistance. The elements geometry maintains almost unaltered. This solution is viable when the dimensions of the concrete element are sufficient to resist compressions, but steel reinforcement is insufficient.

The main problem with this strengthening procedure is the fact that bond relies solely on adherence mechanisms, and no connectors cross the interface. Therefore this solution is especially exposed to the possibility of interfacial failure.

2.3.3.1 Debonding phenomena in the case of structures retrofitted with FRP sheets

A RC beam strengthened with a bonded FRP plate should fail, ideally, either by concrete crushing in the compression zone or a tensile rupture in the FRP plate. However, in most cases, the cause of failure is related with debonding of the FRP plate from the RC beam (Yao & Teng, 2007).

Debonding between the FRP plate and concrete may occur in one of several possible modes. In Figure 2.4 (a), a situation where debonding initiates at a flexural or flexural-shear crack in the high moment region and propagate towards one of the plate's ends is represented. This debonding failure mode is referred as intermediate crack (IC) debonding.

Debonding may also begin near one of the plate's end in three different modes. It can result from a critical diagonal crack (CDC). In this situation, debonding begins at a major shear crack created near the end of the plate and evolves along the interface until reaching the actual end of the plate. This mode might also introduce concrete cover separation at the reinforcement level (Figure 2.4 example (b) and (c), respectively). Another failure mode is related to the separation of the concrete cover, which begins at the end of one of the plates, at the reinforcement level, and propagate towards midspan, see Figure 2.4 (d) and (e). Plate end interfacial debonding is also possible, occurring in the concrete adjacent to the adhesive layer (or even, at the adhesive layer, if the adhesive properties for some reason were not developed), as shown in Figure 2.4 (f), (Yao & Teng,2007).

There are a number of factors can influence the probability of a particular debonding failure mode, for instance the distance from the plate to the supports and the dimensions of the same plate.

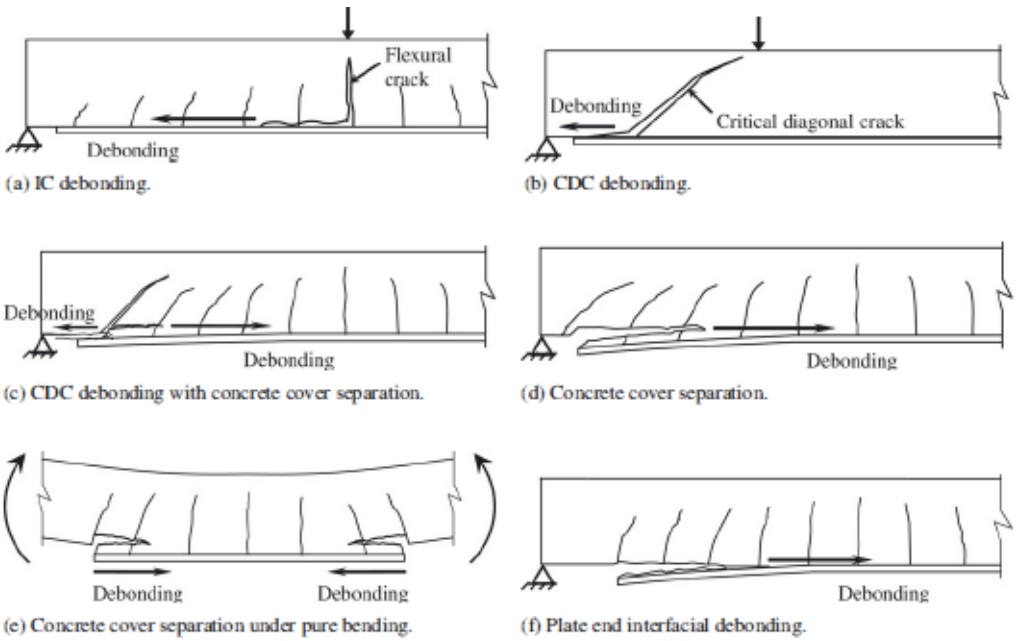

Figure 2.4: Debonding failure modes of a plated RC beam (Yao & Teng, 2007)

2.3.4 External post-tensioning

This method is very effective in increasing flexural and shear capacity of concrete elements, with minimum additional loads to other structural elements (Banu & Taranu, 2010). The post tensioning forces are delivered to the structure at anchor points of prestressing tendons or high-strength steel rods. Prestress can be considered as an imposed deformation or equivalent forces

This technique has been used successfully in bridge rehabilitation.

2.3.5 Altering the structure

It is always possible to alter the structure, introducing new vertical and horizontal elements, such as columns and beams, which allow for loads redistribution and relief from stresses on the initial structure. However, this type of strengthening solution modifies significantly the interior space and may impose limitations in terms of the normal use of the building. Also, this solution may expend a significant amount of material, increasing the cost of the intervention.

2.4 Repairing techniques

Most strengthening interventions may also require localized repairs of RC members, after the cause of the structural problem has been solved. This is important in order to prevent concrete degradation and, obviously, to recover the visual appearance. Most common procedures in concrete repair include injecting cracks with epoxy resins or grout; local repairs with repair mortars (patch repairs) or even the replacement of deteriorated concrete.

2.4.1 Crack repairing

Crack repairing should only be performed once the cause of cracking has been determined and the necessary steps have been taken to avoid recurrence. A crack gage installed across a crack will allow determination of widening or movements of the crack, and regulate whether or not the crack is active (Figure 2.5). With crack repairing the original flexural stiffness may be restored to the RC element, but flexural strength in relation to the initial situation won't be improved (The Concrete Society, 1984; Rodrigues, 2005).

It is recommended to use an epoxy resin to seal cracks with widths from 0,1 to 5mm. For larger cracks, grout can be applied. In water retaining structures it is common to use polyurethane to seal the cracks (Smoak, 2004).

The following steps can be used in crack repairing:

- Cleaning the intervention area
- Widening and enlargement of the crack
- Cleaning the crack, removing loose material. Smoak (2004) suggests cycles of compressed air, followed by water. Using a steel brush is also a possibility.
- Injecting resin or grout.

Figure 2.5: Crack gage installed across a concrete crack (Smoak, 2004)

2.5 Practical examples of reinforced bonded concrete overlays

2.5.1 Building *Visconde de Alvalade*

The *Visconde de Alvalade* is an office building in Lisbon with eight floors, and three underground garages. It was built in 2003, and subjected to a strengthening intervention in two of the underground garage slabs in 2011.

2.5.1.1 Causes and extent of degradation

In the mentioned building, two underground garage flat slabs displayed significant cracking. The top surface of both slabs exhibited radial cracking around the columns due to flexural stresses. In addition, another type of cracking that crossed the slab's entire height was also visible near RC walls, as a consequence of restrained shrinkage. After visual inspections the flexural crack widths revealed to be larger than 0,4mm near the columns. It was also found that between columns the cracks were inferior to 0,4mm and the shrinkage cracks near the wall presented widths superior to 0,3mm. Cracks widths were higher than the limits imposed by EC2.

Table 2.1: Crack width

Type of Cracking	Crack width
Flexural cracks near the columns	w>0,4mm
Flexural cracks between columns	w<0,4mm
Shrinkage cracks	w>0,3mm

To investigate the cause of cracking, the position and quantity of the reinforcement was surveyed, using a pacometer and two investigation cores (Figure 2.6).It became clear that, although the top reinforcement was present, it had been misplaced, at a lower vertical position and covers measured in average 95mm instead of the 25mm specified in the building's project.

The flexural capacity of the slabs was reduced by 40% in relation to the project. Despite the fact that no circumferential cracks were visible around the columns, the punching resistance of the slabs was reduced by 62%.

Figure 2.6: Core extracted from the slab in -2 level (while the thickness is 0,28m, the concrete cover of the top reinforcement measures 0,1m)

2.5.1.2 Strengthening procedures

The slabs were strengthened by the addition of a new concrete layer. In this case, the two possible solutions illustrated in Figure 2.2 could be effective in increasing flexural strength. However, strengthening the slab by an increase in the compression zone, near the column, presented a problem, since the buildings infrastructures circulated under the ceiling. These infrastructures were necessary because the other floors of the building would maintain normal use during the strengthening intervention.

The intervention intended to improve both flexural strength for negative bending moments, and punching shear strength with the addition of flexural and punching reinforcement. A thin reinforced concrete layer was poured into a limited area that had been previously demolished on the top surface the slab around the columns, thus making it possible to maintain the original height (Figure 2.7). The shrinkage cracks and remaining flexural cracks were filled with epoxy injections. Because the slab's dimensions were maintained, there was no significant addition in loads to other structural elements.

The punching reinforcement consisted of steel threaded bars crossing the slab and restrained at both ends by small steel plates. This reinforcement was salient on the lower part of the slab, but at the top part of the slab it was embedded in the new concrete layer. To promote monolithic behavior, shear connectors were distributed

along the intervention area. Some longitudinal reinforcement was also anchored in holes previously drilled in the substrate.

The following procedure was adopted:

- Shoring of the two damaged slabs, and measuring eventual displacements with a deflectometer;
- Demolition of the concrete cover before reaching either the substrate reinforcement or a maximum depth of 80mm. The demolition area corresponded approximately to 1/4 of the span, around each column;
- Repairing the remaining cracks;
- Vertical perforation of the slab, in order to place new punching reinforcement, shear connectors and anchor longitudinal bars (Figure 2.8 and Figure 2.9);
- Placement of the reinforcement;
- Injection of cement grout and epoxy resin, sealing holes;
- Pouring the new concrete: a self-compacting concrete was adopted;

Figure 2.7: Longitudinal and punching shear reinforcement

Figure 2.8: Shear connectors crossing the interface

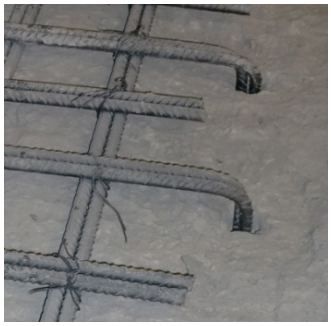

Figure 2.9: Anchorage of the longitudinal reinforcement

2.5.2 Prestressed viaducts in the Netherlands

According to Keesom et al. (2008) seven viaducts in the Dutch highway, A9, built around 1970 have experienced increasing traffic loads. Therefore, it was necessary, either to recalculate the structure for the present standard traffic standards, and prove that either it would maintain, at least, 15 more years of life, or strengthening the viaducts would be necessary. If strengthening revealed to be necessary, it should ensure a surplus life of at least 100 years. Although there were no visible signs of degradation, the present day loads were superior to the designed ones, and an assessment of actual load bearing capacity was required.

The viaducts are built using prestressed girders and a reinforced cast-in-place deck. The cast in place deck was designed to resist negative bending moments at the supports, caused by the statically undetermined system.

The structural dimensions and the steel disposal were obtained from as-built drawings. Cores were drilled on the deck to determine both compressive and tensile strength of the concrete. For this purpose, compressive, direct tension and splitting tests were executed.

The design approach was based on four major principles: assessment of the concrete strength; FEM calculations resorting to the program ESA PT; minimization traffic disruption; the design of the concrete mix and on site testing of the overlay properties and anchor strength.

After assessment of the actual conditions of the viaduct, the slab was modeled in a FEM program. It was concluded that four of the seven bridges needed structural strengthening, because there was insufficient reinforcement near the supports and insufficient transversal reinforcement in the cast-in-place deck, and the girders were under high tension stresses at midspan. The solution consisted of the application of an approximately 100 mm reinforced concrete overlay.

In this case, strengthening the underside of the slab was impossible due to its geometry.

The client had imposed some specifications regarding the concrete overlay. A concrete grade of C53/65 was defined, as well as minimum bond strength of 1,5N/mm^2. It was required that concrete covers measured at least 40mm. In addition, across the interface, steel anchors were to be placed, at least 4 per m^2 and near the edges 10 per m^2. FEM results showed that in the middle of the overlay anchors were not necessary, because the adhesion between layers was more than sufficient to assure bonding. However near the edges, the authors state that anchors were required due to stresses caused by drying shrinkage of the overlay.

The overlay increased the loads transmitted to the base of the piles in 10%. The designers considered that the foundations should resist the increase in loading due to the use of relatively large scale factors.

Another specification of this project was that, six days after casting, the overlay had to be ready for use. A trial casting was preformed, and the strength development was documented and verified. After only six days, a bond strength of 1,5MPa was achieved. The interface surface was roughened resorting to milling.

After milling, some top reinforcement became visible and it was verified that the actual dimension of the slab was inferior to the predicted. Therefore it became necessary to increase the height of the new concrete layer. After milling, holes were drilled in the substrate to anchor the connectors. The longitudinal reinforcement used was prefabricated.

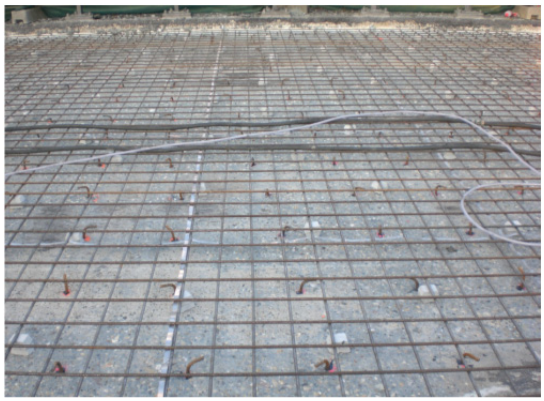

Figure 2.10: Ready to cast overlay (Keesom et al., 2008)

Chapter 3

State of the art

3.1 Introduction

The addition of a new concrete layer bonded to an existing RC element can provide substantial enhancement in flexural resistance. Nevertheless, concrete-to-concrete load transfer across interfaces can lead to premature failure of the composite element. Therefore, strains and stress state at the interface, adhesive bond strength and ultimate shear stress must be quantified in terms of variables that can influence their values.

In this chapter, the stress state at the interface and the main factors that can influence stress transmission between concrete layers cast against each other with different ages, particularly in the case of bonded concrete overlays, are described based on literature about this subject and provisions of EC2 and MC2010.

Moreover, when analyzing bonded concrete layers, it is important to consider the fact that when a new concrete layer is placed, the substrate has already experienced most of its drying shrinkage, thus restraining free deformation of the RC overlay and inducing stresses (which reach maximum values at the interface perimeter).

Another problem associated with this strengthening solution is related to the fact that when the new concrete layer is placed, on site, it is difficult to provide a clean interface surface. Contamination of interface surfaces causes a negative impact on adherence between concretes. Good practices regarding the execution of bonded concrete overlays are also mentioned.

3.2 Bond strength and shear strength at the interface

Bond or adhesion between substrate and overlay is regarded as the way in which these materials can act together, before a crack along the interface is formed.

If the resistance of an interface is assured only by adhesion, it is commonly designated as bond strength. Providing good bonding is a key factor to ensure monolithic behavior and the effectiveness of the strengthening intervention. In literature, several studies have proven that there are a number of factors that can influence bonding, such as cleanliness and roughness of the interface.

According to Omar et al. (2010), the fundamental theories that govern adherence mechanisms between substrate surfaces and overlay materials are mechanical blocking and the adsorption theories. At a macroscopic level, the roughness of surface creates mechanical blocking between overlay and substrate. At the microscopic level, the surface porosity at the interface substrate, comparable to a micro-roughness, facilitates chemical linkage.

Adhesive bond can be enhanced by optimizing fresh concrete properties and roughening of the substrate surface. However, the adhesive component is yet to be completely defined. Roughness and concrete compressive (or tensile) strength are the main parameters used to describe adhesion; other factors that can influence adhesive bond, (e.g. drying shrinkage and w/c ratio) are often neglected. However, as adhesion is quite dependent on the cleanliness of the substrate, on site, a contamination scenario must not be ignored.

Values for adhesion/shear strength are highly dependent on the test measuring procedure, as they are related to stress state of the interface. Bond strength is usually defined as the tensile strength perpendicular to the interface plane and can be determined by pull-off tests (Rilem, 2011). Bond strength in shear has also been considered by several authors, as it is associated to stress states typically found in the field (Bakhsh, 2010).

Often, the adhesion strength between concrete layers is not sufficient to resist interface stresses, requiring the designer to allow for a cracked interface and place reinforcement across both concrete layers. In this case, adhesive bonding can be exceeded (if reinforcement is able to sustain the increase of stress resultant from loss of adhesion). Therefore, it is important to determine both the shear strength at the interface and adhesion strength and guarantee that rupture is not characterized by this weakness plane.

In addition, as adhesive bond is associated with brittle behavior, a certain amount of reinforcement crossing the interface is required. For economic reasons the goal is to take the most advantage of adhesive bonding, and minimize the reinforcement area (Randl, 2011).

According to MC2010, representative mean values for the mean shear resistance vary in the following ranges:

Table 3.1: Representative mean values for the mean shear resistance (MPa)

Rough interface (e. g. sandblasted)	1,5~2,5
Very rough interface (e. g. high pressure watter jetted)	2,5~3,5

3.3 Test methods

The values obtained for bond/shear strength are highly dependent on the stress state at the interface and the test measuring procedure. The tested elements will obviously react differently if the interface is subjected to tension, compression, shear or torsion. Experiments may be performed with large or small scale specimens.

According to Randl and Zilch (2009) large scale specimens reflect the real situation in the structure somewhat better, but small specimens allow for a more precise understanding of the interface stress and a larger number of tests. MC2010 considers the main parameters that influence load bearing capacity observed in tests to be interface roughness, cleanliness, concrete strength and quality, eccentricity/inclination of shear force, strong bond, pre-cracking or debonding before testing and the ratio of reinforcement crossing the interface.

3.3.1 Large scale tests

Large scale tests have been mostly used to study increases in the overall resistance.

3.3.1.1 Flexural tests

Three and four point bending tests are commonly used in experimental research about strengthened beams. Strengthened slabs have also been subjected to bending tests, however, conducted experiments encountered in literature (Pires, 2006; Santos, Júlio & Silva. 2007) are not tests specifically on shear resistance, but on the overall performance of the strengthening solution.

3.3.1.2 Punching shear tests

As an addition in the elements dimensions and steel ratio may lead to an increase in punching shear capacity, punching shear tests may be performed on slabs. Datta and Seraj (2003) studied precisely the effect of a bonded concrete overlay in the punching shear capacity of slabs. The study concluded that punching shear can significantly be increased by this strengthening method, and dowels have a positive effect.

3.3.2 Small scale tests

A number of small scale tests have been developed, and are mostly used to determine interface bond strength.

Tests may be classified in relation to the stress state they impose to the interface. In tension, most popular bond tests are splitting prism and direct tension tests (Figure 3.1), the latter can be carried out in laboratory or in-situ. In the splitting test a prism with a circular or squared cross-section is placed under longitudinal compressive load.

Shear tests usually apply the force in the direction of the interface (Figure 3.2). Modified shear tests, such as the slant shear test are also widely used.

To analyze the effect of reinforcement crossing the interface, push-off tests have been used.

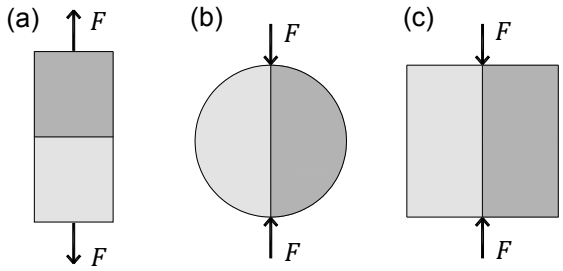

Figure 3.1: Tension tests, (a) Direct tension (b) and (c) Splitting prism, adapted from Rilem (2011)

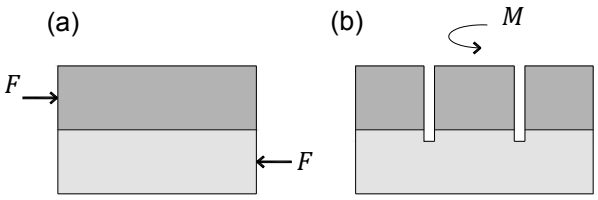

Figure 3.2: Shear tests, (a) Common shear tests and (b) Shear test applying torsion, adapted from Rilem (2011)

3.3.2.1 Pull-off test

The pull-off test is a simple direct tension test that can be useful when evaluating bond strength and failure modes between new and original concretes, both in laboratory and on site conditions. The test usually requires partial coring of the composite elements; at least 10mm bellow the interface. A load frame is glued to the surface of the core through a metallic disc and the element is then loaded, subjecting overlay material, the interface and part of the substrate to the tensile load, F. The pull-off strength, f_t, can easily be determined by Equation 3.1. Failure modes are described in Figure 3.4. This test presents the disadvantage of being sensitive to eccentricities (Ramezianpour et al., 2007).

$$f_t = F/A_i \tag{3.1}$$

Where,

A_i is the area of the interface

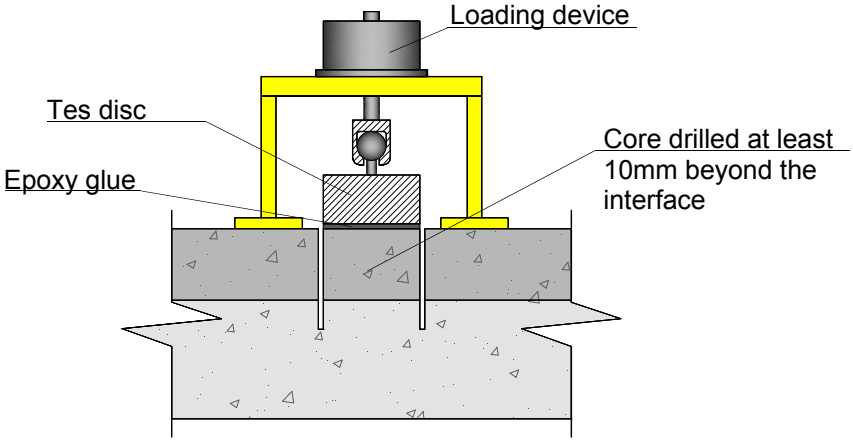

Figure 3.3: Pull-off test setup, adapted from Borges (2008)

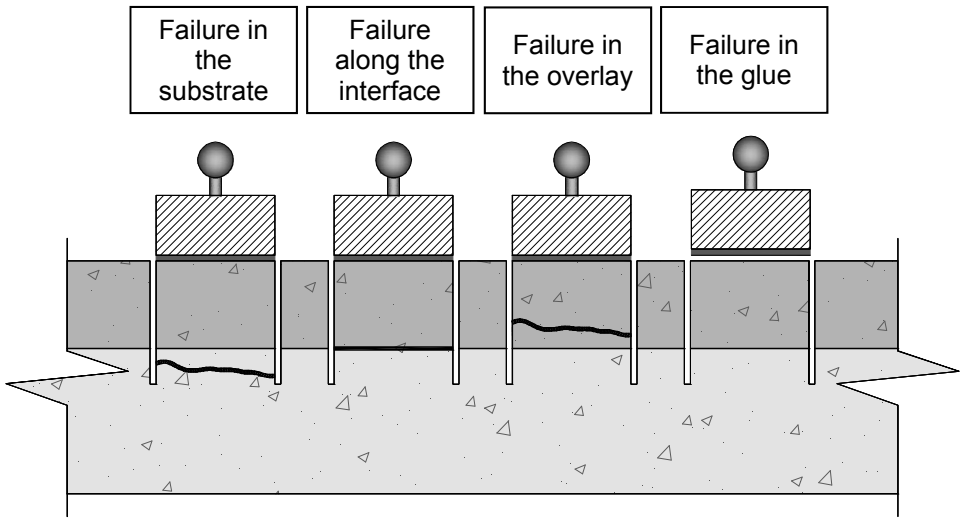

Figure 3.4: Typical pull-off failure modes, adapted from Borges (2008)

A failure in the interface (adhesive failure) indicates bond strength. It is also possible that an interfacial failure is combined with partial substrate failure, which can be the result of, for instance, micro cracks in the substrate. When substrate or repair material failures (cohesive failures) occur, the ultimate strength represents a low estimate of the tensile strength. Results should not be considered when the disc detaches from the core. Failure might also take place while drilling the cores.

Values for pull-off strength are most dependent on the diameter and depth of the core (Rilem, 2011). The related standard methods for the pull-off test are found in EN1504-3. The European procedure requires at least a surface cohesion value of 2MPa for structural repairs, and 5 valid tests.

3.3.2.2 Slant shear test

This test was primarily used to evaluate bond strength of resinous materials and bonding agents in a stress state that combines shear and compression. Some authors have found this test to be particularly sensitive to roughness, and have used it to evaluate bonding between different age concretes.

The test consists on subjecting a composite prism or a core of substrate and repair material that has a joint at an accurate angle, to axial compression. The interface stress state combines shear and compression. It presents the advantage of being easy to perform, as it can be tested in a compression machine. Results are reproducible and sensitive to roughness (Garcia & Clímaco, 2001). The bond strength measured depends of the angle of the interface and rupture occurs at different compressive stresses for different angles. The correct interface angle must be used in order to obtain significant results.

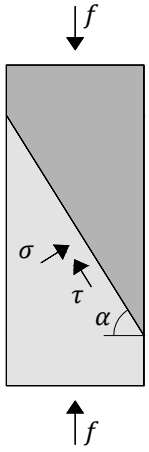

Figure 3.5: Slant shear test, adapted from Clímaco and Regan (2001)

Failure can occur either at the interface, at a plane near the interface or be monolithic. According to Clímaco and Regan (2001), if the bond is effective, failure is characterized by a rupture in concrete, and the joint is subjected to an uneven combination of shear.

If the bond is not effective (joint failure), the Mohr Coulomb criteria can be used to describe bond strength (Equation 3.2). This represents the straight line in Figure 3.6. The inclination of this straight line is the angle of friction, $\Phi = arctan\,\mu$, which represents the maximum angle that shear stress can make with the perpendicular of the facet.

$$\tau = c + \mu\sigma \tag{3.2}$$

The cohesion, c, represents the interception of the straight line with the shear axis. The friction coefficient, μ, is dependent on roughness.

From the equilibrium between the applied force and stresses at the interface (Figure 3.5), it is possible to determine both normal and shear stresses at the interfaced, given by Equations 3.3 and 3.4.

$$\sigma = f\,cos^2\,\alpha \tag{3.3}$$

$$\tau = f\,sin\,\alpha\,cos\,\alpha \tag{3.4}$$

From Equations 3.2-3.4, it is possible to determine the compressive strength of the prism, f, when failure is governed by the weak plane:

$$f = c\frac{1 + tan^2\,\alpha}{tan\,\alpha - \mu} \tag{3.5}$$

As cohesion and friction are dependent on parameters such as surface treatment and joint angle, it becomes complicated to describe the most critical angle. Table 3.2 provides values for α_{crit} and f from a study elaborated by Clímaco and Regan (2001).

Table 3.2: Critical joint angles and minimum compressive strength of prisms adapted from Clímaco and Regan, (2001)

Interface conditions	Cohesion, c	Friction, μ	α_{crit}	f [N/mm^2]
Rough	$0{,}25f_c^{2/3}$	1,4	72,2º	$1{,}56f_c^{2/3}$
Medium	$0{,}25f_c^{2/3}$	0,9	66,3º	$1{,}12f_c^{2/3}$
Smooth	0,5	0,7	62,5º	1,92

Where,

f_c is the cylinder compressive strength of concrete

f is the compressive strength of the composite prism, when failure is governed by the weak plane

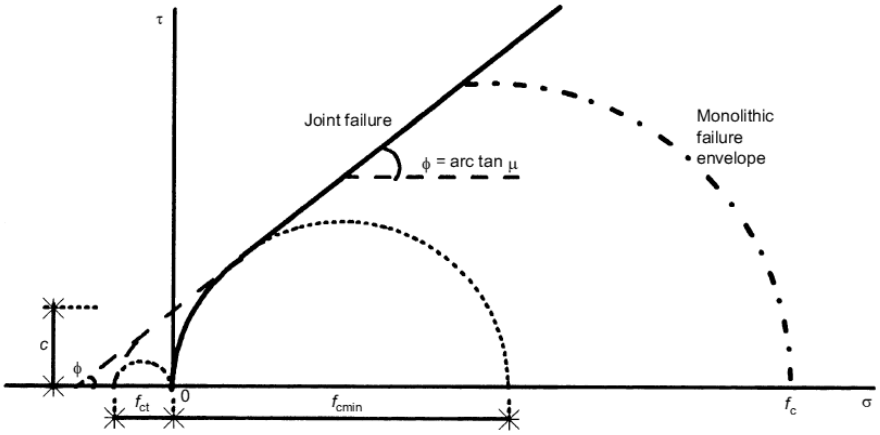

Figure 3.6: Failure criterion for concrete composite prisms (Clímaco & Regan, 2001)

3.3.2.3 Push off test

With the push off test the shear resistance of an interface connected by dowels can be determined. It is used to analyze precisely the effect of dowels perpendicular to the interface plane (Figure 3.7). The relation between shear stress and the applied force is related to the interface dimensions, and $v_i = F/(b_i l_i)$, being b_i is the width of the interface.

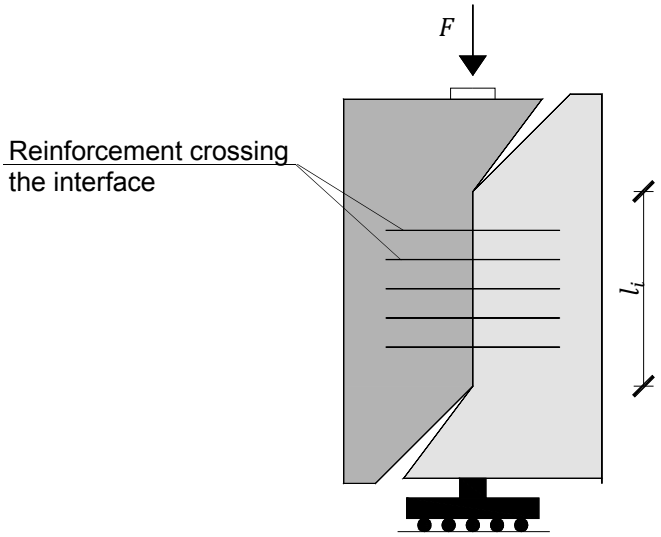

Figure 3.7: Push off test, adapted from Walraven et al., 1987

3.4 Shear stress at the interface

In classic mechanics, when a beam composed of two different materials is subjected to load along the (2) axis, two limit situations may be considered (Figure 3.8). Situation (a) represents a scenario where both materials act together. In situation (b), materials act separately, creating a relative slip between them. Example (a) is also true in the case of beams composed by only one material: as no slip between horizontal planes takes place, the material act together, inducing shear stress in any horizontal plane.

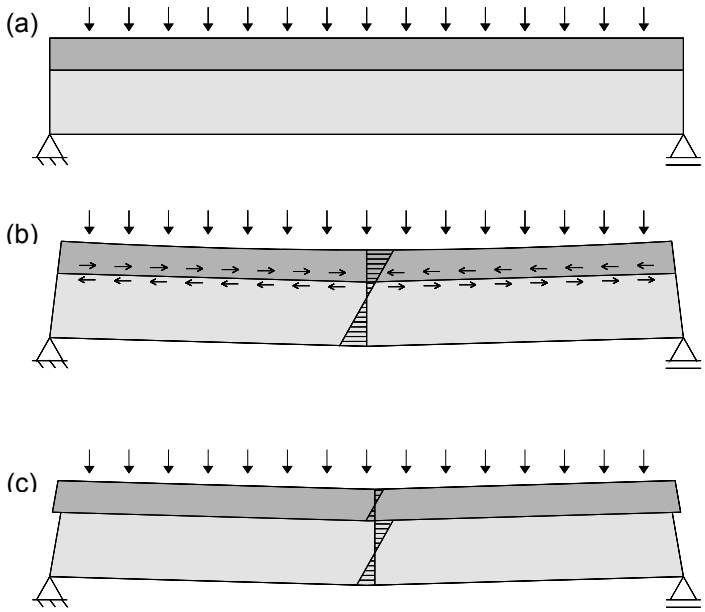

Figure 3.8: Limit situations for stress transfer across an interface (a) undeformed composite beam (b) materials act together (c) materials act separatly

In a system composed of two concrete layers, which is obviously the case of an element strengthened with a concrete overlay, it is important to resist these horizontal shear forces and ensure composite action, with minimal slip between substrate and overlay.

The stress transfer across a concrete-to-concrete interface is considered to occur by adherence, dowel action in the transversal reinforcement (crossing the interface), friction and tension in the transversal reinforcement triggered by aggregate interlock.

3.4.1 Determination of shear stress in the interface

Since an original RC element has probably endured a certain amount of stress prior to the strengthening intervention, the strain distribution on the cross-section of the composite element is not continuous. Strain distribution is also dependent on interface slip. Therefore, usual bending and shear theories might not be valid in the case of strengthened elements.

There are some concerns as to whether or not the assumption of linear strain distribution in a concrete composite cross-section is valid, namely because of concrete cracking and flexibility of the shear connectors (Dritsos et al., 1995). Another issue addressed by Beushausen and Alexander (2007), is related to the fact that strains resulting from restrained shrinkage of the overlay should also be considered in the design.

In Figure 3.9, possible normal strain and stress distributions for concrete overlays in the tension zone are exemplified.

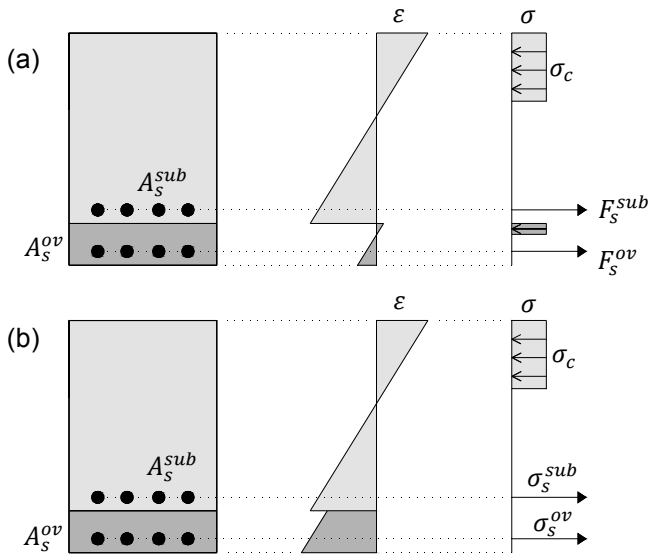

Figure 3.9: Possible normal strain and stress distributions for concrete overlays in the tension zone, adapted from Dritsos et al. (1995) with (a) a differential behavior between substrate and overlay, that implies large slips and (b) materials act together with small interface slip

As a result of the discontinuity in strains, stress distribution becomes complex and expressions related to the problem become lengthy and difficult to analyze. For low values of interface slip and shear flow the behavior may be considered monolithic (Dritsos et al, 1995).

The determination of shear stresses described below is based on the hypothesis of linear strain distribution in the cross-section. As the stress tensor is symmetric (Figure 3.10), the relationship presented in Equation 3.6 is true.

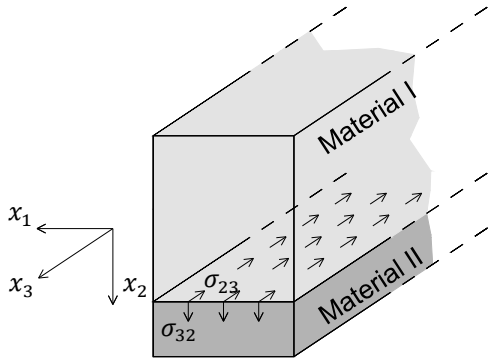

Figure 3.10: Shear stress at the interface

$$\sigma_{23} = \sigma_{32} \tag{3.6}$$

For a simply supported beam, subjected to a concentrated load, assuming linear elastic behavior (uncracked concrete), the equilibrium at the bottom part of the element (Figure 3.11) leads a shear stress distribution of a second degree polynomial, where the shear stress, $\tau = f/b$, is assumed constant along the element's width.

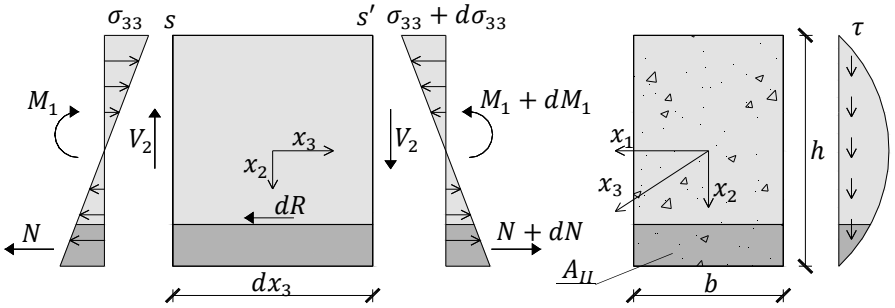

Figure 3.11: Equilibrium of normal stress and shear distribution in the cross-section (uncracked concrete)

Assuming the theory of elasticity for linear elements, the equilibrium of horizontal forces in an element with an area A_{II} and an infinitesimal length dx_3 is given by:

$$N + dR = N + dN \Leftrightarrow dR = dN \tag{3.7}$$

Where N and $N + dN$ are the resultant forces of the normal stress, with N is given by:

$$N = \int_{AII} \sigma_{33} dA_{II} \tag{3.8}$$

With:

$$\sigma_{33}(s) = \frac{M_1}{I_1} x_2 \tag{3.9}$$

Where $M_1$is the bending moment and I_1 is the moment of inertia of the cross-section along x_1. The shear force is then obtained by:

$$V_2 = \frac{dM_1}{dx_3} \tag{3.10}$$

By analogy:

$$dR = dN = \int_{AII} d\sigma_{33} dA_{II} \tag{3.11}$$

$$dR = \frac{dM_1}{I_1} \int_{AII} x_2 dA_{II} \tag{3.12}$$

And,

$$f = \frac{V_2 \int_A x_2 dA_{II}}{I_1} \tag{3.13}$$

And the shear stress,

$$\tau = \frac{f}{b} = \frac{V_2 \int_A x_2 dA_{II}}{b I_1} \tag{3.14}$$

However, linear elastic behavior may only be considered before stress reaches the concrete tensile resistance.

If enough longitudinal reinforcement is present, for an ultimate limit state, tensile resistance has obviously already been exceeded, and the stress distribution of an equivalent rectangular block may be adopted (Figure 3.12).

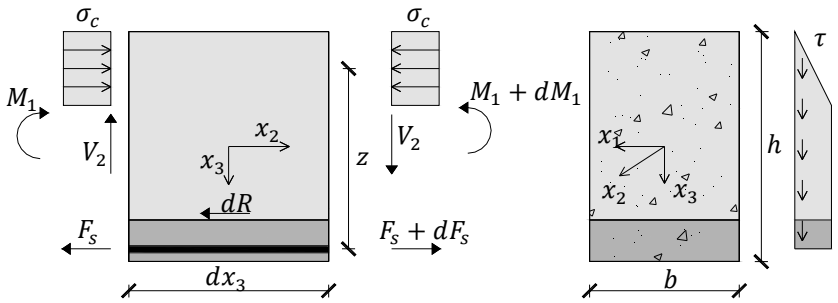

Figure 3.12: Equilibrium of normal stress and shear distribution in the cross-section (cracked concrete)

Shear stress in the tension zone (cracked concrete) can be deduced from the equilibrium of normal forces at the bottom part of the element illustrated in Figure 3.12.

$$\tau = \frac{dR}{b \cdot dx_3} = \frac{dF_s}{b \cdot dx_3} = \frac{dM_1}{b \cdot z \cdot dx_3} = \frac{V_2}{b \cdot z} \tag{3.15}$$

Where,

F_s is the tensile force in the longitudinal reinforcement

z is the lever arm of the binary of the longitudinal forces in the cross-section

In the compression zone, stress is resisted by concrete. The compression zone is displayed in Figure 3.12 as a rectangular block, so shear stress distribution was considered linear. This example is an approximation, since in reality the distribution of normal stress in the compression zone is not linear.

Both in EC2 (Equation 6.24 of the design code) and MC2010 (Equation 7.3.32 of the design code), the adopted design value for shear stress in concrete-to-concrete interfaces is given by:

$$v_{ed,i} = \frac{\beta V_{ed}}{z b_i} \tag{3.16}$$

Where,

β is the ratio of the longitudinal force in the new concrete and the total longitudinal force either in the compression or tension zone, both calculated for the section considered. For the example illustrated in Figure 3.12, $\beta = 1$. In general, $\beta \leq 1$.

b_i is the width of the interface

So the problem consists on calculating correctly both shear stress and strength in the interface region, and ensuring:

$$v_{ed,i} \leq v_{rd,i} \tag{3.17}$$

The latter expression is consistent with requirements of MC2010, expression 7.3-31 and EC2 expression 6.23.

3.5 Prediction for shear strength at the interface

According to Rilem (2011), at this time there is still no generally accepted design methodology for the determination interfacial shear strength. The proposed design expressions are considered by some authors to be unsafe as there is an opinion that structural stiffness and differential shrinkage should be included in the design (Santos & Julio, 2010).

3.5.1 Shear friction theory

Most design codes have adopted shear friction theory to determine ultimate shear stress between concretes cast against each other with different ages. This is relevant not only in the field of strengthening by addition of new concrete layers, but also for other concrete joints in which the hardening process of the older concrete is already finished, such as precast elements that receive in situ topping.

Shear friction theory is related to the resistance mechanism of interfaces after the loss of adhesion (or, in other words, stress transfer across a concrete crack). This theory is explained by comparison to a “saw-tooth” model (Figure 3.13). On a roughened interface, when a slip between the two materials occurs, a crack along the interface is formed. As the crack widens, tensile stress in the reinforcement is generated, compressing the joint (clamping force) and allowing frictional forces between substrate and overlay to develop (Santos & Julio 2010). As the layers slide one over the other, dowel action is also activated in the reinforcement.

Also, as a result of shear friction (after the expected crack along the interface is formed), a rough interface will create a higher crack width, w, hence higher tension in the reinforcement. A smooth interface will allow for large slips, s (Figure 3.14) which promote dowel action.

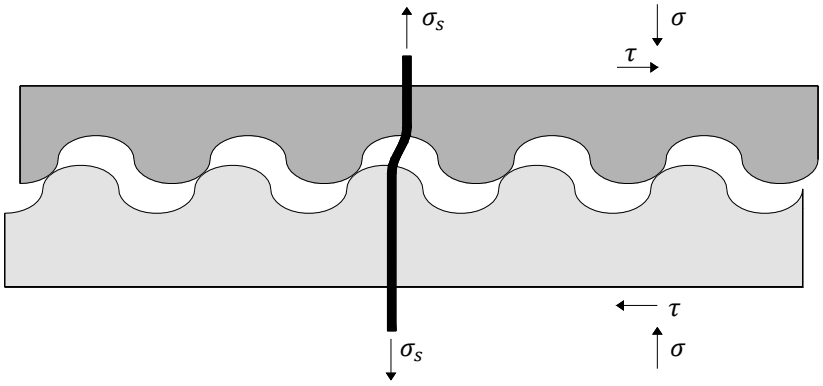

Figure 3.13: Saw tooth model, adapted from Santos and Julio (2010)

The single mechanisms responsible for shear transfer in cracked concrete are represented in Figure 3.14.

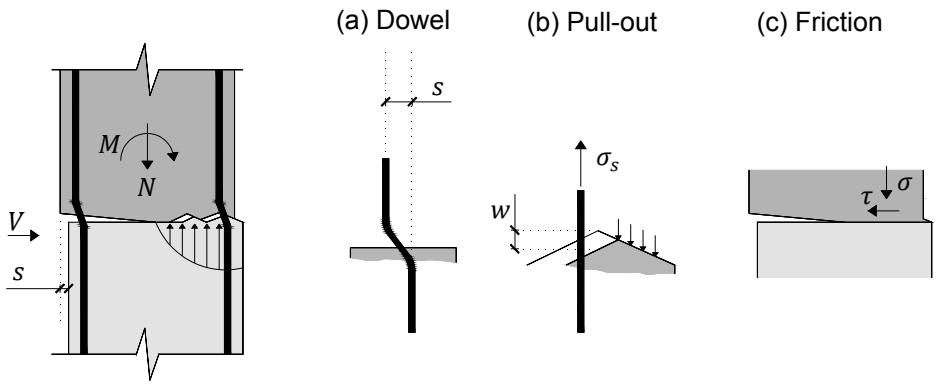

Figure 3.14: Single mechanisms responsible for shear transfer, adapted from Munger et al (1997); (a) Dowel action; (b) Tension in the reinforcement and compression of the interface; (c) friction

These mechanisms interact and affect each other in function of the bond slip, so it would not be correct to formulate shear resistance by adding their contribution considering their maximum values. Most recent approaches to shear resistance have this interaction in account, by introducing coefficients that are dependent on surface roughness. In MC2010 this difference is emphasized:

- Adhesive bonding is considered to be very stiff and only effective at slips under 0,05mm;
- Aggregate interlock is also considered to be very stiff, decreasing its contribution to overall shear resistance with increasing slip, as the aggregates crush;
- Friction shows a slight decrease with increasing slip, due to interface deterioration;
- Only dowel action contribution increases with increasing slip;

Two types of behaviors can be differentiated: “Rigid” bond slip behavior and “Non-rigid” bond slip behavior. Depending on bond strength, roughness and the degree of reinforcement one of this behaviors will dominate the overall load bearing behavior.

In “rigid” bond slip behavior, failure occurs with the loss of adhesion, which is usually the case of smooth interfaces without reinforcing or in rough interfaces with no or small amounts of reinforcement. The resistance is ensured mainly by the single mechanisms of adhesion/mechanical interlock. Typical slip values are under 0,05mm. For larger deformations (higher slips), friction and dowel action deliver the main contribution for interface resistance, provided that a noticeable amount of reinforcement is present $\rho_i \geq 0{,}05\%$

The Model Code 2010 approach for surfaces connected by dowels (Equation 3.24), already describes these two situations (Randl, 2011). In EC2 no reference is made to the possibility of different behaviors between interfaces intersected by reinforcing steel and interfaces connected by dowels.

When superposing different mechanisms that influence shear resistance, it is necessary to account the influence and interrelation between the different single mechanisms, the interaction of tension and bending in the connectors (that leads to an interrelationship between clamping force and dowel action) and that the main contributions of each mechanisms occurs at different slips.

3.5.1.1 Birkland's expression

Shear friction was first proposed by Birkeland in 1966 (Santos & Julio, 2010). According to his approach, ultimate shear stress developed exclusively from the frictional force triggered by the compression of the joint, and could easily be determined by Equation 3.18.

$$v_{rd,i} = \mu \rho_i f_y \tag{3.18}$$

Where,

μ is the friction coefficient

ρ_i is the amount of reinforcement crossing the interface

3.5.1.2 Randl's expression

Over the years, the theory has been revised by several authors to include other parameters. According to the current version, ultimate shear strength is seen as a combination of adhesion, mechanical interlock, friction and dowel action.

As the two concrete layers distant, the contributions of mechanical interlock and friction to bond strength decrease and the influence of dowel action increases (Santos & Julio 2010; MC2010; Randl, 2011). The latter theory can be quantified by Randl's expression.

Randl's expression (Equation 3.19) first parcel is related to the contribution of adhesion and mechanical interlock for shear strength. The middle parcel represents the influence of friction triggered by normal stress at the interface and the steel connectors. The last parcel accounts for dowel action (Santos and Julio, 2010).

$$v_{rd,i} = c f_c^{1/3} + \mu\left(\sigma_n + \rho_i k f_y\right) + \alpha \rho_i \sqrt{f_y f_c} \tag{3.19}$$

Where,

c is a coefficient for cohesion (Table 3.3)

f_c is the concrete compressive strength

f_y is the yield strength of the reinforcement

μ is a coefficient for friction (Table 3.3)

σ_n is the normal stress acting on the interface due to exterior loading

ρ_i is the reinforcement ratio crossing the interface

k is a coefficient of efficiency related to the reinforcement

α is a coefficient for dowel action

If the surfaces are very rough, the reinforcement is primarily stressed in tension, because the roughening prevents the development of higher slip between layers, whereas for smooth interfaces, dowel action is predominant. The coefficients in each parcel of Randl's expression have this effect in account.

Roughness can be quantitatively evaluated by the Sand Patch Test (described in section 3.9.1.3 of this dissertation). Several authors have been successful on relating surface treatments with substrate roughness and its effect on adhesion, this issue will be addressed in detail in section 3.9. The cohesion and friction coefficient are displayed in Table 3.3:

Table 3.3: Comparison between surface treatments and coefficients, adapted from Santos and Julio, 2010

Surface preparation	Surface roughness R_a [mm]	Coefficient of cohesion, c	Coefficient of friction, μ		k	α
			$f_{ck} > 20$ MPa	$f_{ck} > 35$ MPa		
High-pressure water-blasting	≥3.0mm	0.4	0.8	1.0	0.5	0.9
Sandblasting	≥0.5mm	0.0	0.7	0.7	0.5	1.1
Smooth	-	0.0	0.5	0.5	0.0	1.5

3.5.1.3 Walraven's Sphere Model

This model was proposed by Walraven et al. (1987). In this approach, concrete is considered a two phase model, the aggregates are approximated to rigid spherical particles and the paste is considered to be rigid-plastic. Walraven et al (1987) developed a non-linear design expression for ultimate shear strength, based on the results of a large experimental study with push-off specimens.

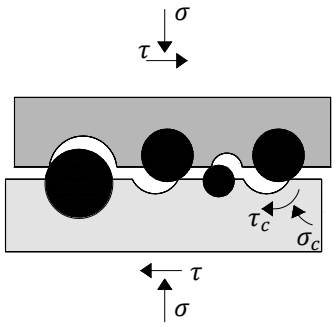

Figure 3.15: Sphere Model, adapted from Walraven (2007)

The ultimate shear strength is given by Equation 3.20.

$$v_{rd,i} = C_1(\rho_i f_y)^{C_2} \tag{3.20}$$

Where $C_1 = 0{,}82 f_{cc}^{0{,}41}$ and $C_2 = 0{,}16 f_{cc}^{0{,}3}$ and f_{cc} is the compressive strength of concrete cubes.

3.5.2 Design code expressions

Despite the fact that for ultimate limit states the design code's philosophy is to ignore the contribution of the concrete's tensile strength, both EC2 and MC2010 accept the contribution of adhesion (related to tensile strength) for shear strength at the interface.

Another issue is related to the differentiation between the "Rigid" and "Non-rigid" bond slip behavior, which is only appreciated in MC2010.

3.5.2.1 EC2 design expression

Shear stress at the interface is given by Equation 3.16, and shear strength must respect the limit imposed by Equation 3.17.

For design purposes, shear strength at the interface in EC2 is similar to Randl's expression, except it is not explicit in the formula the specific contribution of dowel action in the reinforcement. The design shear resistance at the interface is given by Equation 3.21.

$$v_{rd,i} = cf_{ctd} + \mu\sigma_n + \rho_i f_{yd}(\mu \sin\alpha + \cos\alpha) \leq 0{,}5\vartheta f_{cd} \qquad (3.21)$$

Where,

c, μ are coefficients which depend on the roughness of the interface

f_{ctd} is the design tensile strength of the concrete with the lowest strength

σ_n is the stress per unit area caused by the minimum external normal force across the interface that can act simultaneously with the shear force, positive for compression and negative for tension, such that $\sigma_n \leq 0{,}6f_{cd}$. When σ_n is tensile cf_{ctd} should be taken as 0.

ρ_i $= A_{s,i}/A_i$

$A_{s,i}$ is the area of reinforcement crossing the interface, including ordinary shear reinforcement (if any), with adequate anchorage at both sides of the interface

A_i is the area of the interface

α is defined in Figure 3.16, and should be limited by $45° \leq \alpha \leq 90°$

ϑ is a factor that accounts for the reduction of concrete resistance in cracked concrete, given by $\vartheta = 0{,}6\left[1 - \frac{f_{ck}}{250}\right]$, f_{ck} in MPa

This formula has been criticized by some authors, including Randl (2011), because it considers full yield in the reinforcement and disregards displacements parallel to the interface.

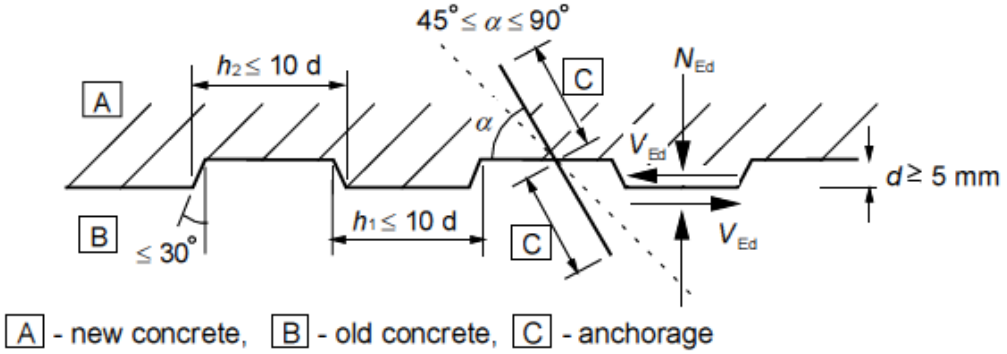

Figure 3.16: Indented construction joint (EC2)

The coefficient values are given by a qualitative classification of interface surfaces as very smooth, smooth, rough or indented, and a brief reference is made to the surface treatment (Table 3.4). The fact that these coefficients directly influence the importance

of each single mechanism for shear resistance has also been criticized, and a more accurate classification for the parameters is necessary (Santos and Julio, 2010).

Table 3.4: Roughness parameters for Expression 3.3, adapted from EC2

Surface	Description	c	μ
Very smooth	A surface cast against steel, plastic or specially prepared wooden molds	0,025~0,10	0,5
Smooth	A slip formed or extruded surface, of a free surface left without further treatment after vibration	0,20	0,6
Rough	A surface with ate least 3mm roughness at about 40mm spacing achieved by ranking, exposing of aggregate or other methods giving an equivalent behavior	0,40	0,7
Indented	A surface with indentations (Figure 3.16)	0,50	0,9

If the joint is significantly cracked, the parameter c should be taken as 0 for smooth and rough joints, and 0,5 for indented joints. Under fatigue or dynamic loads, the values for c should be halved.

3.5.2.2 MC2010 design expressions

Shear stress at the interface is also given by Equation 3.16, and shear strength must respect the limit imposed by Equation 3.17.

The subject of shear at the interface between concretes cast against each other at different times is addressed in sections 6.3 and 7.3.3.6 of MC2010. This design code presents a progress from the EC2 methodology, as it highlights specifically the role of the displacement on the mechanisms that govern shear strength (adhesion, mechanical interlock, friction and dowel action).

The code presents Equation 3.22 as an overall and simplified approach to ultimate shear stress at the interface. The contributions of adhesion (τ_c), friction and dowel action are represented by the first, second and third parcel, respectively.

$$\tau_{Ru} = \tau_c + \mu\left(\rho_i \kappa f_y + \sigma_n\right) + \alpha\rho_i\sqrt{f_y f_{cc}} \leq \beta\vartheta f_{cc} \tag{3.22}$$

Where,

ρ_i is the degree of reinforcement crossing the interface

The interaction factors κ and α take into account that the reinforcement or connectors are subjected to bending and axial forces simultaneously and the maximum values of the different contributions occur at different slips between concrete layers.

For cast-in reinforcement with appropriate end anchorage in the old and new concrete, the tensile loading of bars may be considered as predominant, i.e. $0{,}5 \leq \kappa \leq 1$, the dowel action in turn reduces and for simplified design purposes $\kappa \leq 1$ and $\alpha = 0$ may be adopted.

For post-installed reinforcement, which is the case of concrete rehabilitation, $\kappa = 0{,}5$ shall be taken when the interface has been roughened. For smooth interfaces dowel action is the main resistance mechanism resulting from reinforcement or connectors, i.e. $\kappa = 0$ and $\alpha = 1{,}15$.

Regarding shear strength, the code differentiates between interfaces intersected by reinforcing steel and interfaces connected by dowels.

In the first case, interfaces connected by reinforcement, the design limit value v_{Rdi} for the interface shear is similar to the EC2 approach, and follows from:

$$v_{Rdi} = cf_{ctd} + \mu\sigma_n + \rho_i f_{yd}(\mu \sin\alpha + \cos\alpha) \leq 0{,}5\vartheta f_{cd} \tag{3.23}$$

Where,

c is a cohesion factor

μ is a friction coefficient

ρ_i is the reinforcement ratio of the reinforcing steel crossing the interface

σ_n is an eventual normal force acting on the interface

α is the inclination of the reinforcement crossing the interface

ϑ is a factor that accounts for the reduction of concrete resistance in cracked concrete, given by $\vartheta = 0{,}6\left[1 - \frac{f_{ck}}{250}\right]$, f_{ck} in MPa

Cohesion and friction values in Equation 3.23 depend on the roughness of the interface. The design code proposes the values described in Figure 3.13 and relates, in section 6.3.2 (MC2010) the average roughness R_a and the applied roughening methods with the below mentioned categories, being this the main evolution from EC2.

Table 3.5: Coefficients for the determination of interface shear strength (adapted from MC2010 tables 7.3-1 and the table in section 6.3.2)

Surface	R_a	c	μ
Very smooth (steel, plastic, specially treated timber formwork)	Not measurable	0,025	0,5
Smooth (concrete surface without any curing)	<1,5mm	0,35	0,6
Rough (strongly roughened surface)	>1,5mm	0,45	0,7
Very rough	≥3mm	0,5	0,9

For interfaces connected by dowels, which the code relates to the retrofitting of structures, the following expression is considered more appropriate:

$$v_{Rd,i} = 0{,}09k_c f_{ck}^{1/3} + \mu\left(\kappa \cdot \rho_i \cdot f_{yd} + \frac{\sigma_n}{\gamma}\right) + \alpha_F \rho_i \sqrt{f_{yd} \cdot f_{cd}} \leq \beta_c \cdot f_{cd} \cdot \vartheta \tag{3.24}$$

Note: In the last parcels of Expression 3.24, there is no reference to the presence of ρ_i, and ϑ is typed as b. However, this must be a typing error, as the current version is still a first draft.

Where,

k_c is a coefficient for interface roughness

κ is a coefficient for tensile force activated in the reinforcement or the dowels

α_F is a coefficient for flexural resistance

β_C is coefficient for compressive struts

ϑ is a factor to account for the reduction of concrete resistance in cracked concrete, given by $\vartheta = 0{,}6\left[1 - \frac{f_{ck}}{250}\right]$, f_{ck} in MPa

The coefficients present in Equation 3.24 are shown in Table 3.6. Surface treatments are related with the mean texture depth, R, calculated by the sand patch test (which is described in section 3.9.1.3 of this dissertation).

Table 3.6: Coefficient for surface roughness in interfaces crossed with dowels, adapted from MC2010

Surface Roughness	k_c	κ	α_F	β_c	μ	
					$f_{ck} \geq 20$	$f_{ck} \geq 35$
High pressure water jetting, $R \geq$ 0,5mm	2,3	0,5	0,9	0,5	0,8	1,1
Sand blasting, $R \geq$ 0,5mm	0	0,5	1,0	0,4	0,7	
Smooth	0	0	1,4	0,4	0,5	

3.5.3 Equilibrium of forces across the interface

The relation between the resisting force in the overlay reinforcement and shear stress across the interface is given by Equation 3.25.

$$V_{rd,i} = l_i b_i v_{rd,i} \tag{3.25}$$

Where,

l_i is the length of the interface under review

b_i is the width of the interface under review

$v_{rd,i}$ is the design value of the transferable interface shear stress

This equilibrium highlights the fact that the dimensions of the new concrete layer are also very important, as with higher interface dimensions, less shear stress is created.

For concrete overlays in the tension zone, after concrete has cracked, the equilibrium of normal forces imposes that steel force and shear force at the interface are equal.

3.6 Flexural design

The main goal of the strengthening intervention discussed in this dissertation is to increase flexural capacity of RC elements, such as slabs or beams. Although this technique may also increase the resistance to shear forces and the punching shear capacity, the design methodology is not discussed in this dissertation.

Substrate and overlay must be rigidly connected, to promote, as closely as possible, monolithic behavior and approximately continuous strains. If the strain distribution is approximately continuous, flexural design adopting simple beam theory and a remodeling correction factor for the lack of homogeneity can be used.

In EC8, part 3, for the purpose of evaluating strength in a jacketed member cross-section, full composite action can be considered between new and old concrete, and the bending moment corrected by the mentioned homogeneity factor.

Gomes and Appleton (1997) present an example of a design approach to flexural resistance, which is based on the assumption that the connection between concretes is perfect and the resistance is calculated based on the constitutive relations of new materials. The determined resistance is then reduced by a homogeneity coefficient, and shear stress at the interface is verified. This method allows for the determination of bending moment of a simple beam with two tensile reinforcement layers.

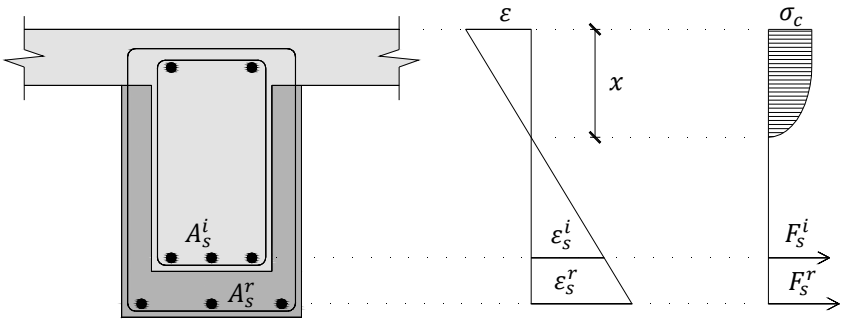

Figure 3.17: Simplified ultimate limit state, adapted from Gomes and Appleton (1997)

If the two longitudinal reinforcement layers are near, the reinforcement area may be calculated considering an equivalent reinforcement area, A_s^{eq}, with the initial tensile resistance f_{yd}^i, located in the centroid of both reinforcement, and defined by the following equations:

$$M_{rd} = \gamma_M \left\{ A_s^{eq} z^{eq} f_{yd}^i = A_s^r z^r f_{yd}^r + A_s^i z^i f_{yd}^i \right\} \tag{3.26}$$

Where,

γ_M is the homogeneity coefficient, equal to 0,9

A_s^{eq} is given by $A_s^i + A_s^r \frac{f_{yd}^r}{f_{yd}^i}$

z^{eq} is given by $z^{eq} = \frac{A_s^i z^i f_{yd}^i + A_s^r z^r f_{yd}^r}{A_s^i f_{sy}^i + A_s^r f_{sy}^r}$

A_s^i is the initial area of longitudinal reinforcement

A_s^r is the area of longitudinal reinforcement in the strengthening layer

f_{yd}^i is the yielding stress of the initial longitudinal reinforcement

f_{yd}^r is the yielding stress of the longitudinal reinforcement in the strengthening layer

z^i is the lever arm of the internal forces of the initial forces

z^r is the lever arm of the internal forces of the strengthening forces

Assuming $z \approx 0{,}9d$,

$$M_{rd} = \gamma_{n,M}\left\{A_s^{eq}0{,}9d^{eq}f_{yd}^{i} = f_{yd}^{i}\left(A_s^{i}0{,}9d^{i} + A_s^{r}0{,}9d^{r}\frac{f_{yd}^{r}}{f_{yd}^{i}}\right)\right\} \quad (3.27)$$

Where,

d^i is the effective depth to the original longitudinal reinforcement

d^r is the effective depth to the longitudinal reinforcement in the strengthening layer

As the initial assumption of linear strains is not real, this analysis must include a verification of shear strength at the interface. The distribution of shear force is illustrated in Figure 3.18.

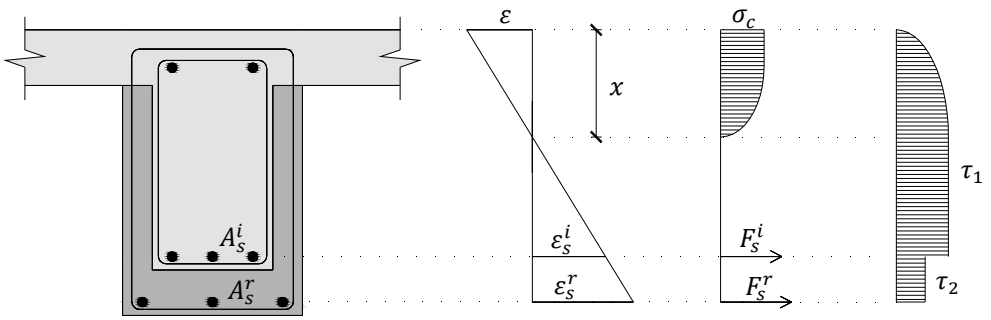

Figure 3.18: Shear stress distribution, adapted from Gomes and Appleton (1997)

In the tension zone, shear stress is given by:

$$\tau_1 = \frac{V}{bz^{eq}} \quad (3.28)$$

$$v_{ed,i} = \tau_2 = \frac{V}{bz^{eq}} \cdot \frac{A_s^r f_{syd}^r}{A_s^i f_{syd}^i + A_s^r f_{syd}^r} \quad (3.29)$$

It is noteworthy that Equation 3.29 is equivalent to Equation 3.16. Gomes and Appleton (2007) also suggest that the value for shear strength in the interface should be limited to:

$$\tau_{rd} = \frac{1}{\gamma_c}\frac{2}{3}f_{ctm} \quad (3.30)$$

Where,

f_{ctm} is the minimum axial tensile strength of the two concretes

3.7 Effect of restrained shrinkage

A restrain is defined as an effect that counteracts the free deformation of a given body. Stresses resulting from shrinkage are always a response to restrains to the free deformation the concrete (Rilem, 2011).

According to Beushausen and Alexander (2007), failure mechanisms associated with RC overlays, such as cracking and debonding, result from differential volume changes between the substrate and overlay. The effect of restrained shrinkage creates stresses, which are concentrated in the interface perimeter.

An experimental research was conducted by the same authors, in order to test fundamental strain characteristics. Two different types of specimens were tested, but it only seems worthy, in the context of this dissertation, to mention the results of specimen A, where strains were measured along the length of the interface.

The geometry of specimen A is illustrated in Figure 3.19. The element has a rectangular cross-section with 160mm width. Concrete strains were measured at approximately 2-3mm distance from the interface in both overlay and substrate.

The substrate surfaces were sandblasted to obtain a rough and sound interface texture. The average interface roughness, R_a, determined by the sand patch test was 0,7mm. The substrate surfaces were kept to moist for 24h using wet burlap and plastic sheets and left to air dry for 30-60min prior to the overlay application.

Overlays were moist cured with wet burlap and plastic sheets for 7 days after casting. Subsequently, specimens were left uncovered in the laboratory. Overlay strains were compared with free shrinkage strains measured on control specimens with the same cross-sectional dimensions as the overlay.

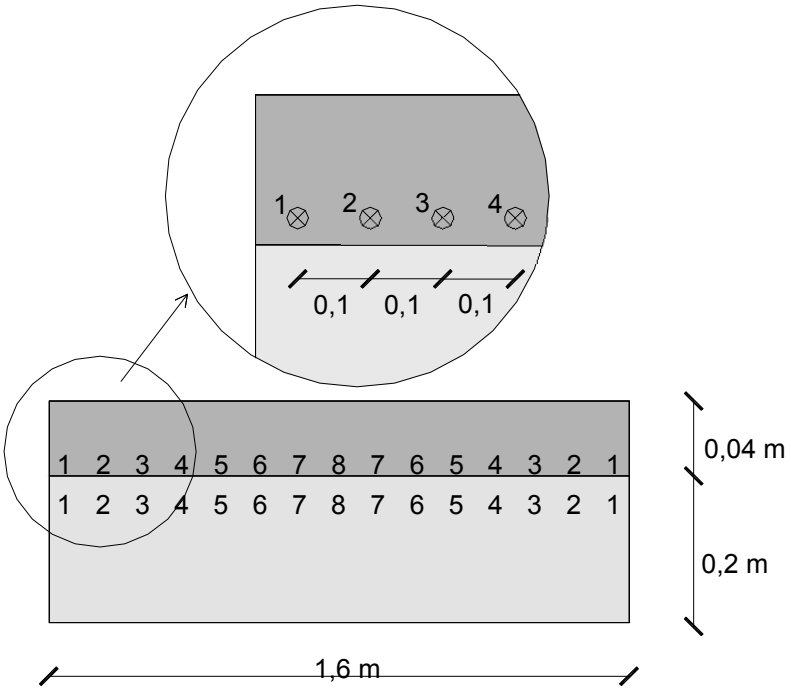

Figure 3.19: Beam geometry and strain gauge location, adapted from Beushausen and Alexander (2007)

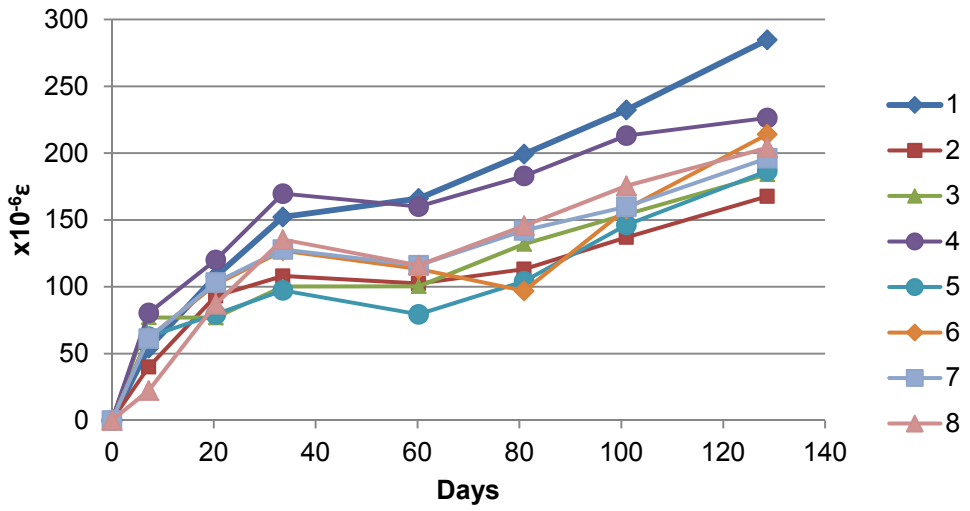

Figure 3.20: Overlay interface strains with time in relation to the location along the member, adapted from Beushausen and Alexander (2007)

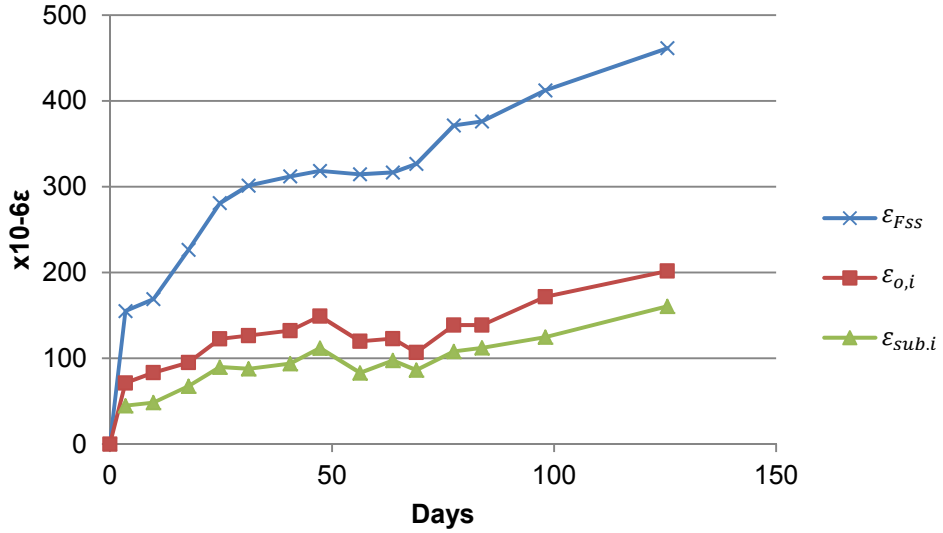

Figure 3.21: Interface strains in the overlay, ($\varepsilon_{o,i}$), and substrate strains, ($\varepsilon_{sub,i}$) and free overlay shrinkage strain ε_{Fss}, adapted from Beushausen and Alexander (2007)

The results showed that substrate and overlay strains developed virtually at the same rate, indicating full bond between the two layers. Both in the substrate and the overlay, similar strains were measured, with the exception of the elements ends (Locations “1”) that exhibited higher values.

Free shrinkage strains in the control specimen with the overlay geometry were much higher than the ones observed for specimen A, indicating that, as shrinkage was restrained, stress is likely to develop.

In addition, the authors affirm that no sign of debonding or cracking was observed in the concrete elements. However, from the results displayed in Figure 3.21, and the relation presented in Equation 3.31 it is possible to conclude that stresses resulting

from differential shrinkage are superior to the concrete tensile resistance. This indicates that some cracking might have occurred, however, it wasn't visible.

$$\sigma_c = E_c(\varepsilon_{o,i} - \varepsilon_{Fss}) \tag{3.31}$$

The relation in Equation 3.31 allows for an approximate quantification of the stress of the interface, which is about 7,4 MPa, and larger than the average tensile resistance of the overlay.

Table 3.7: Properties of the concrete overlay

E_c (28 days)	29,6 MPa
f_{ctm} (28 days)	3,0 MPa
ε_{Fss} (maximum value, based on Figure 3.21)	-450×10^{-6}
$\varepsilon_{o,i}$ (maximum value, based on Figure 3.21)	-200×10^{-6}

Beushausen and Alexander (2007) elaborated experimental research, which results indicate that the existing models based on simple beam theory are deficient in modeling overlay strains realistically.

Binachi (2007) emphasizes that stress due to shrinkage creates not only higher tension stresses near the overlay's borders, but also tension stress perpendicular to the interface.

3.8 Debonding mechanism

In RC elements strengthened with the bonded concrete overlay technique, substrate and overlay should work monolithically, ensuring continuity of deformations between materials. Rilem (2011) relates debonding with two causes, differential length changes and so called "flexural effects" (Figure 3.22). Debonding due to these "flexural effects" is a consequence of flexural straining of the structure. The tensioned area is one of the most critical areas for debonding to occur, because of cracking of the overlay.

Debonding due to length changes is also a consequence of cracking of the overlay (which is why cracks due to differential shrinkage can influence debonding).

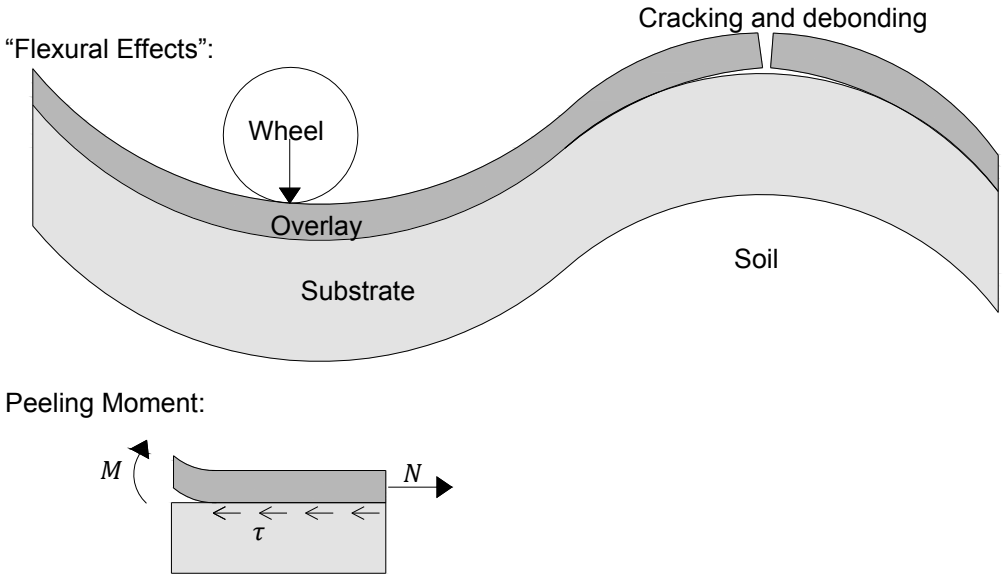

Figure 3.22: "Flexural Effects" and peeling moment, adapted from Rilem (2011)

Regardless of the causes, debonding is related to the creation of tension perpendicular to the interface. At both sides of a crack, a peeling moment induces tensile stresses perpendicular to the overlay (Rilem, 2011).

3.9 Surface preparation and its influence on shear strength

Surface preparation has a strong influence on adhesion and ultimate shear stress. Concrete removal, cleanliness and wettability of the substrate are key aspects to consider.

3.9.1 Surface treatments

3.9.1.1 Concrete removal

To achieve proper bonding, the interface surface must be prepared before the new concrete layer is placed. Casting the new layer against poor quality concrete will create other weak regions near the interface (Julio et al., 2004). In order to prevent this, deteriorated concrete and any unsound concrete in the interface area (e.g. laitance) must be removed, and the coarse aggregate exposed. Depending on the type of deterioration, it might be necessary to expose some rebars or even demolish the old concrete behind them. Also, when preparing a concrete overlay maintaining slab's previous height, it becomes necessary to demolish a part of the substrate concrete, even if there are no evidences of corrosion.

Removal tasks must be performed in a manner that ensures that the remaining concrete and the reinforcing steel retain its structural identity (Rilem, 2011).

3.9.1.2 Roughening the substrate

According to Julio et al. (2004), a surface treatment is recommended both to enlarge and roughen the interface area. Roughening the surface will create a certain degree of mechanical interlock between the concrete layers. Surface treatments have been related to roughness and bond strength in numerous studies; Perez et al. (2009) achieved monolithic behavior for beam core's, tested under direct tension and shear that presented a substrate with a rough interface, whereas large debonding was

recorded for those having smooth surfaces. The author achieved bond strengths ranging from 1,5-2,8.

Depending upon which technique is used and the level of energy induced, different surfaces and results for bond strength will be achieved. However, some roughening techniques might cause micro cracking to the substrate, and contribute to the deterioration of bond quality. Garbacz et al. (2004) related surface treatments with type of failure and analyzed that micro cracking of the interface surface induced cohesion failures rather than adhesive failures. Table 3.8 presents a description of some surface treatments.

Table 3.8: Concrete removal methods, adapted from Rilem, (2011)

Removal method	Principle behavior	Concrete removal capability (Action depth)	Important advantages	Important disadvantages
Sandblasting (Figure 3.23)	Blasting with sands	No	No microcracking	Not selective, leaves considerable sand
Scrabbling	Pneumatically driven bits impact the surface	Little (6mm)	No microcracking, no dust.	Not selective
Shotblasting	Blasting with steel balls	Little (12mm)	No microcracking, no dust	Not selective
Grinding (planning)	Grinding with rotating lamella	Little (12mm)	Removes uneven parts.	Dust development, not selective
Flame-cleaning	Thermal lance	No	Effective against pollutions and painting, useful in industrial and nuclear facilities.	The reinforcement may be damaged, smoke and gas development, safety considerations limit use, not selective
Milling (scarifying)	Longitudinal tracks are introduced by rotating lamellas	Yes (75mm)	Suitable for large volume work, good bond if followed by water flushing	Microcracking is likely, reinforcement may be damaged, dust development, noisy, not selective
Pneumatic (jack) hammers (chipping), hand-held or boom mouted	Compressed air operated chipping	Yes	Simple and flexible use, large ones are effective	Microcracking is likely, reinforcement may be damaged, dust development, noisy, not selective
Explosive blasting	Controlled blasting using small densely spaced blasting charges	Yes	Effective for large removal volumes	Difficult to limit to soley damaged concrete, safety and environmental regulations limit use, not selective
Water-jetting (hydro-demolition)	High pressure water jet from a unit with a movable nozzle	Yes	Effective (especially on horizontal surfaces), selective, does not damage reinforcement or concrete, improved working environment	Water handling, removal in frost degrees, costs for establishment

Table 3.9: Laboratory tests: influence of microcracking, adapted from Rilem, (2011)

Interface treatment	Presence of microcracking	All tests		Interface Failures	
		Number of cores	Average failure stress [MPa]	Number of cores	Average failure stress [MPa]
Waterjetting	No	16	1.86	1	2.23
Pneumatic hammers	Yes	16	1.10	5	0.94

Figure 3.23: Sandblasted surface (left) and left as cast (right)

Figure 3.24: : Wirebrushed surface (left) and left as cast (right)

Although it is one of the parameters that highly influences bond, there is still no standard measure for roughness. In EC2, roughness is evaluated qualitatively and it is considered to be mainly dependent on the technique used and visual observance. In MC2010 roughness is divided in categories and to some extent, related to roughness parameters and surface treatments.

Authors agree that there is a need to measure and quantify roughness, as it is one of the factors that most influences bond strength and ultimate shear strength (Santos, Julio & Silva, 2007; Courard et al., 2006).

3.9.1.3 Roughness measurements and parameters

The sand patch test (Figure 3.25) is a volumetric measure for pavement texture, commonly used in the highway field. The testing apparatus presents the advantage of being quite simple. A certain volume, V, of sand is placed on the concrete surface and regularized forming a circular shape. The diameter, d, is measured. The mean texture depth, R, represents the ratio between the volume and the area of sand (Equation 3.32) Relations between the latter parameter, surface treatments and values for the cohesion and friction coefficients are already used to quantify shear strength in MC2010.

$$R = \frac{4 \cdot V\ [mm^3]}{\pi \cdot d^2\ [mm^2]} \tag{3.32}$$

The sand patch test presents the disadvantage that it can't be used in very rough surfaces (Patel, 2007).

Other methods that determine roughness parameters based on the measurement of surface profiles – profilometry – have been described in literature. Although these are

adequate for laboratory testing, they seem complicated to perform on site; Abu-Tair et al. (2000) proposed a profile texture meter, which basically consisted on recreating the shape of a certain substrate profile with needles, and defined the texture depth of the sample by analyzing the picture of the recreated profile (Figure 3.26). Santos, Julio and Silva (2007) characterized the profile's texture simply by using a digital image of the profile with an auxiliary metric scale (Figure 3.27). The authors suggest that the evaluated length should be 2,5 to 3 times larger than the average roughness, R_a. Garbacz et al. (2004) used a commercial device that consisted on a stylus, a conditioner/amplifier, a mechanical unit and a computer unit for data acquisition.

Figure 3.25: Sand patch test

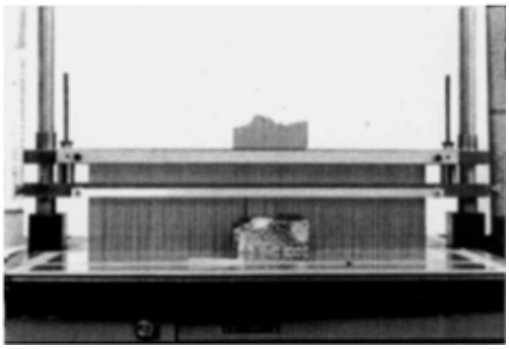

Figure 3.26: Mechanical profile texture meter (Abu-Tair et al., 2000)

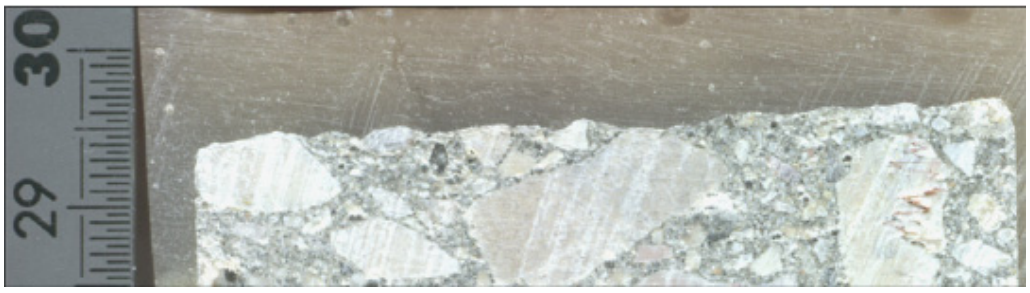

Figure 3.27: Digital image of a concrete specimen (Santos, Julio & Silva, 2007)

MC 2010 describes two commonly used roughness parameters that can be determined with the knowledge of the profile's texture. The average roughness, R_a, which represents the average deviation of the profile from a mean line, is given by Equation 3.33. It is defined as the mean value of profile heights along a certain length l_m. The mean to peak valley height, $R_{z(DIN)}$ represents the average of maximum valley-to-peak-heights, z_i, within a certain number of assessment lengths (Equation 3.34).

$$R_a = \frac{1}{l_m}\int_0^{l_m} y(x)\cdot d(x) \approx \frac{1}{n}\sum_{i=1}^{n} y_i \tag{3.33}$$

$$R_{z(DIN)} = \frac{1}{5}\sum_{i=1}^{5} z_i \tag{3.34}$$

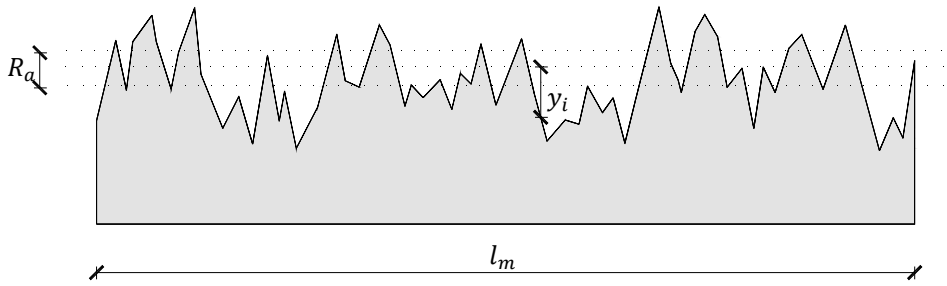

Figure 3.28: Average roughness, adapted from MC2010

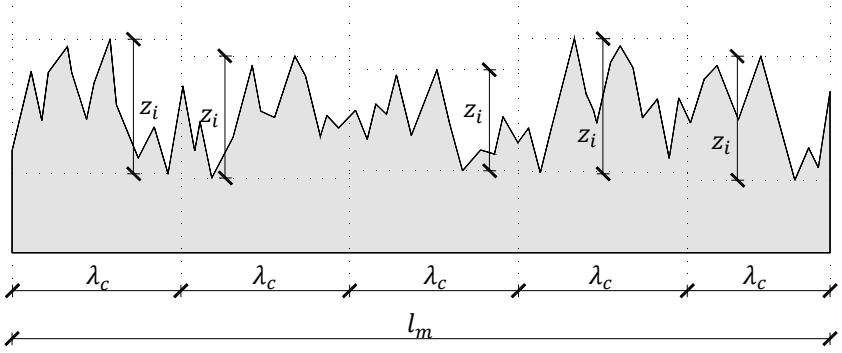

Figure 3.29: Mean to peak valley height, adapted from MC2010

MC2010 emphasizes that identical values of the same average roughness R_a might still lead to different shear resistances. These differences can be explained by variations in the actual surface topography and, as always, engineering judgment is required when determining the appropriate roughness category.

Both Santo, Julio and Silva (2007) and Issa et al. (2003) describe in their research other parameters that can be used to quantify roughness.

Fractal analysis can also be a powerful tool to evaluate roughness (Issa et al., 2003).

3.9.1.4 Correlations between bond strength, surface treatments and roughness

Julio et al. (2004), studied the effect of different surface treatments on bond strength and compared sandblasted, wire brushed, partially chipped, and left as cast substrate surfaces. The concrete compressive strength was about the 50MPa. The sandblasted specimens presented higher values for bond strength both in combined shear and compression (slant shear test) and in pure tension (pull-off test). All specimens experienced adhesive interface failure. However, the specimens left as cast experienced debonding while drilling the core, so testing the specimens was obviously impossible. The occurrence of debonding while drilling the core was regarded as an indicator of deficient interfacial properties. The results obtained are displayed in Figure 3.30.

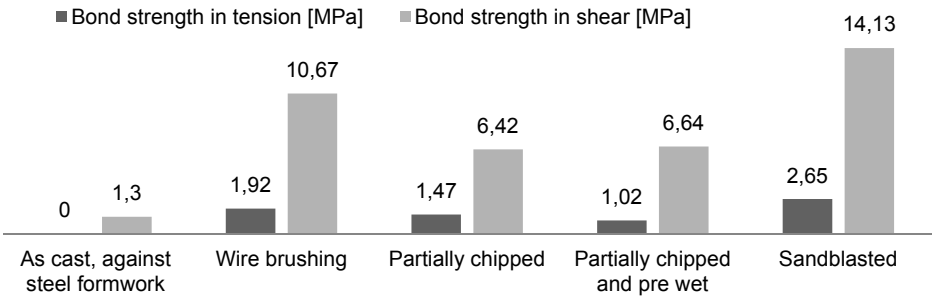

Figure 3.30: Values for bond strength, adapted from Julio et al. (2004)

Santos, Julio and Silva (2007) compared surface textures with surface treatments and related them with test results on bond strength in shear (slant shear test) and in tension (pull-off test). A number of parameters to describe roughness were analyzed. From this parameters it was concluded that the mean to peak valley high correspond to a high degree of correlation with bond strength. The results obtained are displayed in Figure 3.31.

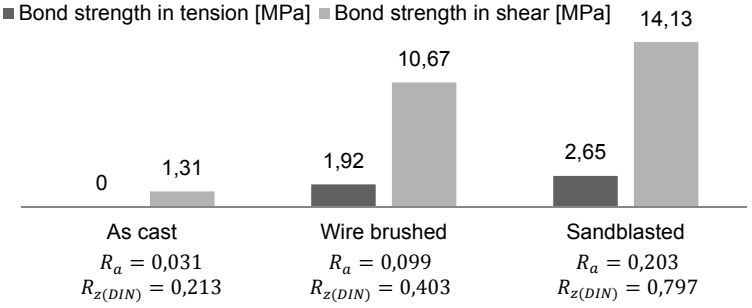

Figure 3.31: Relation beween surface parameters described in MC2010 and surface treatments, adapted from Santos Julio & Silva (2007)

3.9.1.5 Cleanliness of the interface and reinforcement bars

It is also required to provide a clean interface surface at the time of the overlay placement, because loose concrete particles, dust, grease and other contaminating particles resulting from construction works will prevent proper bonding. Cleanliness of the substrate surface has been described as the single most important factor to influence bond (Rilem, 2011). Randl and Zilch (2009) alert to the fact that even though surfaces have already been clean, the concrete surface may be contaminated just before the overlay is placed. The interface may be cleaned with a water jet, compressed air or a vacuum cleaner.

Reinforcement should also be clean and free from dust, oil and corrosion, in order to promote good bond to concrete.

3.9.1.6 Pre-wetting the interface

A study about this subject (Rilem, 2011) analyzed the effect of pre wetting the interface surface on the bond between concretes cast against each other at different times. Three prismatic composite specimens (10x10x40cm) were subjected to a four point bending test. One of the specimens had a wet substrate surface, which was immersed in water for two days, another had a substrate surface with the same humidification, but the surface water was wiped by sponge. A surface that had been

dried for 24h at 105º was also tested. In all the studied specimens, the best resistance was obtained for a saturated substrate with a dry surface, followed by a saturated wet surface. The worst results were obtained for dry surfaces. The study concluded that in order to ensure good bond, the substrate must be saturated with a dry surface, without water stagnation. The results obtained were justified by the fact that stagnant water can clog the pores and prevent absorption of the overlay material. Furthermore, dry surfaces could absorb too much water from the overlay material, resulting in incomplete hydration of cement in the interface zone.

The results of the previous study have shown that the best procedure is to provide a saturated and dry surface. Walraven (2007) explains that a dry substrate can suck water from freshly placed overlay, resulting in bad interface quality. The presence of superficial water can prevent the interlocking effect, as it dilutes the overlay near the interface and prevents absorption, leading to bad interface quality. And a saturated-dry substrate prevents suction and provides open cavities for interlocking, resulting in good interface quality, hence it is considered to be the best procedure.

3.9.1.7 Eventual use of a bonding agent

According to Garbacz et al (2004) bond coats should be avoided as they present an extra plane of weakness. Moreover, in very rough surfaces a bond coat could have a negative effect, limiting the mechanical interlock between substrate and repair material. However, other authors have shown that a presence of bond coat can significantly increase the adhesion.

According to Rilem, (2011) bonding agents are not necessary and should be avoided since they provide an additional layer that can cause failure, and emphasizes the possibility that a bonding agent that is allowed to cure prior to concrete placement, becomes a bond breaker.

3.10 Connectors and reinforcement crossing the interface

Reinforcement crossing the interface is required, either because it's necessary to overcome adhesive bonding, which is usually the case when high interfacial stresses are involved, and to provide a safety margin in order to avoid brittle failure. This is especially important because on site, issues like contamination of the surface just before the overlay is cast, or insufficient quality of the new concrete (provoking shrinkage cracks) may cause debonding to occur for lower loads than the expected, resulting in premature failure modes associated with the interface. As ordinary reinforcement, steel becomes relevant after the concrete tensile resistance has been exceeded. Reinforcement crossing the interface becomes stressed, and effective in increasing shear strength after a predicted crack along the interface is formed.

When strengthening by means of RC concrete overlays, in order to place new reinforcement crossing the interface, it is, obviously, necessary to anchor this reinforcement in the original RC element, which requires drilling and proper sealing of the holes. Usually holes are sealed with epoxy resins, cements or mortars. The mentioned tasks should be performed carefully, in order to prevent damage to the substrate beam. Perforation should not coincide with crossing reinforcement.

Because post-installed connectors, in the case of concrete rehabilitation, were probably not predicted in the element's design, difficulties might outcome regarding the necessary anchorage lengths and in situ placement, as drilling the substrate might be predicted in an area where substrate reinforcement already exists.

According to MC2010, rebar connections using post-installed rebars are permissible for all applications where straight cast-in-place rebars are allowed. The design can be performed in a simplified way, using provisions for cast-in-place rebars.

The relative displacement between concrete the layers is both parallel to the interface surface, and due to roughness, also perpendicular. The parallel displacement, s, is associated with dowel action and the perpendicular displacement, w, is associated with crack width and tension in the reinforcement that creates friction (Figure 3.14).

MC2010 highlights the fact that for bar in tension, the tensile strength of the bar is reduced when a bar is also subjected to dowel action.

3.10.1 Tension

3.10.1.1 Steel bar embedded in a concrete element

Stress between steel and concrete is transmitted through adherence mechanisms. Chemical adhesion between materials, friction and the mechanical interlock created by ribs in the rebar are the single mechanisms involved in stress transfer. The most important contribution to stress transfer is precisely the effect of these ribs; therefore adherence stress can be simplified to the longitudinal forces that the rebar's ribs apply in concrete (Lúcio & Marreiros, 2005).

Adherence between steel and concrete can be evaluated experimentally by the pull-out test. A steel bar crossing both opposite surfaces of a cubic concrete element is submitted to tension stress, in one of the ends. The displacement of the reinforcing bar is measured in the opposite end, along with the applied force. In this test, four stages of the adherence behavior between steel and concrete can be identified. These stages are described briefly in the next paragraphs:

- The first stage is characterized by uncracked concrete, which is related to a low adherence stress, inferior to the concrete tensile strength. Adherence is provided essentially through chemical adhesion and micro-interlocking due to a microscopic roughness. Although the slippage between the elements is considered irrelevant, stress begins to concentrate around the ribs.
- A second stage is characterized by micro-cracking around the reinforcement, and the loss of chemical adhesion. The ribs introduce large stresses in the concrete, which originate micro-cracking. However no slippage between the elements occurs in this phase.
- Radial cracks appear in the concrete surrounding the steel bars and the reinforcement ribs start to crush the concrete, introducing stress in the surrounding concrete. These stresses are resisted by the confinement of concrete. Ruptures can occur by splitting or pull-out. In case of insufficient transverse reinforcement in the concrete specimen, rupture will occur by splitting. If there is a large concrete cover, or for higher reinforcement ratios, splitting can be prevented, and cracks are limited to the area around the steel bar. In this case, rupture is by pull-out. However for long anchorage lengths and moderated confinement, a mixed rupture mode may also occur.

Although the transmission of stress between reinforcement bars and concrete is not uniformly distributed, for design purposes, bond strength, f_b, can be considered constant, and the transference rate linear. The minimum anchorage, l_b, in order to ensure that failure is characterized by rupture in steel may be described by Equation 3.35.

$$F_s = A_b f_b \Leftrightarrow l_b = \frac{F_s}{\pi \cdot \emptyset \cdot f_b} \Leftrightarrow l_b = \frac{\emptyset \cdot f_{yd}}{4 \cdot f_b} \tag{3.35}$$

Where,

A_b is the surface area of the rebar

f_b is the bond strength between steel and concrete

$\emptyset$ is the diameter of the reinforcement bar

3.10.1.2 Post-installed connectors

Although post-installed connections can also be sealed by epoxy resins, in this dissertation only the grouted anchorages will be addressed.

The design of post-installed connectors sealed with grout is similar to reinforcement embedded in concrete. The main difference relies in the loading transfer mechanism, as illustrated in Figure 3.32.

In cast in place reinforcement, steel must transmit stress (though adherence) to concrete, as explained in the section above. However, for post-installed connections, stress must transfer across another interface, which is between grout and concrete. In this case, stress is transmitted by adhesion between concrete and grout.

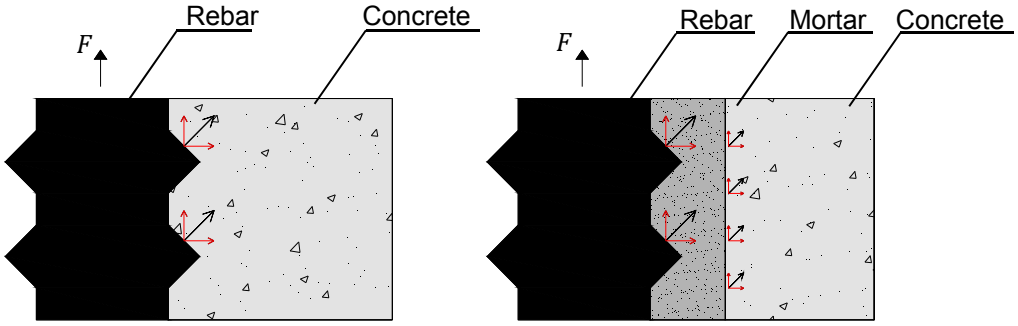

Figure 3.32: Cast in place (a) and post-installed (b) steel bars, adapted from Simmons (2004)

Miltenberger (2001) describes the possible tensile failure modes for a post-installed reinforcement system, which are represented in Figure 3.33. Mode 1 corresponds to failure of the steel and indicates that the bond between steel and grout, as well as the bond between grout and concrete, are effective, as rupture occurs in the steel bar. All other ruptures indicate insufficient bond strength/anchorage length.

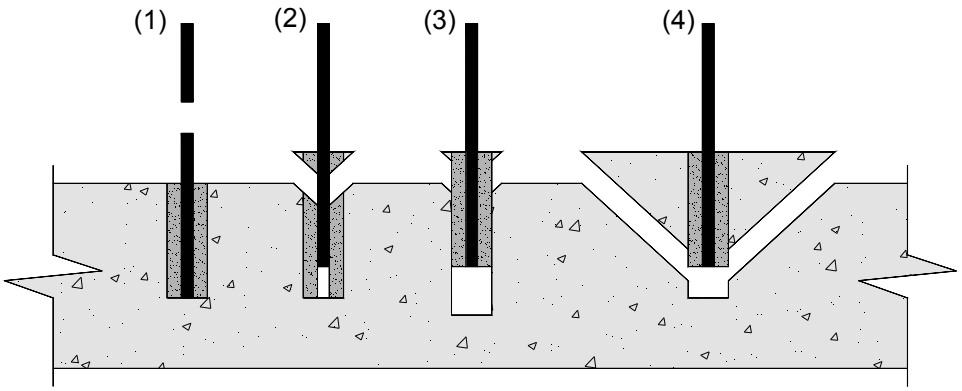

Figure 3.33: Failure modes, adapted from Miltenberger (2001)

Failure in steel:

$$F_{rd,1} = A_s \cdot f_{yd} \tag{3.36}$$

Bond failure between steel and “grout” (adhesive):

$$F_{Rd,2} = \pi \cdot \emptyset \cdot h_{ef} \cdot f_{grout,s} \tag{3.37}$$

Bond failure between grout and concrete (plug):

$$F_{Rd,3} = \pi \cdot d \cdot h_{ef} \cdot f_{grout,c} \tag{3.38}$$

Concrete Failure (conic shaped or concrete breakout):

$$F_{Rd,4} = 12{,}5 f_{cd}^{0,5} \cdot h_{ef}^{1,5} \quad , h_{ef} < 280\text{mm} \tag{3.39}$$

$$F_{Rd,4} = 4{,}75 f_{cd}^{0,5} \cdot h_{ef}^{1,67} \quad , 280\text{mm} < h_{ef} < 635\text{mm} \tag{3.40}$$

Where,

A_s is the area of the tensioned reinforcement

f_{yd} is the concrete tensile resistance

$\emptyset$ is the diameter of the reinforcement

h_{ef} is the depth of the tensioned reinforcement

$f_{grout,s}$ is the adherence between steel and grout

d is the diameter of the hole drilled for the post-installed connection

$f_{grout,c}$ is the adherence between grout and concrete

f_{cd} is the design value for the compressive resistance of concrete

Both in Equations 3.39 and 3.40, if f_{cd} is in MPa and h_{ef}in millimeters, the value obtained for $F_{Rd,4}$ is in Newtons.

Simmons (2004), elaborated a study about post-installed reinforcement, in which the holes were sealed with a commercial cement mortar, the following procedure was used:

- Drilling a hole in concrete;
- Cleaning the hole with compressed air and/or brushes;
- Pre-wetting the surface six hours prior to the mortar's placement;
- Carefully weighing the mortars components and mix them together with a special mixer;
- Pouring the mortar into the hole;
- Compacting;
- Install the reinforcement;

The study compared the effect of the cleanliness of the interface between the concrete and the repair mortar. The test result proved that simply blowing the holes with compressed air once presented lower bond strength than blowing and brushing and the best result for bond strength was a situation where the bond was consecutively blown with compressed air and brushed for three times. The study also proved that the system is highly influenced by curing time and the amount of water of the mix. The effect of cracks existing near the post-installed reinforcement was also studied and it was concluded that bond strength is reduced in approximately 50%, not depending on crack width.

Reguengo (2010) experimentally tested several types of post-installed reinforcement sealed with grout. For what concerns this dissertation, a post-installed rebar was anchored to a concrete element, and the hole was sealed with Sika® grout. The hole measured 52mm in diameter and 200mm in depth. A pull-out rupture occurred, or a type two rupture, according to Miltenberg (2001).

As the maximum force obtained by Reguengo (2010) was 196,76kN. It is possible, through Equation 3.37 to calculate $f_{grout,s} = 15{,}6\text{MPa}$.

3.10.2 Dowel action

Experimental research conducted by Júlio et al. (2010) intended to analyze the difference in dowel action between post-installed reinforcement sealed with epoxy resin and reinforcement placed before casting. The test were performed on push off specimens, and the results demonstrated that the difference in shear resistance between specimens was very small. The obtained interface resistances were 3,8 and 3,9MPa, respectively for the post-installed and placed before casting connectors.

However, the expressions mentioned below were elaborated for cast in place dowels, so an eventual extrapolation to the case of post-installed dowels must be studied

Rasmussen experimental researches led to Equations 3.41 and 3.42, which may be used to describe dowel action (Leonardt & Monning, 1979). The following equations are used in the case when concrete rupture is not restricted (Figure 3.34). If concrete rupture is restricted, one must use different expressions.

$$P_u = 1{,}3\left(\sqrt{1 - 1{,}69e^2} - 1{,}3e\right)\emptyset^2\sqrt{\beta_p\beta_s} \tag{3.41}$$

When the distance $e \to 0$, Equation 3.41 becomes:

$$P_u = 1{,}3\emptyset^2\sqrt{\beta_p\beta_s} \tag{3.42}$$

Where,

$\emptyset$ is the diameter of the connector [cm]

β_s is the steel yield strength [kg/cm^2]

β_p is the concrete compressive strength [kg/cm^2]

e is the distance from the force's application point to the concrete element

P_u is the ultimate load [kg]

The connector must be anchored at a distance $l \geq 6\emptyset$.

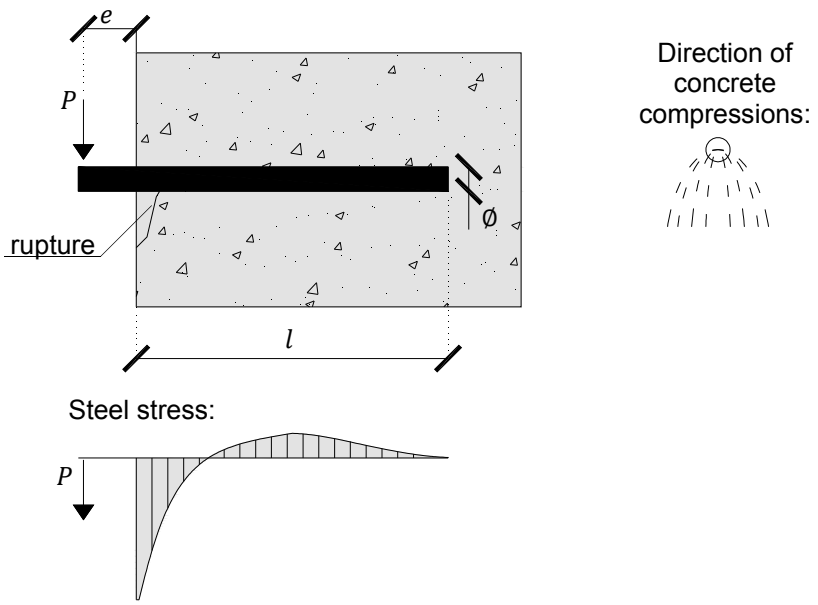

Figure 3.34: Dowel Action, adapted from Lenohardt and Monning (1979)

For dowels placed before casting concrete, according to MC90, the design value of the maximum shear force which may be transferred by a reinforcing bar crossing a concrete interface may be calculated by means of Equation 3.43, provided that the geometrical conditions displayed in Figure 3.35 are satisfied.

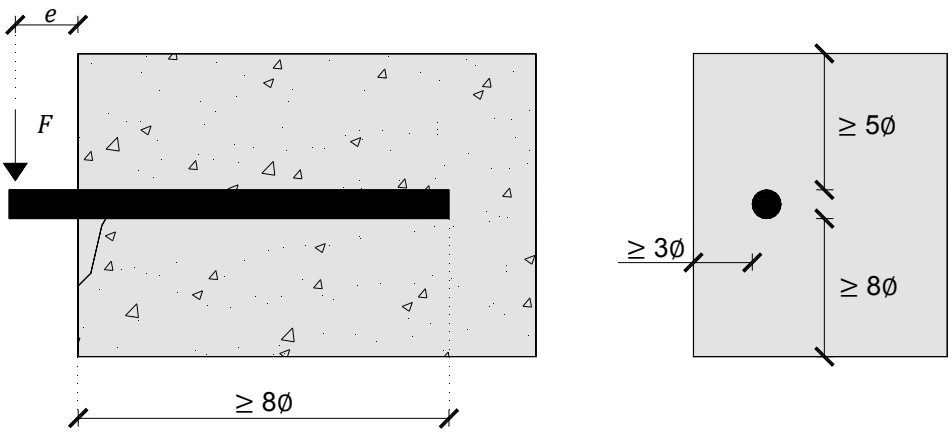

Figure 3.35: Geometrical conditions, adapted from MC90

$$F_{ud} = \frac{1{,}30}{\gamma_{Rd}} \emptyset^2 \left\{ \sqrt{1 + (1{,}3\varepsilon)^2} - 1{,}3\varepsilon \right\} \sqrt{f_{cd} f_{yd} (1 - \zeta^2)} < A_s f_{yd} / \sqrt{3} \qquad (3.43)$$

Where,

γ_{rd} is the supplementary partial coefficient, may be taken equal to 1,3

$\emptyset$ denotes the diameter of the dowel

A_s denotes the cross-sectional area of the dowel

f_{cd} is the design value of the compressive strength of concrete

f_{yd} is the design value of the steel yield stress

ζ $= \sigma_s / f_{yd}$(where σ_s is the simultaneous axial stress on the bar)

ε $= 3\, e / \emptyset_b \sqrt{f_{cd} / f_{yd}}$

e is the load eccentricity

Regarding the approach to dowel action in MC2010, the bending-resistance of a reinforcement or connector is approximated in function of the relative slips (Equation 3.44).

$$F(s) \approx F_{0,max} \cdot \left(\frac{s}{s_{max}} \right)^{0,5} = k A_{s,i} \sqrt{f_c f_y} \left(\frac{s}{s_{max}} \right)^{0,5} \qquad (3.44)$$

Where,

s_{max} is the slip when $F_{0,max}$ is reached. $s_{max} \approx 0{,}1 - 0{,}2 d_s$

k~1,6 for circular cross-sections, $C \leq C50/60$

$A_{s,i}$ is the area of reinforcement crossing the interface

f_c is the cylinder compressive strength of concrete under uniaxial stress

3.10.3 Interaction between dowel action and tension

As it was mentioned, the reinforcement crossing a rough interface is subjected to simultaneous bending and tension. Bending is related to a displacement parallel to the interface (slip) and tension is related to the opening and widening of an interfacial crack (due to roughness).

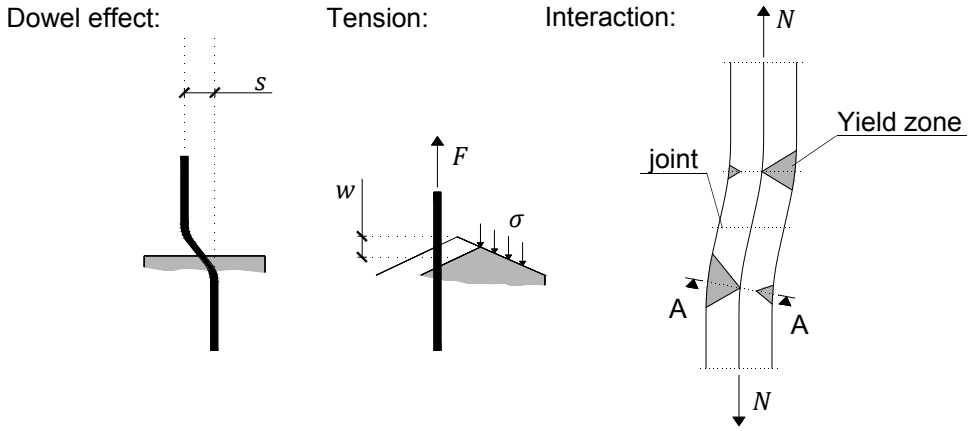

Figure 3.36: Interaction between dowel action and tension, adapted from MC2010 and Munger et al. (1997)

Interaction of tensile forces and bending leads to a reduction of the maximum possible dowel action, which is especially the case when surfaces are rough. The reduction of the shear strength can be approached, as described in MC2010, by multiplying $F_{0,max}$ with an interaction factor taking in to account the degree of utilization (κ). Dowel action with simultaneous tension is given by Equation 3.45.

$$F_{max} = F_{0,max} \cdot \sqrt{1 - \left(\frac{\sigma_s}{f_y}\right)^2} = F_{0,max} \cdot \sqrt{1 - \kappa^2} \tag{3.45}$$

Where,

κ is given by σ_s / f_y

σ_s is the tensile stress in the steel reinforcement

3.10.4 Minimum amount of reinforcement

Ideally, after adhesive bond failure, reinforcement resistance must be sufficient to bear the actual adhesive resistance, preventing the structural element to succumb to brittle failure, as the reinforcement will not be able to take up the loss of adhesive resistance completely. In EC2 the issue of brittle failure is not addressed. MC2010 already predicts (in section 6.3.5) a minimum amount of reinforcement. Equation 3.46 is adequate for beam members whereas Equation 3.47 should be used in the case of slabs.

$$\rho_{i,min} = 0{,}20\, f_{ctm} / f_{yk} \geq 0{,}001 \tag{3.46}$$

$$\rho_{i,min} = 0{,}12\, f_{ctm} / f_{yk} \geq 0{,}001 \tag{3.47}$$

Lenz and Zilch (2011) suggest estimating the reinforcement area with a design approach that involves separating the resistance components based on the required joint displacement. The maximum shear strength must be limited to either the mechanisms of adhesion/mechanical interlock or the reinforcement resistance. Reinforcement resistance should overcome adhesion.

3.10.5 Type of connectors

Several designs for connectors (Figures 3.37-3.41) are available. In order for the connectors to be effective, appropriate anchorage is necessary both in substrate and repair layer. In both practical examples mentioned in section 2.5 of this dissertation bent reinforcing bars crossing the interface were adopted.

Figure 3.37: Shear connectors

Figure 3.38: Dowel (Bianchi, 2007)

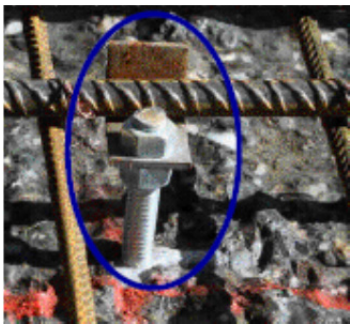

Figure 3.39: Dowel (Bianchi, 2007)

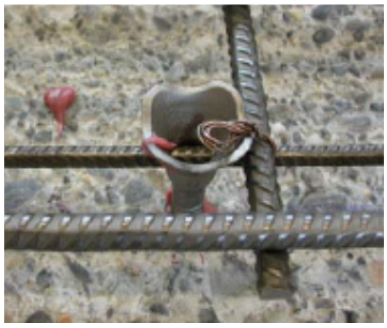

Figure 3.40: Hilti HCCB connector (Bianchi, 2007)

Figure 3.41: Connector with expansion (Santos, Shehata & Shehata, 2007)

3.10.6 Disposal of reinforcement crossing the interface

Debonding in RC overlays often begins near the edges of the new concrete layer. In this region, interface surface stresses (resulting from drying shrinkage) are higher, and the concrete may eventually be cracked before load is applied. Also, tension forces perpendicular to the interface, which are considered the main cause of debonding, are likely to develop in this region. Therefore appropriate edge reinforcement is recommended.

As mentioned, reinforcement is obviously required, for the development of resistance after adhesive bond failure. However, according to Randl and Zilch (2009) the installation of connectors is also time consuming and costly, so there is an interest in reducing the number of connectors crossing the interface, optimizing the disposal where the debonding is expected to start or higher stresses are predicted.

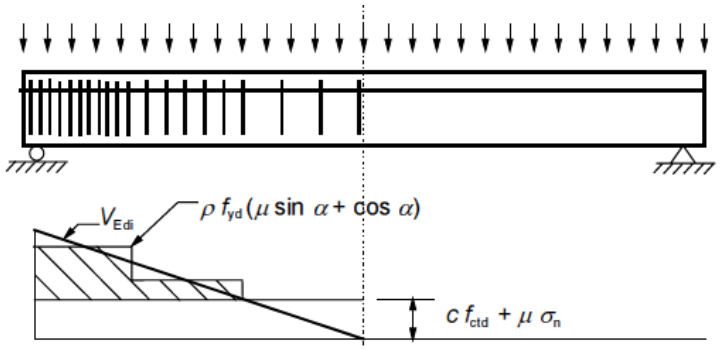

Figure 3.42: Shear diagram representing the required interface reinforcement (EC2)

Both MC2010 and EC2 allow for a stepped distribution of the transverse reinforcement, to be used as indicated in Figure 3.42. However in EC2 there is no reference to the fact that debonding would start in cracks and near the edges of the new concrete, and that in this area, a possible increase in reinforcement crossing the interface could improve the combined behavior of both layers.

In item 6.3 of MC2010 the fact that edge zones have to be sufficiently secured is already emphasized, and Equation 3.48 provides an upper limit to the maximum shear force to be expected along the edges of the new layer:

$$V_{Ed} = t \cdot b \cdot f_{ct,eff} \tag{3.48}$$

Where,

t is the thickness of the new concrete layer

b is the width of the interface

3.10.7 Anchorage of new longitudinal reinforcement

It is possible to calculate the length of a longitudinal reinforcement in the new concrete layer, resorting to Equation 3.35. However, due to practical aspects, in strengthening interventions, it is not always possible to respect the necessary anchorages. For instance, there might be some difficulties in respecting the anchorage length in a slab strengthened for positive bending moments with a RC overlay in the tension zone. When strengthening for negative bending moments, the main concern is related to how the rebars cross the column.

Another reason for the increase of anchorage near the interface perimeter is to assure that steel forces are transmitted to the substrate. Dowels at the edge of the new concrete layer might present a possible solution.

Some proposed anchorages for the longitudinal reinforcement are displayed in Figure 3.43.

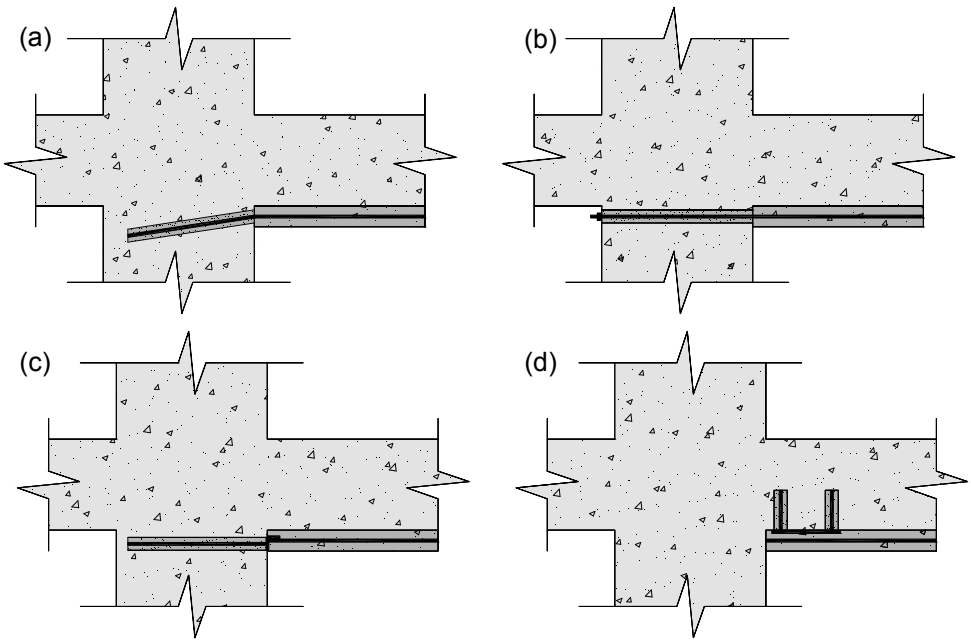

Figure 3.43: Different types of anchorage, adopted from Gomes and Appleton (1997). This example is in the context of strengthened concrete beams.

Figure 3.43 (a) illustrates the anchorage of longitudinal rebars into a hole in the column, filled with grout or resin. In Figure 3.43 (b) the rebar crosses the column and is fixed, either using threaded rebars, or with a mechanic system. The hole must also be sealed. In Figure 3.43 (c) and (d) the rebars are welded to metallic connectors that have been previously placed (Gomes & Appleton, 1997).

The tensile resistance of the post-installed reinforcement is given by Equations 3.36-3.40.

3.11 Flexural tests on reinforced concrete overlays

3.11.1 Santos et al

Santos, Shehata & Shehata (2007) investigated the structural behavior of beams strengthened for positive bending moments. Two beams were strengthened by means of a reinforced concrete overlay in the tension zone – V1R and V2R, shown in Figure 3.44 – and compared with two reference beams (non-strengthened) – Ref1 and Ref2. All beams were designed in order to ensure a flexural failure. Therefore, to avoid shear failure, sufficient shear reinforcement was placed. In the beams that were strengthened, the necessary bond area to prevent failure along the interface was calculated. In addition, crossing the interface, expansion connectors (Figure 3.41) were placed, in order to contribute with some resistance to shear. In Table 3.10 characteristics of the experimental beams are detailed.

The substrate beams of VR1 and VR2 had a similar amount of longitudinal steel to beam Ref1.

The dimensions of the strengthened beams and the calculation model are presented in Figure 3.44.

Table 3.10: Beam characteristics, adapted from Santos, Shehata & Shehata (2007)

Beam	f_{cm} (MPa)		d	d'	ρ	A_s	ρ'	A_s	ρ_{sw}	A_{sw}/s
	Value	age	[mm]	[mm]	[%]	[mm^2]	[%]	[mm^2]	[%]	[mm^2/m]
V1R	36,4	50	369	27	1,08	600 (3ϕ16)	0,18	100 (2ϕ8)	0,45	0,67 (ϕ8//15)
V2R	41,4	57	369	27	1,08	600 (3ϕ16)	0,18	100 (2ϕ8)	0,45	0,67 (ϕ8//15)
Ref1	41,4	36	369	27	1,08	600 (3ϕ16)	0,18	100 (2ϕ8)	0,45	0,67 (ϕ8//15)
Ref2	40,8	37	351	27	2,33	1230 (3ϕ16+ 2ϕ20)	0,19	100 (2ϕ8)	0,45	0,67 (ϕ8//15)

The length of the beams was 4500mm and the cross-section measured 150x400mm. They were simply supported with a 4000mm span. The beams that were strengthened originally had identical longitudinal reinforcement to the “Ref1” beam.

The new reinforced layer is characterized in Table 3.11. The contact area was calculated by the equilibrium between steel forces and overlay shear force, which is schematized in Figure 3.44.

$$l_{min} \cdot P_i \cdot \tau = F_{max} \tag{3.49}$$

The values of τ used to calculate the interface area were found in literature. The chosen contact section, P_i, allowed for a reduced amount of cross-section enlargement, and the minimum length.

Table 3.11: Strengthened beams, adapted from Santos, Shehata & Shehata (2007)

Beam	Dimensions [mm]				A_s [mm^2]	A_s [mm^2]	ρ [%]		Stirrups
	b	h	d	d'	(1)	(2)	(1)	(2)	
V1R	150	455	360	27	600 (3ϕ16)	300 (6ϕ8)	1,11	0,55	Φ5//150mm
V2R	150	455	377	27	600 (3ϕ16)	600** (4ϕ8+3ϕ16)	1,06	1,06	Φ5//150mm

(1)→Original Reinforcement; (2)→New reinforcement;

*f_{cm} of the new concrete layer in rupture: 32,5MPa V1R at 16days and 31,9MPa at 23 days

**600mm^2 do not correspond to the reinforcement described, this must be a typing error

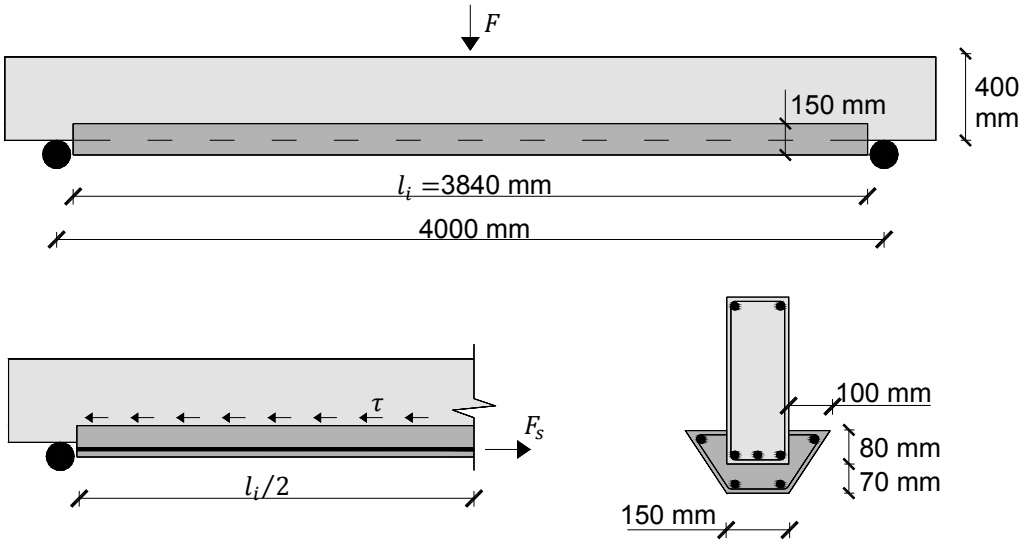

Figure 3.44: Strengthening model, adapted from Santos, Shehata & Shehata, (2007)

The beams were pre-cracked before the strengthening took place, and roughened by hand milling. A few moments before the cast was filled with concrete the surface was pre wetted with a sponge.

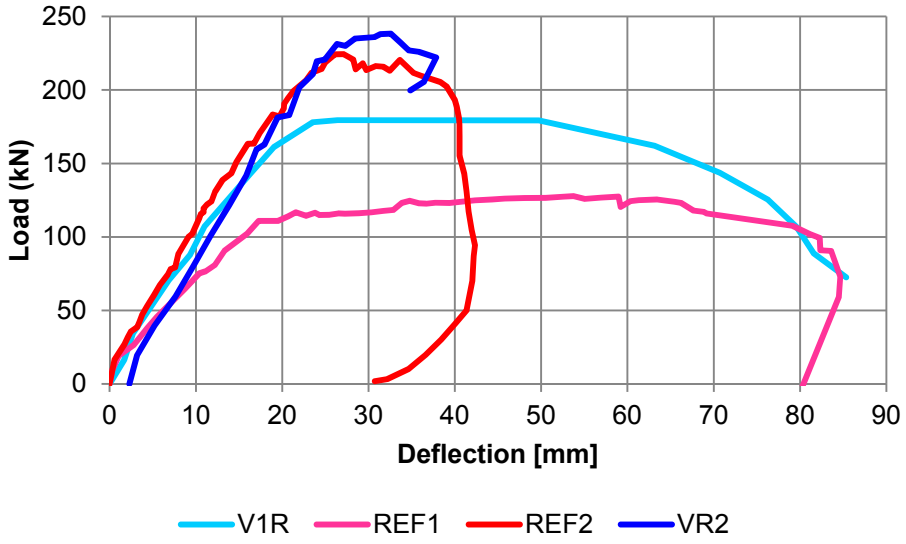

Figure 3.45: Load-displacement graph for the different beams (Santos, Shehata & Shehata, 2007)

The beams were subjected to a three point bending test. No cracking was observed in the interface zone and the deflections values, the rupture mode and ultimate load all indicate monolithic behavior. The tests showed that it is possible to significantly increase flexural strength by the concrete jacketing solution, provided that there is enough distance for shear transmission.

Chapter 4

Experimental program

4.1 General considerations

The aim of the present research is to analyze the behavior of strengthened beams under bending loads and the performance of the interface, in the context of structural rehabilitation. The beams had different types of reinforcement crossing the interface, which influenced the overall load bearing behavior, shear stress and failure mechanisms.

In the present chapter, the strengthening concept is presented, the experimental models are detailed and the test setup is described. The materials used in the beams conception are also characterized in terms of their mechanical properties.

The experimental program consisted on the creation and strengthening of nine beams (with a RC overlay), that were later subjected to bending tests. The original beams presented high resistance to shear, but a discontinuity in the longitudinal reinforcement at midspan imposed low resistance to bending. To increase the flexural resistance, new longitudinal reinforcement was placed on the tensioned side of the beams, and covered with a thin (60mm) concrete layer.

The strengthened beams were subjected to three point bending tests. To simplify the test setup, beams and tests were executed upside down. The shear load and bending moment diagrams are displayed in Figure 4.1.

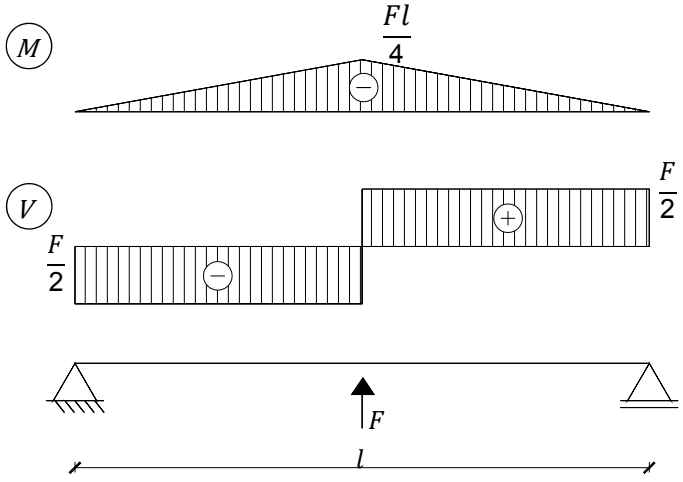

Figure 4.1: Bending moment and shear diagram

The concept was to establish a stress state that forced failure to occur at the interface. Consequently, it would be possible to quantify ultimate shear stress in that plane.

As mentioned in Chapter 3, as interfacial slip increases, the main contributions for the shear resistance of the interface are provided by different mechanisms. In SMI the only contribution for shear resistance is adhesion. In SMII and SMIII adhesion, mechanical interlock friction and dowel action, all contribute for shear strength.

Values for bond strength are extremely dependent on the stress state of the interface, so in order to relate the addition of steel reinforcement with adherence, strengthening model I was developed. With this model, a stress state similar to the remaining beams is recreated, except since no reinforcement crosses the interface, stress transfer relied solely on concrete-to-concrete adherence.

To quantify bond strength in tension, pull-off tests were performed. The goal was to compare bond strength in tension with values for bond strength that could be found in strengthened horizontal elements. Also, as concrete properties for each model are different it would be possible to compare the adhesions of the different specimens.

4.2 Characterization of the experimental models

The experimental models simulate simply supported concrete beams, strengthened for positive bending moments by means of a new concrete layer with embedded steel reinforcement. Since the beams were executed upside down, in reality the strengthening intervention intended to increase the resistance to negative bending moments.

The first phase of the experimental research consisted on the creation of nine substrate beams, with the particularity that the tensile reinforcement was interrupted at mid-span, thereby presenting very low resistance for negative bending moments. The substrate beam geometry is represented in Figure 4.2.

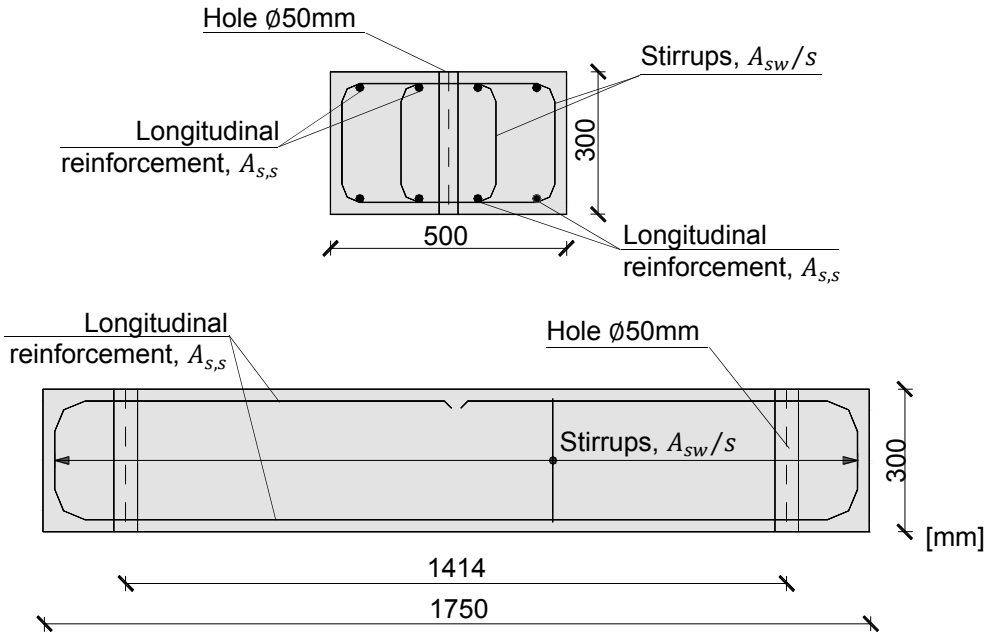

Figure 4.2: Geometry of the substrate beam

With the intention of increasing flexural strength, the beams were then strengthened by means of a RC overlay. The materials used in the overlay had identical properties to the ones used in the substrate. In the region where the new concrete would be placed, grooves were created in the substrate, using pneumatic hammers.

For each strengthening model, the concrete overlay is at least 60mm thick (roughness increases the height of this layer). Concrete covers measure approximately 20mm, so the effective depth of the new longitudinal reinforcement, d, is 332mm. All strengthened beams have identical longitudinal steel, with a reinforcement area, $A_{s,o}$ of 20,11cm^2. In Figure 4.3, SMI is represented.

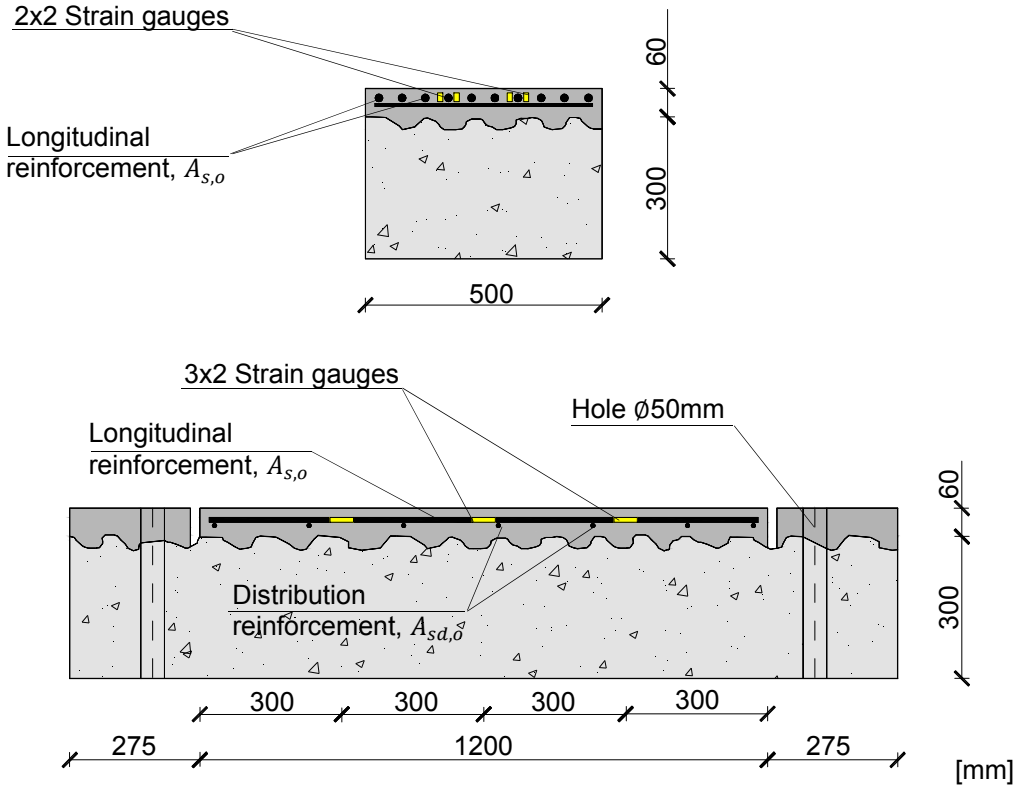

Figure 4.3: Geometry of strengthening mode I (SMI)

The choice of surface treatment is related to the fact that, using jackhammers to roughen concrete, can create a highly rough surface. Also, this treatment is common practice in many countries, mostly for economic reasons, and can be easily performed on site by ordinary workman.

However, jackhammering may introduce micro-cracks in the substrate that weaken the interface region. Although Rilem, (2011), points out hydro jetting and sandblasting as the best surface treatments regarding the performance of the bond, they can significantly increase the cost of the strengthening intervention.

Because roughness is one of the factors influencing results, it seemed important to provide some information about this parameter. Therefore, profile heights were measured on a 100x50mm grid. Description and values characterizing roughness can be found in Appendix A. The result was highly rough surface ($\overline{R_a}$ =3mm) – or considered indented according to the EC2 characterization.

Since at midspan there is a discontinuity in the substrate reinforcement, the bending resistance of the substrate is considered the one of the first crack. Any increase in bending resistance is considered to be provided by the strengthening solution

In the first strengthening solution (SM I, represented in Figure 4.3), stress transfer across the interface relied solely on the concrete-to-concrete capacity to transmit stress, as the overlay was simply cast against the roughened substrate, and no reinforcement crossed the interface. For SMI brittle failure with large debonding was expected, which would allow for a quantification of bond strength. This strengthening solution also acted as an indicator for eventual increases in bending resistance (and ultimate shear strength) provided by the post-installed reinforcement in SM II and SMIII.

As mentioned, SMII and SMIII were developed in order to analyze the contribution of two different types of reinforcement crossing the interface. The substrate was perforated for the reinforcement installation, and holes were sealed with *Sika® Grout*. Although failure across the interface was expected for the strengthening solutions with reinforcement crossing the interface, it was predicted a higher mobilization of flexural resistance.

In SM II, shear connectors were evenly distributed along the interface, as illustrated in Figure 4.4. Regarding SM III, the intention was to test the effectiveness of reinforcement crossing the interface concentrated near the edges, combined with the effect of an increase in anchorage length of the new reinforcement bars (Figure 4.5). The rebars were bent into an *L* shape, and anchored in the substrate (Figure 4.6). Although a more ductile behavior is expected, failure along the interface is still predicted for the beams of both strengthening models.

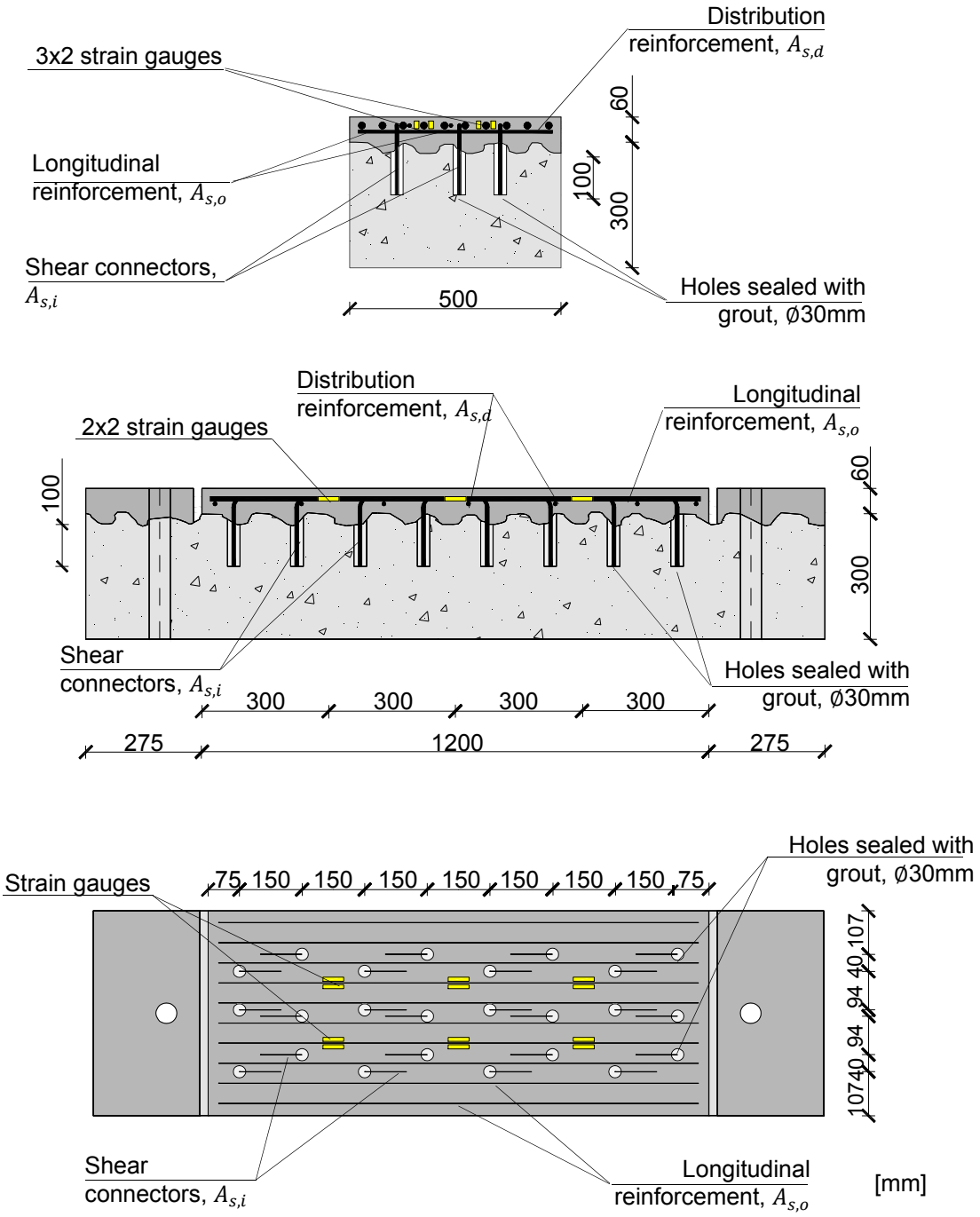

Figure 4.4: Geometry of strengthening model II (SMII)

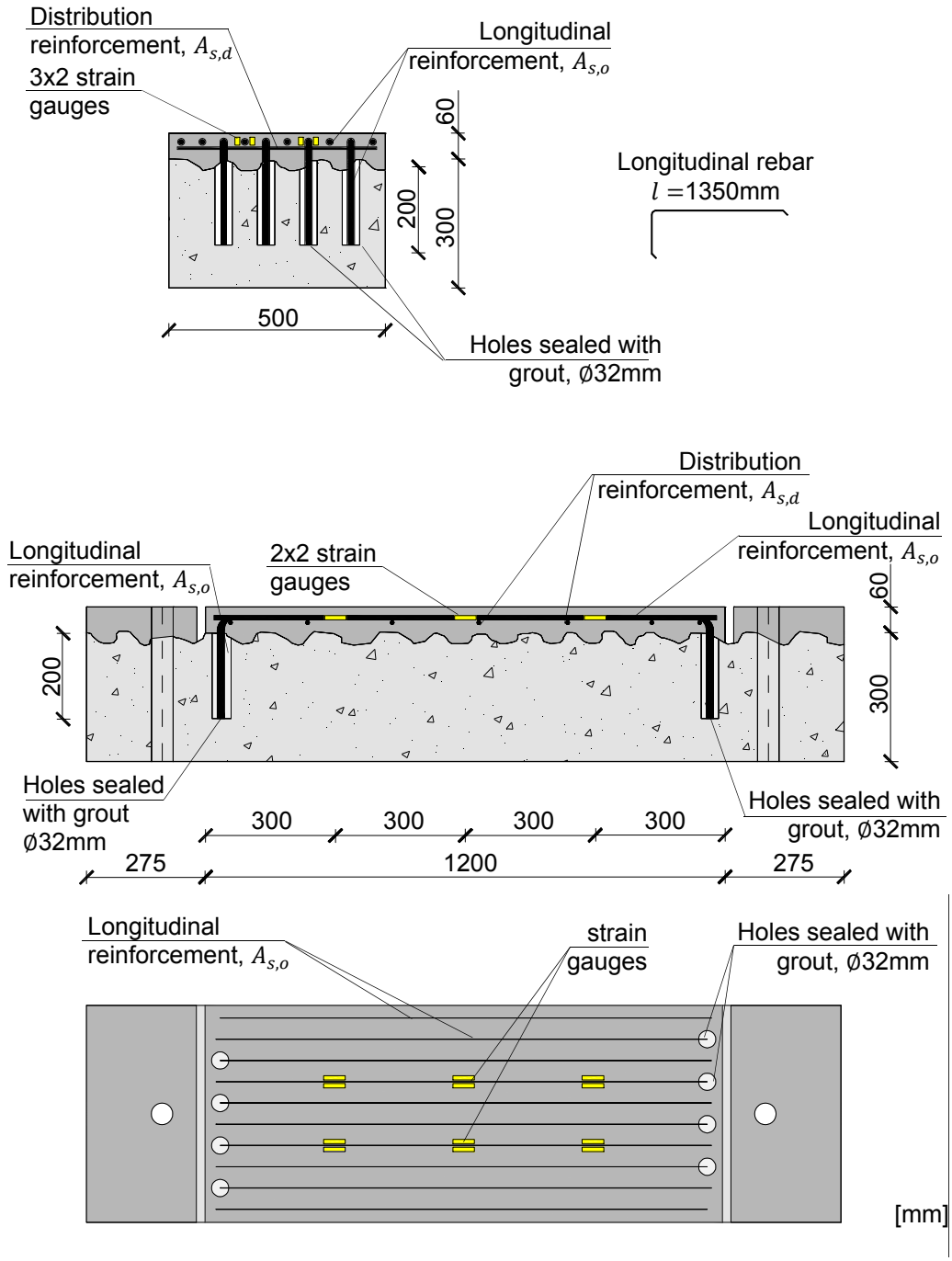

Figure 4.5: Geometry of strengthening model III (SMIII)

Figure 4.6: Instrumented L-shape rebar (used in SMI III)

For each model, three specimens, labeled A, B and C, were produced.

As mentioned, the following production steps were performed at the precast plant *CONCREMAT*:

1) The substrate reinforcement was prepared with regard to Figure 4.2 (see also Figure 4.7).
2) Because there was only one formwork available, the substrate beams were created at a rhythm of one a day. For each beam, three cubic specimens were kept, in order to evaluate concrete compressive strength. Shortly after it was poured, the concrete was compacted with a vibrator.
3) The substrate beams were kept in the formwork for at least 24h, and cured at exterior weather conditions, for at least 28 days.
4) The interface was roughened with pneumatic hammers that introduced grooves in the surface (Figure 4.10). For strengthening models II and III, holes were drilled into the substrate (Figure 4.11). Care was taken not to damage the substrate reinforcement during these operations. Interface heights were measured with a slide gauge in order to quantify roughness.
5) The reinforcement was prepared and strain gauges were attached to some rebars, as illustrated in Figure 4.10.
6) For models II and III, reinforcement crossing the interface was placed, as described:
    a. Holes were cleaned of dust and loose particles with compressed air and a wire brush (Figure 4.12).
    b. The substrate holes were sprinkled with water and eventual remaining superficial water was cleaned with a sponge
    c. Before the grout was poured, the holes were cleaned again with compressed air.
    d. Grout was poured, sealing the holes
    e. Reinforcement was installed shortly after the grout was poured (Figure 4.13)
    f. The grout was left to cure for three days
7) The interface surface that received the concrete overlay was cleaned of dust and loose particles with compressed air (Figure 4.14).
8) The remaining overlay reinforcement was placed onto the substrate beams.
9) The interface surface was previously wet and cleaned again. Superficial water was removed with a sponge.
10) The new concrete was poured and compacted. In SM I a concrete vibrator was used and three cubic specimens were kept. In models II and III, concrete was compacted in a vibrating table. Six cubic and cylindrical specimens were kept of the concrete used in the overlays of SMII and SMIII, in order to evaluate the relation between cubic and cylindrical compressive strengths.
11) The beams were left to cure at weather conditions for at least 28 days.

Figure 4.7: Interrupted longitudinal reinforcement (substrate)

Figure 4.8: Concrete placement

Figure 4.9: Concrete vibration

Figure 4.10: Roughening the substrate

Figure 4.11: Perforations for the post-installed reinforcement

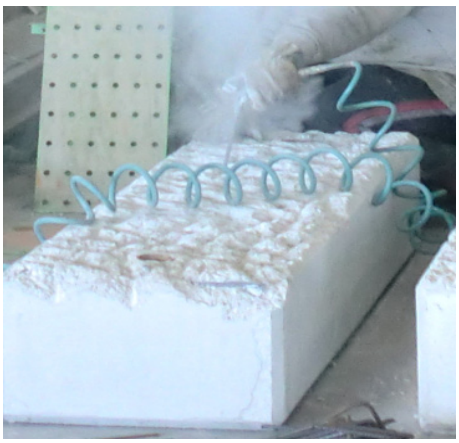

Figure 4.12: Cleaning the holes with compressed air

Figure 4.13: Post-installed reinforcement (SM II)

Figure 4.14: Cleaning the interface surface with compressed air

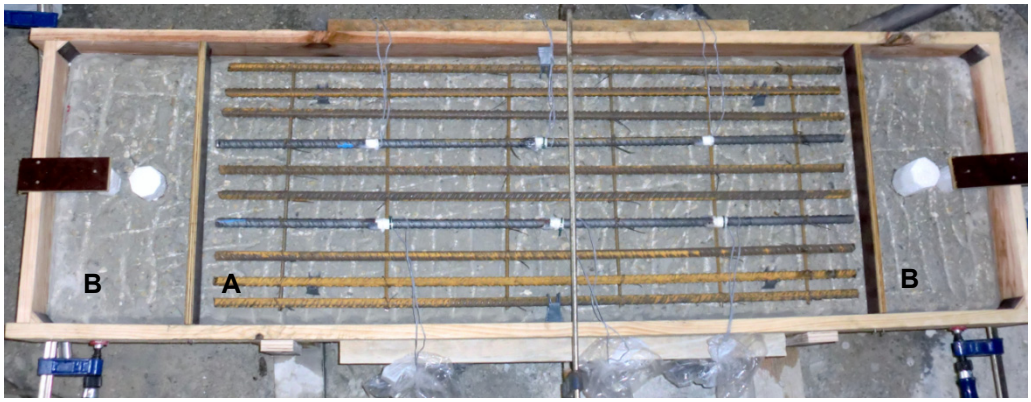

Figure 4.15: Reinforcement in the concrete overlay (SM I)

Two different zones were filled with concrete but kept separate, as illustrated in Figure 4.15. The area marked as “A” represents the RC overlay, and is responsible for the flexural strengthening of the slab. With no strengthening purpose, area B was also filled up with concrete. The purpose of this area was to carry out pull-off tests and evaluate adhesion. No longitudinal or crossing the interface reinforcement was placed in area B.

4.2.1 Substrate beam

The geometry of the substrate beam is represented in Figure 4.2.

Since the tension rebars are interrupted, the beam’s resistance to negative bending moments can be considered the one of the first crack, which is given by Equation 4.1.

Stirrups were placed along the beam in order to provide high resistance to shear.

The shear resistance of the substrate beam is described in section 6.2.3 of EC2. The design concept was to create high resistance to shear in the substrate, in order to avoid a shear failure of the composite beam and induce an interfacial failure mode. However, shear resistance is based on a struts and ties model, which in this case can only be completed with the overlay reinforcement, because of the interruption in the longitudinal rebars. Shear resistance is considered the minimum value between Equations 4.2 and 4.3.

$$M_{cr_{sub}} = \frac{bh_{sub}{}^2}{6} f_{ctm_{sub}} \quad (4.1)$$

$$V_{rd,s} = \frac{A_{sw}}{s} z f_{ywd} (cot\,\theta + cot\,\alpha)\, sin\,\alpha \quad (4.2)$$

$$V_{rd,max} = \alpha_{cw} b_w z v_1 f_{cd} / (cot\,\theta + tan\,\theta) \quad (4.3)$$

With,

$$v_1 = 0{,}6 \left[1 - \frac{f_{ck}}{250}\right],\ f_{ck} \text{ in MPa} \quad (4.4)$$

And, where,

A_{sw} is the cross-sectional area of the shear reinforcement

s is the spacing of between stirrups

α is the angle between shear reinforcement and the main tension chord

θ is the angle between concrete compression struts and the main tension chord

b_w is the minimum width between tension and compression chords

The reinforcement of the substrate is presented in Table 4.1.

Table 4.1: Substrate reinforcement

Longitudinal Reinforcement ($A_{s,s}$)	4Ø16	6,03 cm^2
Transversal Reinforcement (A_{sw}/s)	4 legs Ø8//0,10	20,12cm^2/m

4.2.2 Strengthening solutions

In order to increase overall flexural resistance, a new concrete layer of 1,2x0,5m, with embed longitudinal reinforcement was placed over the substrate.

The equilibrium between steel forces and shear stress adopted to determine shear stresses at the interface, which assumes shear stress to be constant, along $l_i/2$ is illustrated in Figure 4.16.

The relation between steel force and shear strength is given by Equation 4.5.

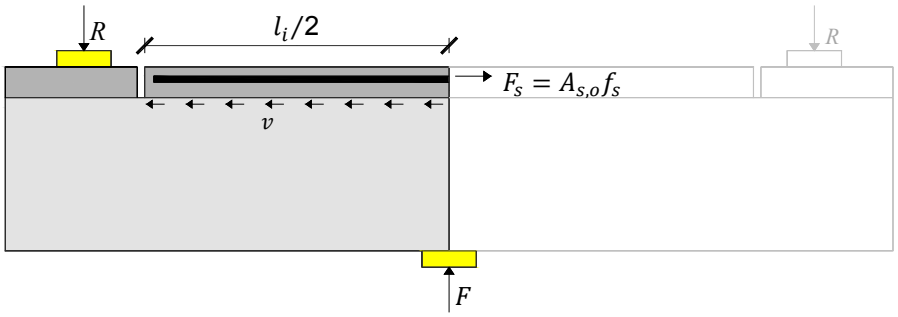

Figure 4.16: Equilibrium for shear transmission across the interface

$$\sum F = 0 \Leftrightarrow \frac{l_i \cdot b_i}{2} \cdot v = A_{s,o} f_s \tag{4.5}$$

Where,

b_i is the width of the interface, $b_i = 0{,}5$ m

l_i is the length of the interface, $l_i = 1{,}2$ m

$A_{s,o}$ is the area of longitudinal reinforcement in the overlay

f_s is the tensile stress

v is the stress transmitted along the interface, which is assumed constant

No debonding along the interface is expected to occur for a given stress value in the interface, $v_{ed,i}$, inferior to the interface resistance $v_{rd,i}$ (Equation 3.17).

If maximum steel stress is achieved, the stress transfer rate, or shear stress along the interface, would be given by:

$$v_{max} = \frac{2A_{s,o}f_{yk}}{l_i b_i} \tag{4.6}$$

However, the mentioned maximum steel stress is difficult to achieve, not only because of weaker interfacial properties, but also derived from the lack of stirrups around the new reinforcement. In addition, the fact that longitudinal steel does not have enough anchorage, and still needs to transfer tensile stresses to the substrate's interrupted longitudinal steel, presents more difficulties in achieving maximum steel stresses and the full bending capacity of the cross-section.

According to Gomes & Appleton (1997) the bending resistance of the composite cross-section may be considered:

$$M_{rd} = \gamma_M A_{s,o} 0{,}9 d f_{yd} \tag{4.7}$$

4.2.2.2 Strengthening model I (SMI)

The geometry of strengthening model I is represented in Figure 4.3. The reinforcement steel is shown in Table 4.2.

According to the MC2010 approach, the mechanisms responsible for stress transfer between the substrate and overlay materials are adhesive bonding and mechanical

interlock, which are referred to as τ_c. A "rigid" bond slip behavior is therefore expected.

As mentioned, strengthening model I was developed in order to analyze the contribution of the adherence between concretes in a stress state similar to SMII and SMIII. This is important because, when adhesion is lost, the main contribution for stress transfer is given by the reinforcement. Therefore this model can not only provide values for the interface resistance delivered by adhesion, but also works as an indicator of when the reinforcement crossing the interface becomes relevant in the resisting mechanism.

Table 4.2: Model I – overlay reinforcement

Longitudinal reinforcement ($A_{s,o}$)	10Ø16	20,11 cm^2
Distribution Reinforcement ($A_{sd,o}$)	Ø6//0,20	2,83 cm^2/m

4.2.2.3 Strengthening model II (SII)

The geometry of strengthening model II is represented in Figure 4.4 and the reinforcement steel is shown in Table 4.3.

Despite the fact that the addition of dowels may increase shear strength, full bending capacity is not expected to be achieved. Ultimate shear stress at the interface, considering both MC2010 and EC2 provisions is still expected to be caused by a load that is inferior to the one that would promote a flexural/shear monolithic failure.

A shear crack along the interface is expected, creating stress in the reinforcement crossing the interface. Dowels are expected to overcome the loss of adhesion and continue to resist, being subjected both to tension and bending.

Table 4.3: Model II – overlay reinforcement

$A_{s,o}$	10Ø16	20,11 cm^2
$A_{sd,o}$	Ø6//0,20	2,83 cm^2/m
$A_{s,i}$	24Ø8	12,06 cm^2

The adopted anchorage length for the post-installed reinforcement was 100mm, and took into account the limit imposed for dowel action in MC90, $l_b \geq 8\text{Ø}$ (Figure 3.35), as well as the failure mechanism for post-installed reinforcement under tension, described in item 3.10.1.2 of this document. In section 4.6.1 the maximum steel force in the post-installed reinforcement is calculated.

4.2.2.4 Strengthening model III (SMIII)

Strengthening model III geometry is represented in Figure 4.5 and the reinforcement steel is shown in Table 4.4.

The concepts related with the development of model III are an increase in anchorage length combined with crossing the interface reinforcement concentrated near the edges of the interface, where shear stress is larger, and tension perpendicular to the interface is likely to develop.

A crack along the interface is also expected to occur once adhesion is lost, transferring stress to the reinforcement crossing the interface.

Table 4.4: Model III – overlay reinforcement

$A_{s,o}$	10Ø16	20,11 cm^2
$A_{sd,o}$	Ø6//0,20	2,83 cm^2/m
$A_{s,i}$	8Ø16	16,08 cm^2

The adopted anchorage length for the post-installed reinforcement was 200mm. Anchorage length respected the limits for dowel action, however, it did not respect the limits for tension in the reinforcement, and failure between grout and concrete is expected (in section 4.6.1 this issue is presented in more detail).

Due to difficulties while drilling the holes in MIII.C, two anchorages did not respect the designed position. The difference in geometry of the anchorages is indicated in Figure 4.17.

Figure 4.17: Anchorage holes in specimen III.C

4.3 Test setup

4.3.1 Pull-off test

To determine bond strength in tension, pull-off tests were performed in area “B” (Figure 4.15).

Several cores with 45mm diameter were drilled on the top side of the beam. The cores distanced approximately one diameter from the edges of the overlay and from each other. As mentioned in section 3.3.2, it is required that the cores are drilled at least 10mm into the substrate. Since superficial treatment increased the depth of the new concrete layer, the depth of the cores reached about 80mm (coinciding with the reinforcement plane).

The 80 mm measure was marked in the drilling crown, and cores were dilled as exemplified in Figure 4.18.

Figure 4.18: Drilling the cores

The testing equipment, illustrated in Figure 4.19 and Figure 4.20, registers peak tensile stresses on a manometer for increases in loading. The readings admit a 50mm diameter core.

The test discs were attached to concrete with an epoxy glue (araldit®) that, according to the manufacturer, had a tensile resistance of 35 MPa. After the glue had hardened for about 24h, a bolt was attached to each disc, and the specimens were manually loaded at an approximately constant speed. Results were registered.

Figure 4.19: Test discs attached with an epoxy adhesive (*araldit*®) to the concrete

Figure 4.20: Pull-off test

4.3.1.1 Problems encountered while performing pull-off tests

A number of specimens experienced failure, in the interface plane while drilling the cores (Figure 4.21). Other subjects did not display a perceptive failure at that time, but when tested exhibited rather small tension stresses. Ruptures occurred between the substrate and the overlay.

Debonding while drilling the core and low adhesion values could be explained by some vibration introduced by the drilling crown, which might have cracked the concrete in the interface area. Also, the fact that the drilling depth coincides with the reinforcement plane in the substrate might create an extra plane of weakness in the bond between concrete and steel. However, this fact would not explain concrete debonding while drilling the core.

A possible explanation is that difficulties in drilling, accentuated by the reinforcement, may introduce extra vibrations in concrete and cause failure along the interface, or only in some regions.

Julio et al (2004) also describes debonding while drilling, in the situation where the pull-off test specimens were located in a concrete joint where the interface surface was left as cast.

For the purpose of this dissertation the test results are considered to have no meaning regarding the tensile resistance of the interface. Nevertheless, these results are shown in Appendix B.

Figure 4.21: Specimen that experienced debonding while drilling the core

Another test procedure was attempted, which involved the cutting of concrete into squared “cores” with a 50x50mm cross-section. Prismatic steel plates specially developed for this purpose would be glued to the concrete, and the test would be performed as described previously. However, while cutting the concrete, it was no longer possible to test the cores, since all had detached at the time they were cut.

4.3.2 Flexural test

As illustrated in Figures 4.22-4.25, the system simulated a simply supported beam to which a concentrated load was applied. The two supports consisted on 150x120x35mm steel plates, mechanically fixed to 26mm diameter threaded bars. The load was applied to the composite beams by a 200x200x50m steel plate connected to a hydraulic jack.

Figure 4.22: Flexural test setup

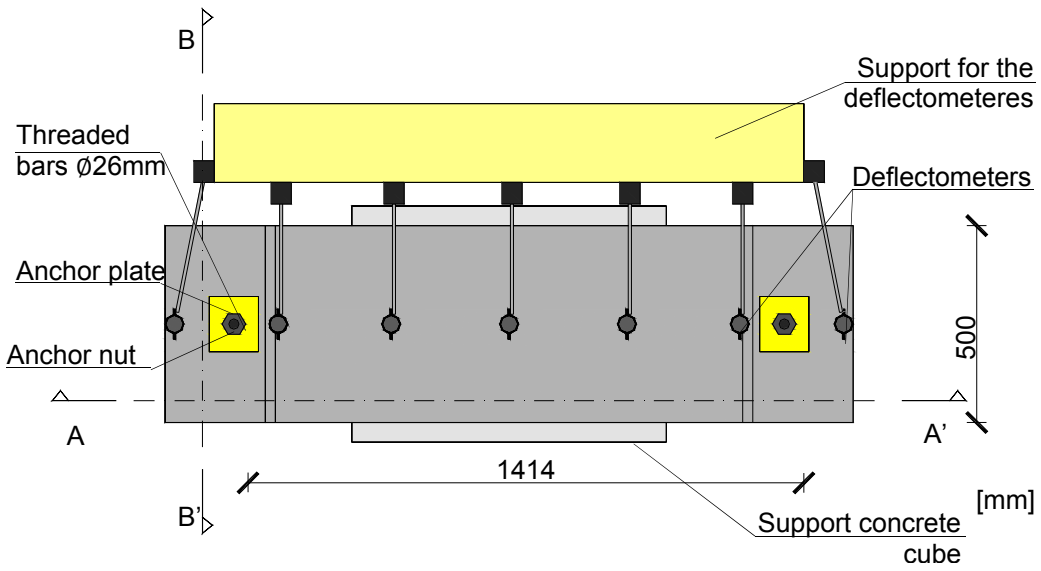

Figure 4.23: Test setup plan

As the flexural stiffness of the concrete beam (EI/l) is about 800 times greater than the flexural stiffness of the threaded bars (EI/l), the moment created by eventual bending of the threaded bars is relatively small and was considered null, validating support conditions.

During the tests on SMI a 600kN hydraulic jack was used (ENERPAC RCH603) that was manually controlled. For SMII and III, a 1000kN hydraulic jack was used (ENERPAC RRH1006), which was operated with an automatic pressure control unit.

The substrate was not submitted to any type of initial loads in order to simulate possible cracking caused by service loads.

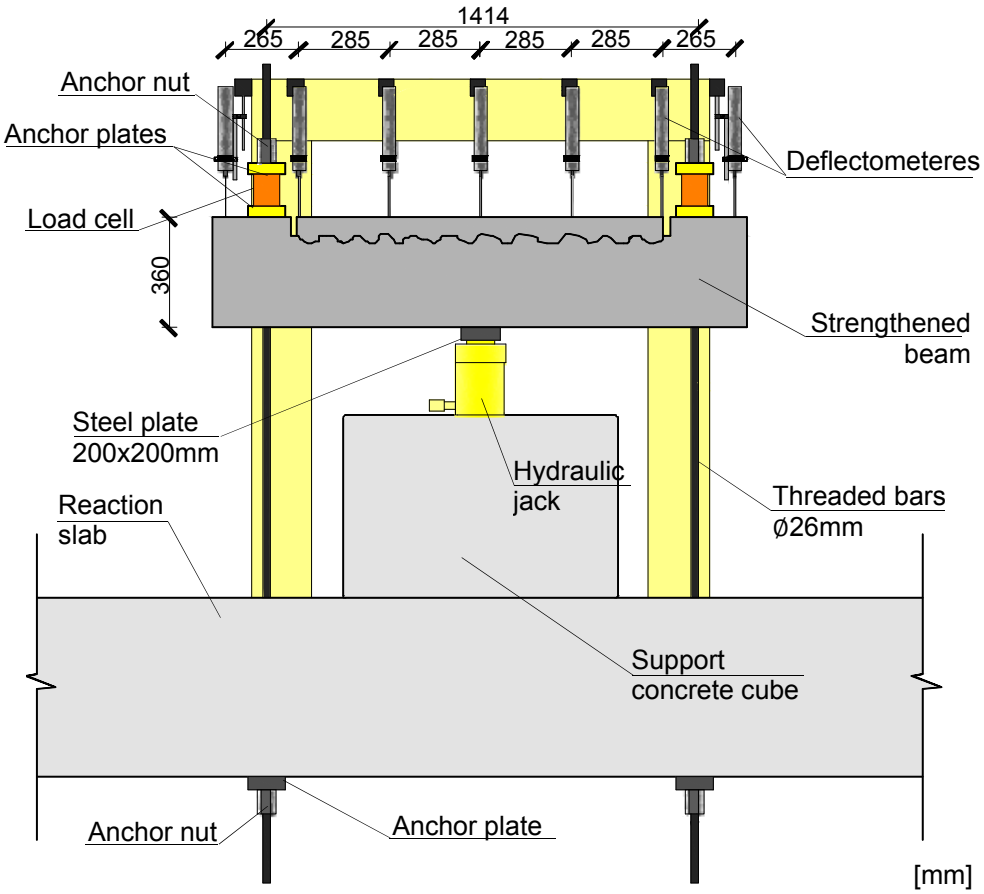

Figure 4.24: Test setup – AA' cross-section

During the experimental test several factors that could influence the results were monitored. The applied load and shear force, as well as deformation and steel strains in the overlay were measured.

Information about the vertical load applied by the hydraulic jack (Figure 4.26) and reaction values (shear force) was collected by two 300kN load cells installed between steel plates, as shown in Figure 4.27.

Vertical deflections in the overlay were measured by seven deflectometers, positioned as indicated in Figure 4.28. The deformations of the substrate might not accompany the deflections in the overlay, so this factor must be accounted for when analyzing results.

Strain gauges were attached on two of the longitudinal reinforcement bars, as illustrated in Figure 4.29, allowing for a quantification of steel strains. On each bar, six strain gauges were placed both at midspan and distancing 300mm from each end. Therefore it would be possible not only to calculate the maximum steel force, but also a rate for stress transfer between steel and concrete.

It would have been interesting to know steel strains in more locations. However, the employment of strain gauges is expensive and has a negative impact on the bond between steel and concrete.

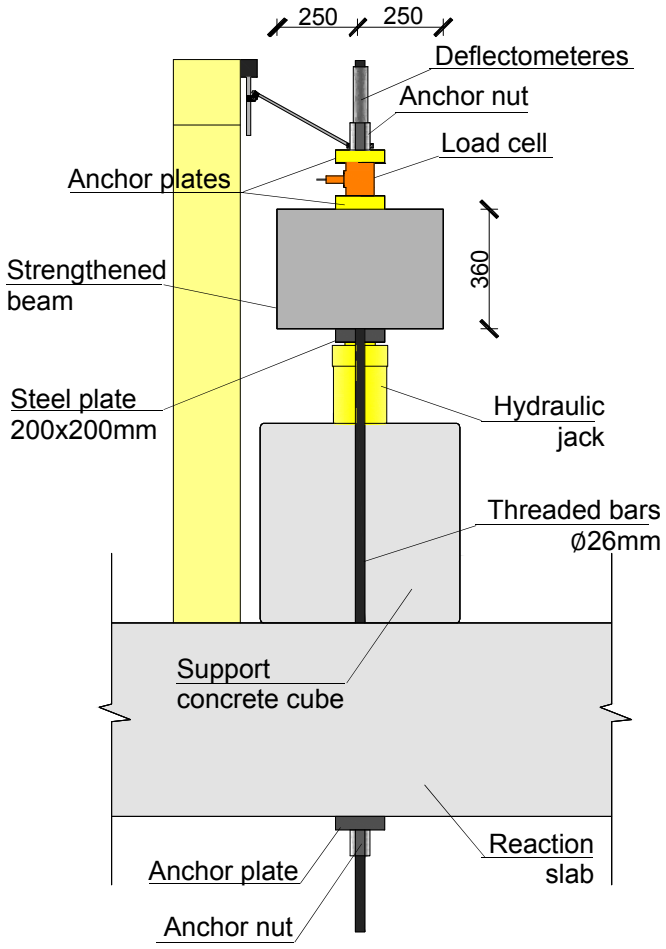

Figure 4.25: Test setup – BB' cross-section

Figure 4.26: Hydraulic jack

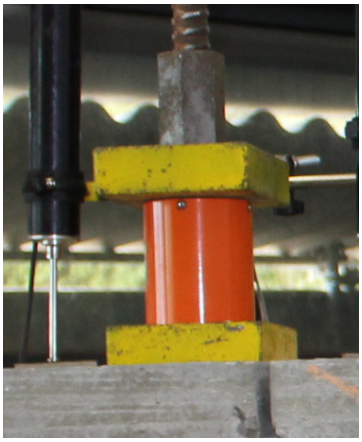

Figure 4.27: Load cell

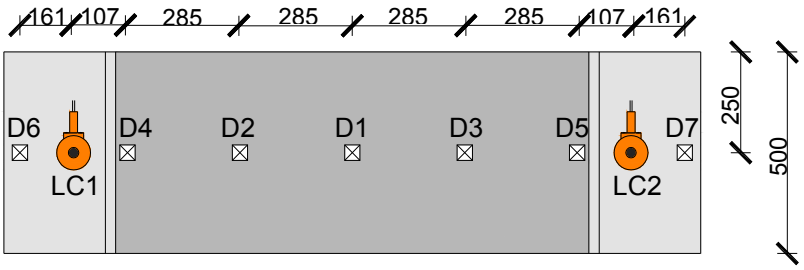

Figure 4.28: Load cells(LC) and deflectometer (D) location and nomenclature

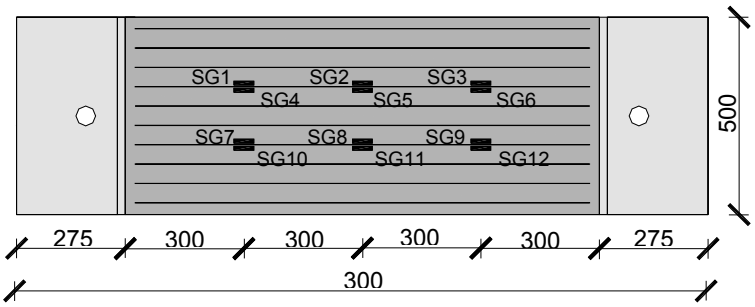

Figure 4.29: Strain gauges (SG) locations and nomenclature

For the application of the strain gauges, it was necessary to create a smooth area, which was achieved by careful grinding of the reinforcement ribs. The strain gauges were attached to the reinforcement with cyanoacrylate glue and impermeabilized with silicone (Figure 4.30 and Figure 4.31).

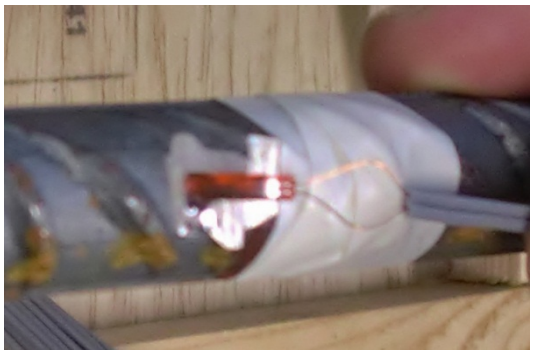

Figure 4.30: Strain gauges installation

Figure 4.31: Impermeabilized strain gauges

The instruments – two load cells, seven deflectometers and twelve strain gauges – were connected to 21 channels of the “Data Logger HBM Spider 8”, and results were saved for each half second (Figure 4.32).

Figure 4.32: Data aquisition system

4.4 Materials

4.4.1 Reinforcement

The adopted mechanical properties of the reinforcement are described in Table 4.5. For longitudinal reinforcement both in the substrate and overlay, 16mm diameters were used. The stirrups diameter was 8mm, as for distribution reinforcement in the overlay, $A_{sd,o}$ 6mm diameters were adopted.

Table 4.5: Mechanical properties

Steel	Yield strength, f_{yk} [MPa]	Ultimate strength, f_{tk} [MPa]	Elasticity modulus, E_s [GPa]
A500NR	500	550	200

4.4.2 Concrete

For each concrete production, at least three cubic specimens with standard dimensions (150x150x150mm^3) were kept and tested approximately at the time of the bending tests, which allowed for concrete characterization.

In order to compare the compressive strengths of cylindrical and cubic specimens, six concrete cylinders were also kept in the last concrete production.

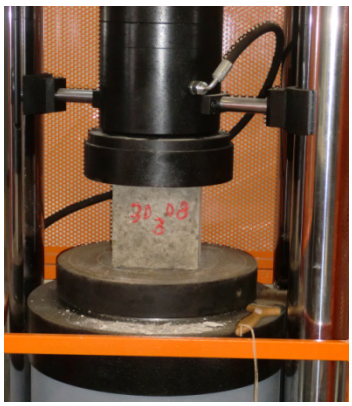

Figure 4.33: Concrete compression test

In Table 4.6, concrete is characterized in terms of its mechanical properties, obtained from compressive tests on cubic specimens.

$$f_{c,cm} = \frac{\sum f_{c,ci}}{n} \tag{4.8}$$

Where,

$f_{c,cm}$ is the average compressive strength, measured in cubic specimens

$f_{c,ci}$ is the measured compressive strength for each cubic specimen

The values for compressive strength in cylindrical specimens, f_{cm}, can be related to cubic specimens, taking in consideration the following relationship:

$$f_{cm} = 0{,}8 f_{c,cm} \tag{4.9}$$

The average tensile resistance, f_{ctm}, may be quantified by:

$$f_{ctm} = 0{,}3 f_{ck}^{2/3} \tag{4.10}$$

With,

$$f_{ck} = f_{cm} - 8 \text{ MPa} \tag{4.11}$$

The adopted value for the secant modulus of elasticity, E_{cm}, is given by:

$$E_{cm} = 22[(f_{cm})/10]^{0,3} \tag{4.12}$$

The value of the elasticity module was reduced in 10%, according to provisions for limestone aggregates, described in item 3.1.3 (2) of EC2.

Table 4.6: Stress characteristics for concrete

Concrete Production	specimen	age	$f_{c,ci}$ [MPa]	$f_{c,cm}$ [MPa]	f_{cm} [MPa]	f_{ctm} [MPa]	E_{cm} [GPa]
substrate I-A	1	105	28,5	29,1	23,3	1,8	25,5
	2		29,5				
	3		29,4				
substrate I-B	1	106	40,9	39,7	31,7	2,5	28,0
	2		41,7				
	3		36,3				
substrate I-C	1	101	30,4	29,6	23,6	1,9	25,6
	2		29,3				
	3		29,1				
substrate II-A	1	201	43,8	43,6	34,9	2,7	28,8
	2		42,3				
	3		44,6				
substrate II-B	1	200	50,6	51,5	41,2	3,1	30,3
	2		52,6				
	3		51,2				
substrate II-C	1	196	38,3	37,9	30,4	2,4	27,6
	2		36,5				
	3		39,1				
substrate III-A	1	208	35,8	36,9	29,6	2,3	27,4
	2		36,9				
	3		38,1				
substrate III-B	1	207	33,7	34,7	27,8	2,1	26,9
	2		33,2				
	3		37,2				
substrate III-C	1	199	47,6	47,1	37,6	2,9	29,5
	2		46,1				
	3		47,4				
overlay SM I	1	32	23,0[1)]	29,3	23,4	1,9	25,6
	2		29,2				
	3		29,3				

Note:[1)]This value was not considered (according to NP EN 206-1 item 8.2.1.2).

Table 4.7 presents compressive strengths of concrete cylinders of the overlay material from strengthening models II and III. The cylinders measured 150mm in diameter and 300mm in height. The relation between cubic and cylindrical compressive strengths in Equation 4.9 was obtained by comparison of compressive strength regarding cubic and cylindrical specimens of concrete produced for the overlays of models II and III.

Table 4.7: Compressive strength for the cylindrical specimens (concrete used in overlays of SMII and SMIII)

concrete production	specimen	age (days)	f_{ci} [MPa]	f_{cm} [MPa]	f_{ctm} [MPa]	E_{cm} [GPa]
overlay SM II and SM III	1	46	46,5	44,6	3,31	31,0
	2		43,3			
	3		41,9			
	4		44,9			
	5		43,8			
	6		47,0			

The design compressive and tensile strengths, in EC2 and MC2010, are respectively given by:

$$f_{cd} = \alpha_{cc}\, f_{ck}/\gamma_c \tag{4.13}$$

$$f_{ctd} = \alpha_{ct}\, f_{ctk_{0,05}}/\gamma_c \tag{4.14}$$

Where,

α_{cc} is a coefficient taking account of long term effects on the compressive strength and unfavorable effects resulting from the way the load is applied. The recommended value in EC2 for $\alpha_{cc} = 1$.

α_{ct} is a coefficient taking account of long term effects on the tensile strength and unfavorable effects resulting from the way the load is applied. The recommended value for $\alpha_{ct} = 1$.

f_{ck} $f_{cm} - 8$ [MPa]

$f_{ctk_{0,05}}$ $0{,}7 \cdot f_{ctm}$

f_{ctm} $f_{ct} = 0{,}3 f_{ck}^{2/3}$

γ_c is the partial safety factor for concrete, $\gamma_c = 1{,}5$

4.4.3 Grout

Sika® grout was used for sealing the post-installed reinforcement holes. According to the manufacturer, properties are described in Table 4.8. The adherence to steel reinforcement provided by the manufacturer is proximate to the one obtained experimentally by Reguengo (2010).

Table 4.8: Grout properties provided by the manufacturer

Adherence to steel reinforcement	Compressive strength
15 MPa	57,5~63,8 MPa

As no information was provided regarding the bond between grout and concrete, design value $f_{grout,c} = 2{,}7$ MPa was adopted.

4.5 Minimum amount of reinforcement crossing the interface

Steel must be able to take up the shear load after the loss of adhesion. Therefore, the adopted amount of reinforcement was superior to the provisions of MC2010.

Table 4.9: Minimum amount of reinforcement crossing the interface (Equation 3.46) compared with the adopted reinforcement

Beam	II.A	II.B	II.C	III.A	III.B	III.C
$\rho_{i_{min}}$ [%]	0,108	0,124	0,095	0,093	0,088	0,115
$\rho_{i_{adop}}$ [%]	0,201	0,201	0,201	0,268	0,268	0,268

The ratio for the adopted amount of reinforcement, $\rho_{i_{adop}}$, is given by:

$$\rho_{i_{adop}} = \frac{n \cdot \pi \emptyset^2}{4A_i} \tag{4.15}$$

Where,

n is the number of concrete rebars crossing the interface, (for SMII, $n = 24$ and for SM III $n = 8$)

$\emptyset$ is the diameter of the rebar

A_i is the area of the interface

4.6 Resistance of the post-installed reinforcement

4.6.1 Maximum tension force in the reinforcement

Maximum tension forces in the reinforcement were determined through Equations 4.16-4.19. Tensile resistance of post-installed reinforcement is represented in Table 4.10.

$$F_{r,1} = A_{s,i} \cdot f_{yk} \tag{4.16}$$

$$F_{r,2} = \emptyset \cdot h_{ef} \cdot f_{grout,s} \tag{4.17}$$

$$F_{r,3} = \pi \cdot d \cdot h_{ef} \cdot f_{grout,c} \tag{4.18}$$

Where,

$\emptyset$ is the diameter of the reinforcement crossing the interface, 8mm and 16mm for SMII and SMIII, respectively

h_{ef} is the anchorage length of the reinforcement, 100mm and 200mm for SMII and SMIII, respectively

d is the diameter or the hole in the substrate, 30mm and 32mm, for SMII and SMIII, respectively

To determine the force that causes a conic shaped failure mode, the design value for the concrete compressive resistance, f_{cd} was used (Equation 4.13). Since the force necessary to create this failure mode is higher than the other failure modes, maximum tension in the reinforcement will not be related to $F_{r,4}$.

$$F_{r,4} = 12{,}5 f_{cd}^{0,5} \cdot h_{ef}^{1,5} \quad (4.19)$$

Table 4.10: Resistance of a tensioned post-installed reinforcement (Equations 4.16-4.19)

Model		SMII			SMIII	
$F_{r,1}$[kN]		25,1			100,5	
$F_{rd,2}$[kN]		37,7			150,8	
$F_{rd,3}$[kN]		25,4			54,3	
$F_{rd,4}$[kN]	II.A	II.B	II.C	II.A	II.B	II.C
	52,9	58,8	48,3	134,0	128,3	157,2

For a SMII tensioned reinforcement bar (Ø8mm), failure can occur in two possible modes (Mode 1 and 3 – also because the value of $f_{grout,c}$ might not be realistic).

For a SMIII tensioned rebar (Ø16mm), failure is expected to occur at the connection between grout and concrete ($F_{rd,3}$). The necessary anchorage length in the substrate would have been $l = 0{,}37$ m. However, this value seemed unrealistic both for the experimental models developed in the present research, and for in situ applications. Therefore an anchorage length of $l = 0{,}20$ m was adopted and rupture in tension is expected to be at the bond between concrete and grout.

4.6.2 Dowel action in the reinforcement

Rasmussen expression (Equation 3.42) can be used to calculate dowel action in the reinforcement. It would also be interesting to compare the effect of pure dowel action with the predictions of MC90 and MC2010 that take in account simultaneous tension in the reinforcement. However, as no strain gauges were placed in the dowels, it is not possible to account for the parameter ζ (Eq. 3.43).

Equation 3.42 approximates the resistance of a single dowel, $V_{rd_{dowel}}$. To determine the resistance of the dowels placed along the interface and somehow compare with the obtained shear resistance, the parameter $v_{rd,i_{dowel}}$was determined, according to the following equation:

$$v_{rd,i_{dowel}} = \frac{V_{rd_{dowel}} \cdot n}{l_i \cdot b} \quad (4.20)$$

Where,

$V_{rd_{dowel}}$ is the resistance of a single dowel, obtained through equation 3.42

n is the number of dowels crossing the interface

l_i is the length of the interface, in this case 1,20m

b is the width of the interface, which is 0,5m

Equation 4.20 is proportional to the last parcel of Randl's expression and the provision for shear resistance for interfaces connected by dowels of MC2010 (respectively, Equations 3.19 and 3.24 of this dissertation).

Table 4.11: Resistance of a single dowel (V_{rd}) and of the interface ($v_{rd,i}$)

Specimen	II.A	II.B	II.C	III.A	III.B	III.C
f_{cm} [MPa]	34,9	41,2	30,4	29,6	27,8	37,6
f_{yk} [MPa]	500					
∅ [mm]	8	8	8	16	16	16
$V_{rd_{dowel}}$ [kN]	11,0	11,9	10,3	40,5	39,2	45,7
$v_{rd,i_{dowel}}$[MPa]	0,44	0,48	0,41	0,54	0,52	0,61

The obtained values for the shear resistance, in what concerns the mechanism of pure dowel action, are quite low, however, when combined with the other resisting mechanisms (namely friction and mechanical interlock) the expected result is much higher.

The value of $v_{rd,i_{dowel}}$can be compared with the shear stress along the interface, if maximum steel stress is considered (Equation 4.6), which is equal to 3,35 MPa.

Chapter 5

Results and discussion

5.1 General considerations

In this chapter, test results are exhibited and analyzed. The values for the maximum load and bending moment are presented, in addition to the progressions in strain and vertical displacements with increasing load.

As expected, all beams had failure modes associated with the interface and SMIII exhibited the best results regarding maximum load.

Both the experimental shear resistances and their expected values are determined and compared with each other. With results of SMI it is possible to isolate the influence of adhesion, and compare this parameter with the concrete compressive strength. The influence of reinforcement crossing the interface, equally distributed in the interface area or concentrated in the edges of the new concrete layer is also demonstrated.

The expected values for the cracking load are determined, assuming that when the first crack is formed, the slip between substrate and interface is negligible and strain distribution is linear. This expected value is compared with two possible approaches that can be used to determine the cracking moment.

A comparison between the different strengthening solutions is also presented.

5.2 Experimental results

In Figure 5.1, the maximum loads applied to the beams, F_{max}, estimated from the reaction values measured in the load cells, are displayed. It is visible that a significant improvement of the overall load bearing capacity was accomplished with the connectors' solution (SMII) and with the anchorage of the ends of the new longitudinal reinforcement (SMIII).

It is also noticeable that, for SM I, the compressive strengths of the substrate might be the variable influencing the results, as this is the main parameter that was different between specimens (the compressive strength of concrete was kept constant in the overlays of each model). This observation is in agreement with design code expressions, which relate the influence of adhesion solely with roughness and the compressive (or tensile) concrete strengths (section 3.5).

Other variables that influence results might outcome from differences in roughness and concrete vibration. Small eccentricities in the test setup could also lead to differences in results.

The relation between concrete strength and overall bending resistance is not clear for specimens of SMII and SMIII, as after the loss of adhesion, the main contribution for stress transfer across the interface is provided by the reinforcement.

In strengthening model III, the difference in results could be explained due to small differences in the geometry of beam III.C. Also, during the test of this beam, the hydraulic jack lost pressure before the beam reached failure, and it was necessary to load in two cycles.

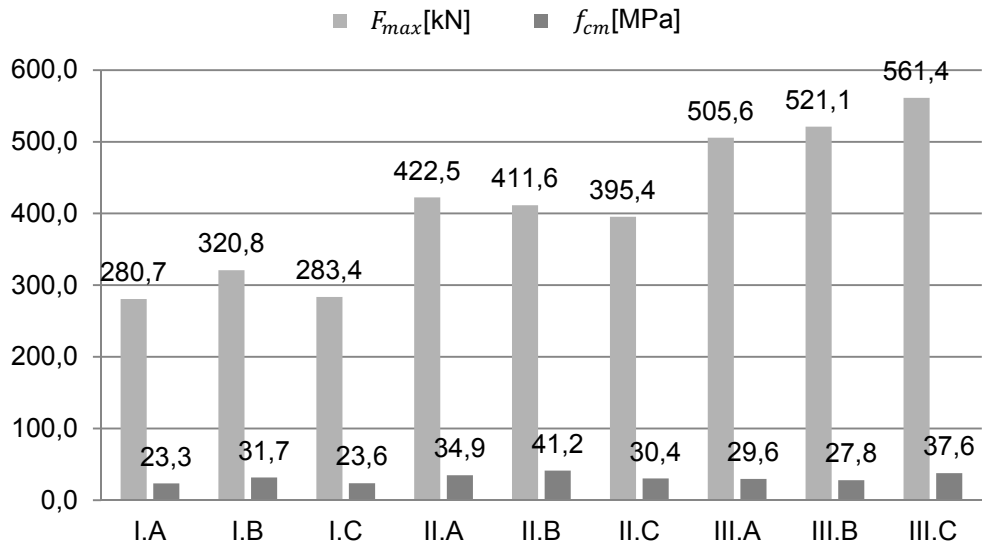

Figure 5.1: Maximum load and substrate concrete compressive strength (cylinders)

5.2.1 Strengthening model I

5.2.1.1 Description of the failure mode

As expected, all three beams with no reinforcement crossing the interface experienced brittle failure, with large debonding, that always began in one of the beam's sides.

As the beams were loaded, the first crack observed corresponded to a midspan flexural crack. The only other type of cracking visible before failure were two shear cracks that were formed in the substrate, near both supports.

Shortly after the appearance the shear cracks, the new RC layer suddenly detached from the substrate, with no indication given of failure. Debonding always started at the intersection of the secondly formed shear crack and the interface, and progressed along the interface plane until reaching midspan, where the gap in reinforcement existed. Then the crack took the path of the flexural midspan crack (see Figures 5.2 and 5.3).

Little deformation and steel strains were associated with this failure mode. No crack along the interface was detected prior to debonding, which suggests that failure occurred simultaneously with the appearance of a crack along the interface. In the side that did not experience interface failure, no crack along the interface was detected.

After failure, several small cracks were visible in the substrate concrete, just under the interface (Figure 5.3). This type of failure is consistent with the creation of tension

perpendicular to the interface, near the supports, which in this case also corresponds to the end of the strengthening layer.

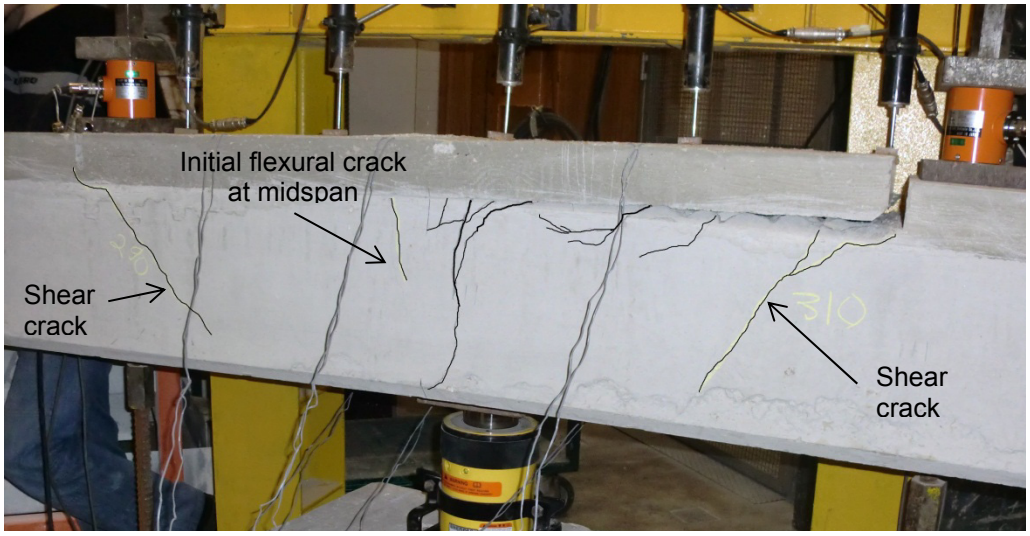

Figure 5.2: Failure mode for specimen I.B (cracks are highlighted)

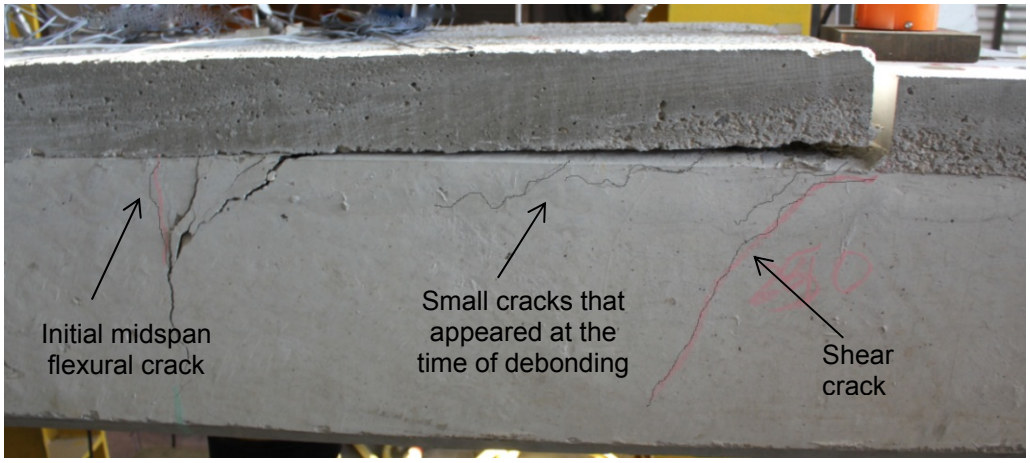

Figure 5.3: Failure mode for specimen I-A (with some highlighted cracks)

5.2.1.2 Measured strains and deflections

Deflections and steel strains were measured in all three tests. For each beam of this particular model, rather small deflections prior to debonding were measured (inferior to 2mm). Therefore, it does not seem relevant to display deflection values. The low values for deflections are related the fact that the beams are very rigid; consequently experiencing little deformation prior to failure.

The evolution in steel strains along the steel reinforcement is presented in Figures 5.4-5.6. The points in the graph correspond to known steel strains (at the end of the steel bars, strains were considered null). The lines joining the known points assume that stress transmission is constant between points.

Regarding the evolution of steel strains (and consequently steel stresses) with increasing load, the strain distribution doesn't always progress at a constant rate. At first, steel is more stressed in the midspan region, where the bending moment is higher. However, just before failure, the slope of the lines joining known strain points becomes approximately constant (Figures 5.4-5.6).

From this results, the consideration of an uniform distribution of shear stress (constant shear strength, $v_{rd,i}$), provided by adhesion seems realistic. The only exception rests on the left side of Figure 5.6 where steel strains (Gauges 3-6-9-12) just before failure, present a small difference in the slope. An explanation can be related to the fact that steel tension along a tensioned rebar embed in concrete is not constant. Therefore the measured strains will vary if the strain gauge is located in a crack or in between cracks.

In Figures 5.7-5.9 it is possible to see the development in steel extensions with increasing load. It can clearly be observed that, as load increases, the initial steel response to load is approximately linear. After reaching a certain threshold value, steel becomes increasingly stressed, and the increment in load loses the initial rate. The latter threshold value is the cracking load, F_{cr}, which indicates the load for which concrete tensile resistance is exceeded, and steel becomes relevant in the load bearing capacity of the element.

Usually the cracking moment, M_{cr} is used to quantify this stage. Given the bending moment diagram for a simply supported beam with a concentrated load at midspan (Figure 4.1), obviously, this moment is reached first at midspan (Gauges 2-5-8-11) and progresses towards the edges with increasing load. This can be observed, namely in the load-steel strains curve of specimen I.C (Figure 5.9). Steel becomes more stressed first in Gauges 2-5-8-11 (midspan). At a much higher load, both Gauges 1-4-7-10 and 3-6-9-12 experience a virtually instantly increase in strains, for the same load.

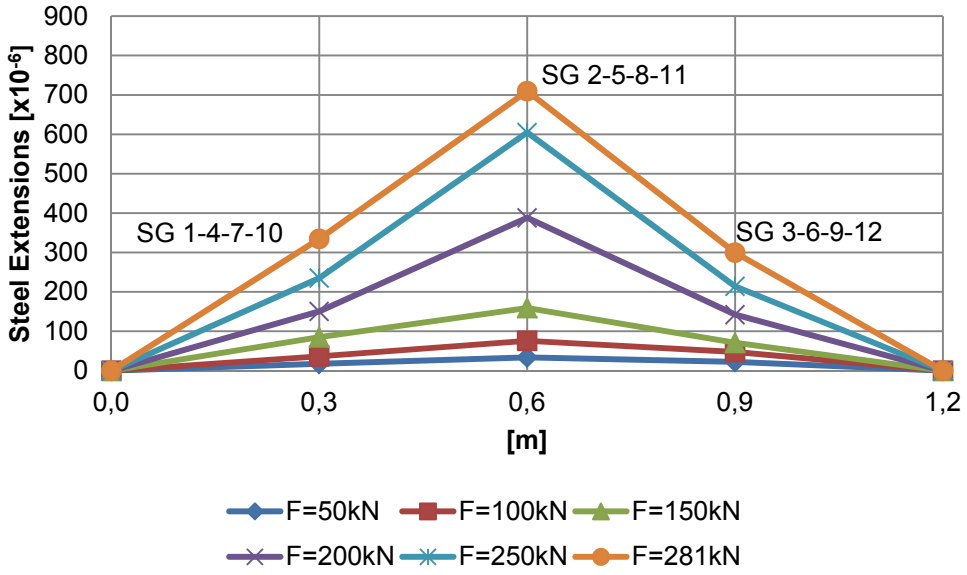

Figure 5.4: Specimen I.A – Evolution in steel strains. Failure along the interface occurred in the left side of this graph

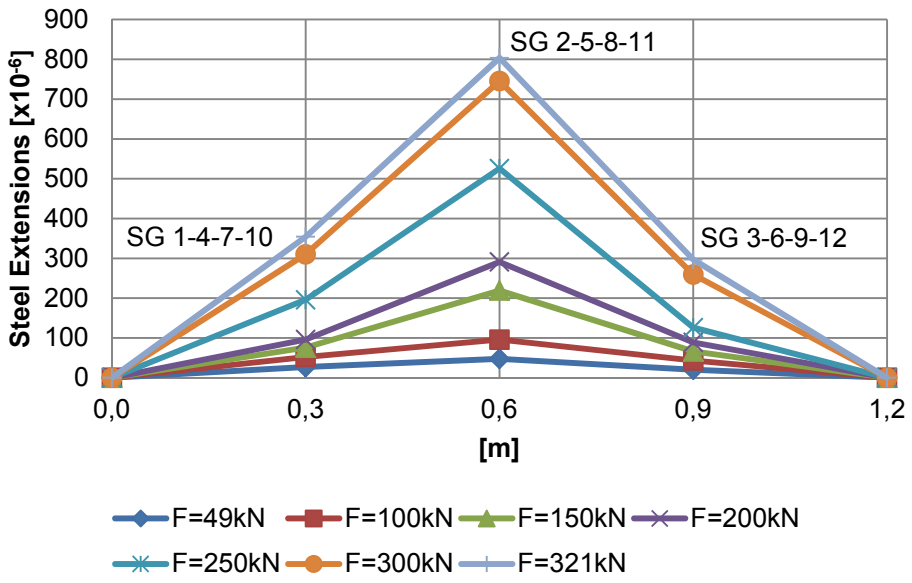

Figure 5.5: Specimen I.B – Evolution in steel strains. Failure along the interface occurred in the left side of this graph

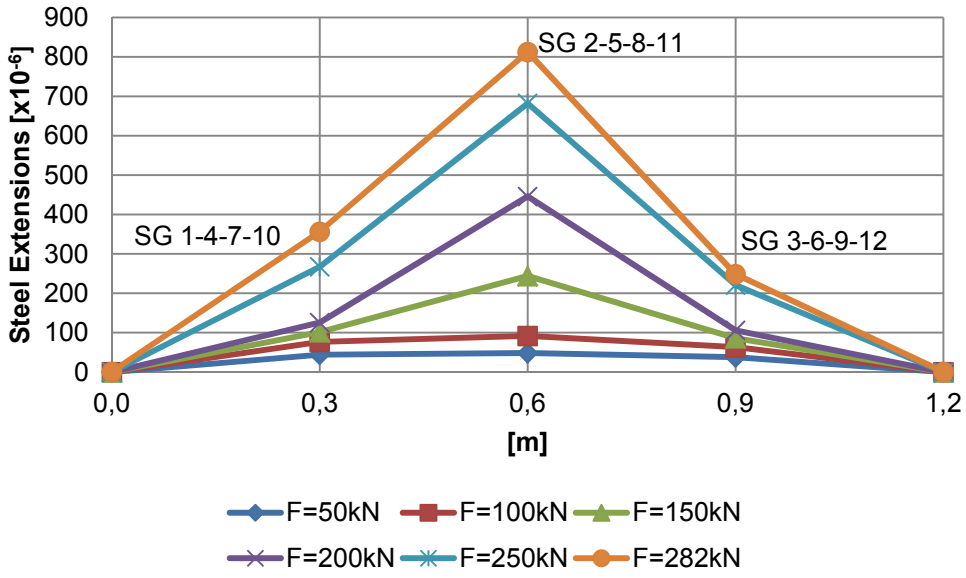

Figure 5.6: Specimen I.C – Evolution in steel strains. Failure along the interface occurred in the right side of this graph

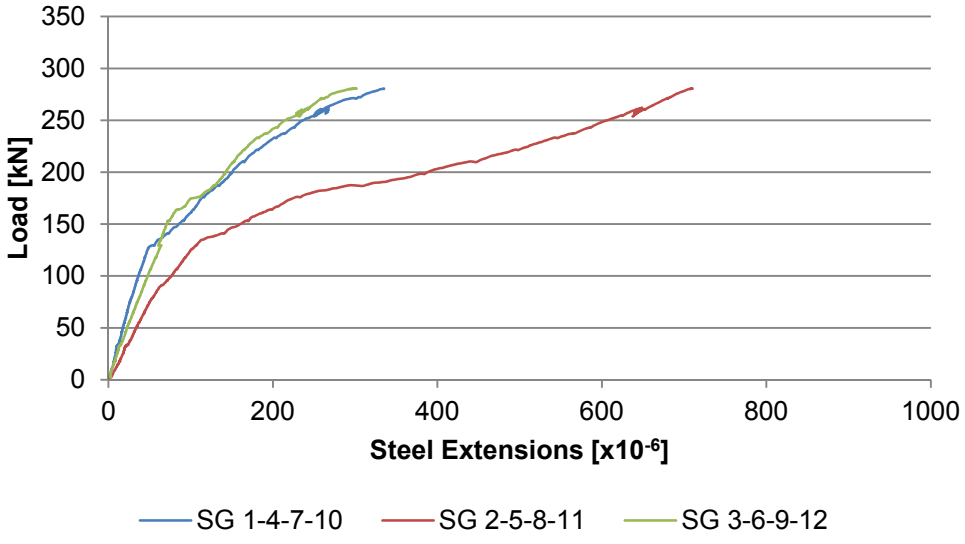

Figure 5.7: Specimen I.A – Load-steel strains curve (F_{max} = 281kN)

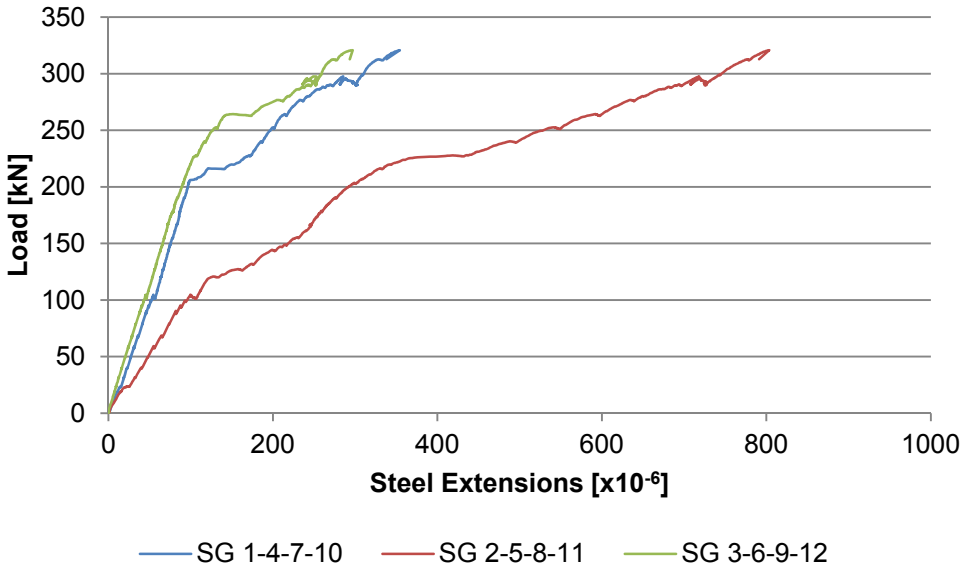

Figure 5.8: Specimen I.B: Load-steel strains curve (F_{max} = 321kN)

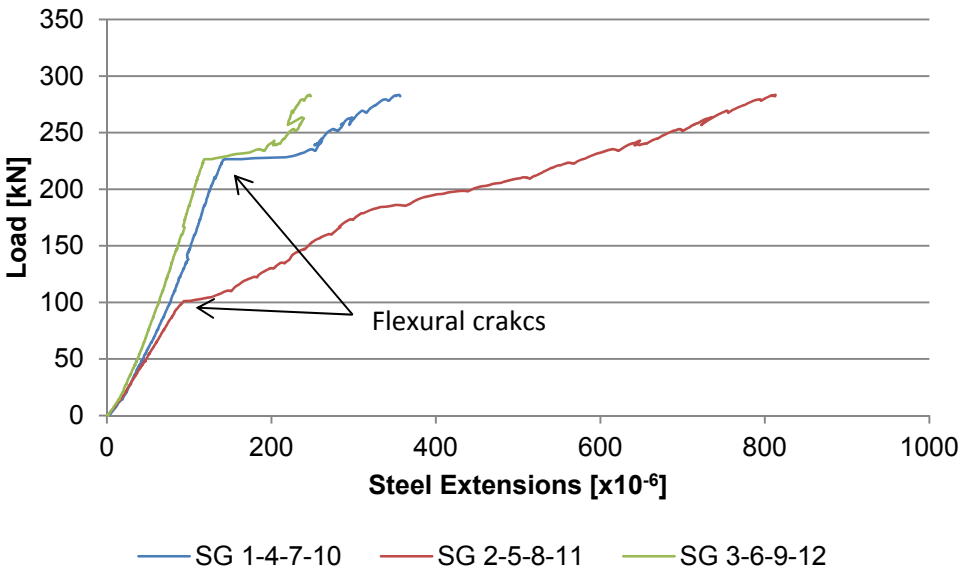

Figure 5.9: Specimen I.C – Load-steel strains curve (F_{max} = 282kN)

5.2.2 Strengthening model II

As mentioned, deflection values are not representative of the substrate deformation, but of the new RC layer. It was observed that deflections in the substrate and strengthening layer were different, which is explained by differential behavior between the substrate and overlay.

This differential behavior can be related to tension existing in the edges of the new concrete layer, perpendicular to the interface and, obviously to the fact that the interface is cracked, at least in this region.

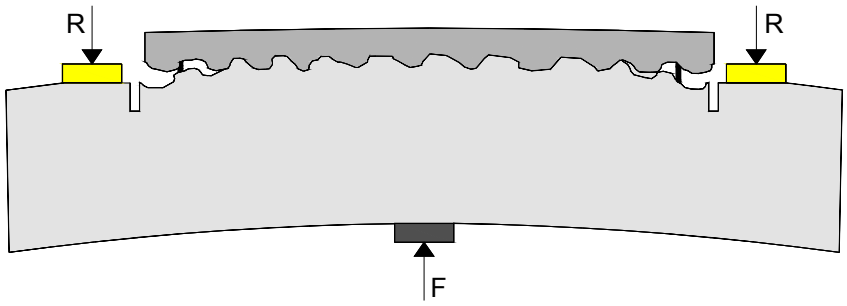

Figure 5.10: Differential behavior between substrate and overlay

5.2.2.1 Description of the failure mode

The beams with evenly distributed 8mm diameter connectors resisted to higher loads than specimens of SMI and exhibited more deformation and cracking prior to failure.

After a first midspan crack was observed, several other flexural-shear cracks started to appear, as the beam deformed. Two shear cracks also became visible near the

supports, and shortly after, some cracks along the interface were also formed (Figure 5.11). These cracks along the interface progressed from the edges of the new concrete layer (which also coincide with the beginning of the shear crack), until a new crack was formed, only in the substrate region (Figure 5.11).

In agreement with the previous model, failure always started at one of the beams ends, which is also consistent to the development of tension in this area. But for this model, failure started at the end anchorage of the new reinforcement in the new concrete (similar to a concrete cover separation of the overlay reinforcement) and then evolved along the interface until reaching the flexural crack at midspan (Beams II.A – Figure 5.13 – and II.B – Figure 5.14) or evolved parallel to the interface, near the bond between concrete and steel (II.C - Figure 5.15).

As it can be observed in Figure 5.13, failure began by anchorage, between the overlay's concrete and steel, and evolved to the already existing crack along the interface.

The beam still continued to resist after the interface cracked, which is the main difference in behavior in comparison to the previous model. Dowels made resistance possible, after a crack along the interface plane appeared (Figure 5.13).

Some perforations were made in beam II.B. It was observed that there was no failure in the reinforcement crossing the interface. However, due to a short anchorage length of the longitudinal reinforcement, failure evolved rapidly along this plane of weakness. Therefore it is not clear whether or not the consideration of an interface shear resistance is correct for this particular model. Nevertheless, ultimate shear stress is quantified.

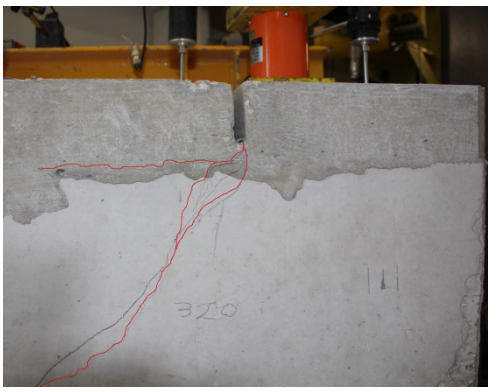

Figure 5.11: Crack along the interface and the shear crack (Beam II.B)

Figure 5.12: Appearance of a grouted dowel, after the beams were tested

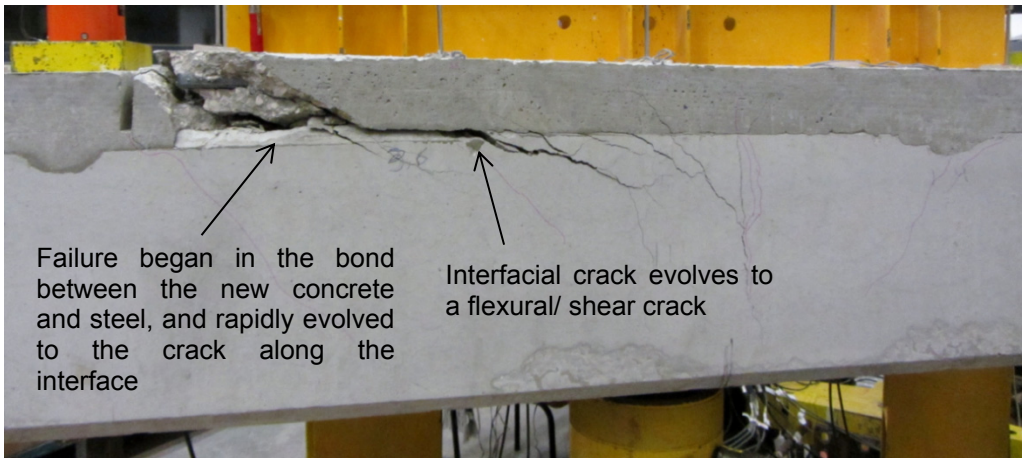

Figure 5.13: Failure mode (Beam II.A)

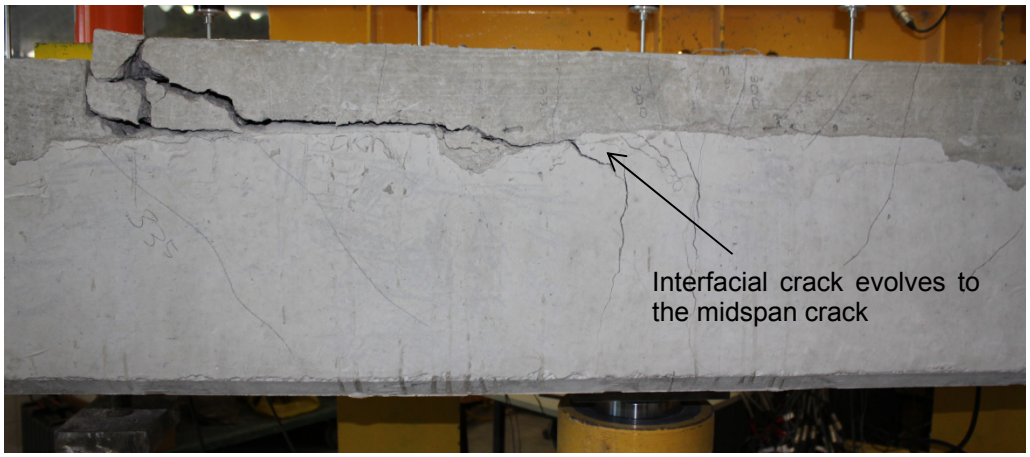

Figure 5.14: Failure (Beam II.B)

Figure 5.15: Failure mode (Beam II.C)

5.2.2.2 Measured strains and deflections

The measured strain and deflection values are not demonstrated for specimen II.A, as a human error occurred in the monitoring device during the test.

Regarding Figure 5.16 and Figure 5.17, it is noteworthy that the distribution of steel strains (and consequently steel stress) for an applied load equal or inferior to about $F = 300$kN, is similar to the results obtained in SMI (Figures 5.4-5.6).

In the evolution of steel strains of beam II.B, it is noticeable that for an applied force superior to $F = 300$kN, stress transmission becomes lower at midspan, inverting the initial tendency.

Between the applied loads of $F = 300$kN and $F = 350$kN there is a zone where the distribution of steel strains is linear. Before failure, steel strains become higher towards the edges, implying that stress transfer in this part of interface is greater before failure. Although it's an approximation, linear stress distribution along the interface was also adopted for this strengthening solution.

This inversion of the initial tendency, indicates that beam II.B was probably able to mobilize a higher resistance than the one provided solely by adhesion, namely in the edges of the overlay, due to the effect of the connectors.

The same process was perhaps beginning in beam II.C (Figure 5.17), however, failure occurred before this behavior became visible. Nevertheless, it is undeniable that the interface was already cracked, namely at about $F = 320$ kN (approximate load value when the interface crack first became visible, during the test) and failure occurred at $F = 395$kN, so the transmission of forces across the interface would not be possible without the effect of the dowels. It can be concluded that tension in the dowels was activated, also because the interfacial crack had a significant width.

From the load-strains curve exhibited in Figure 5.18 and Figure 5.19 it is visible that the failure load occurred with no special increase in steel strains, so although there is a more ductile behavior, with more deformation and cracking, failure is still quite brittle.

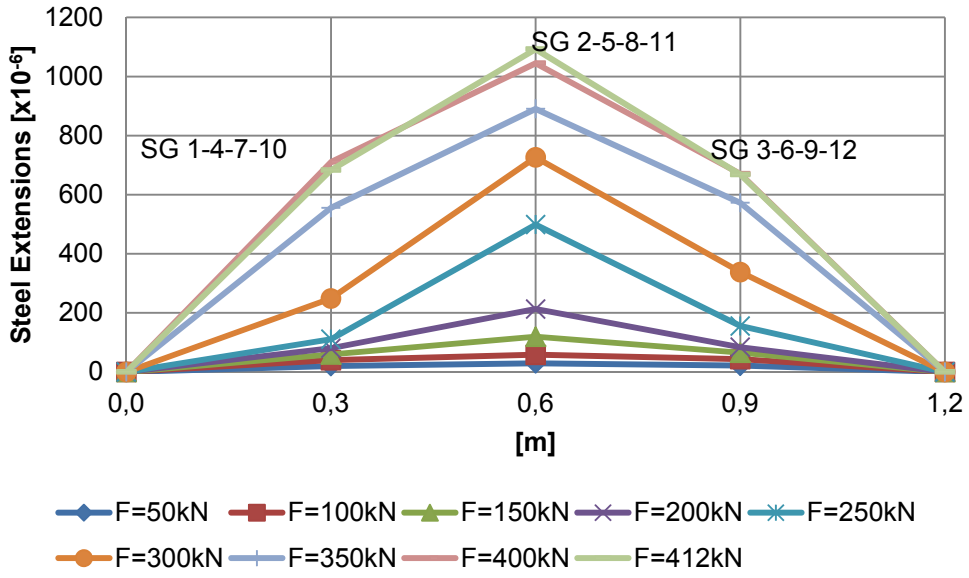

Figure 5.16: Specimen II.B – Evolution in steel strains. Failure along the interface occurred in the left side of this graph

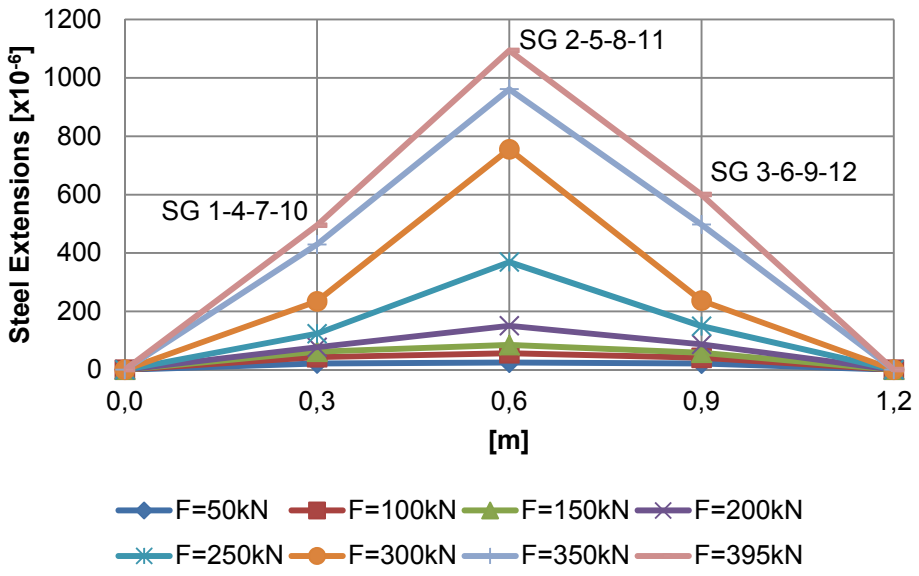

Figure 5.17: Specimen II.C – Evolution in steel strains. Failure along the interface occurred in the left side of this graph

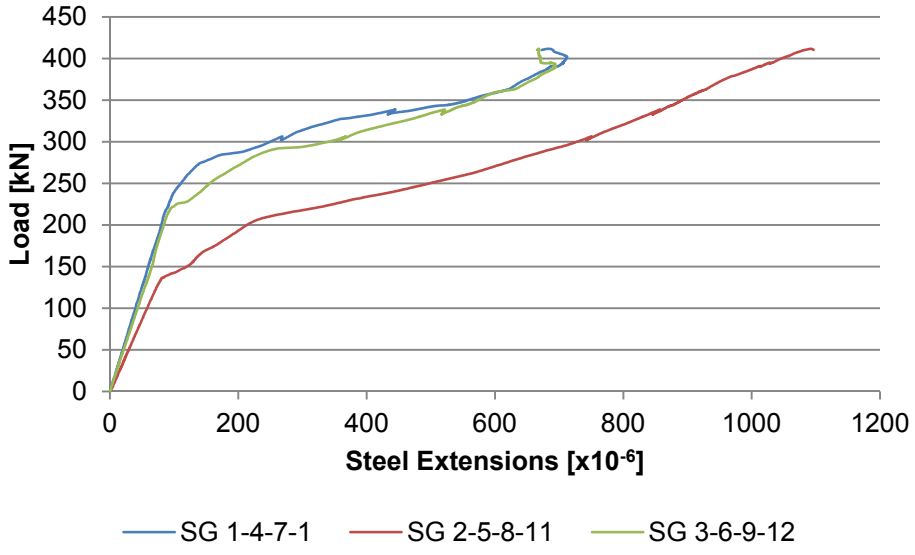

Figure 5.18: Specimen II.B – Load-steel strains curve (F_{max} = 412kN)

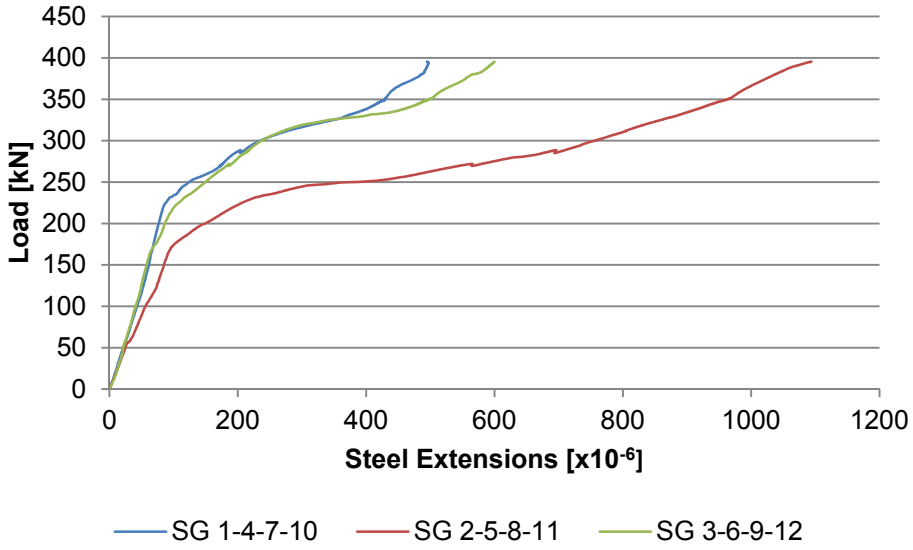

Figure 5.19: Specimen II.C – Load-steel strains curve (F_{max} = 395kN)

Vertical displacements measured in relation to the points D6 and D7 are presented in Figure 5.20 and Figure 5.21. In both beams, it is visible that deflections in relation to D6 and D7 become relevant, for a force superior to F = 300kN. The deflections in the overlay are somewhat uniform, however, in relation to the reference points they begin to differ. Although it would have been interesting to have measured the deformations in the beams underside, it is clear that the overlay's deformation does not accompany the substrate's deformation. This fact can also be observed in the load-deflection curves shown in Figure 5.22 and Figure 5.23. .As the crack along the interface is formed, the overlay tends to distance itself from the substrate. This behavior is also schematized in Figure 5.10.

It is also evident that the overlay is very rigid, because there are little variations in deflections in the overlay. The main difference between the vertical deflections is in comparison with the substrate deflections.

The fact that deflection values in relation to D6 and D7 only became relevant after an applied load of about F = 300kN, which is also approximately the failure load of SMI, can also be related to the loss of adhesion and the creation of a interfacial crack (activating dowel action and tension in the reinforcement, especially at the edges of the new concrete layer). It is an indicator that a non-uniform distribution of reinforcement, with a higher concentration near the edges is more realistic than a uniform distribution.

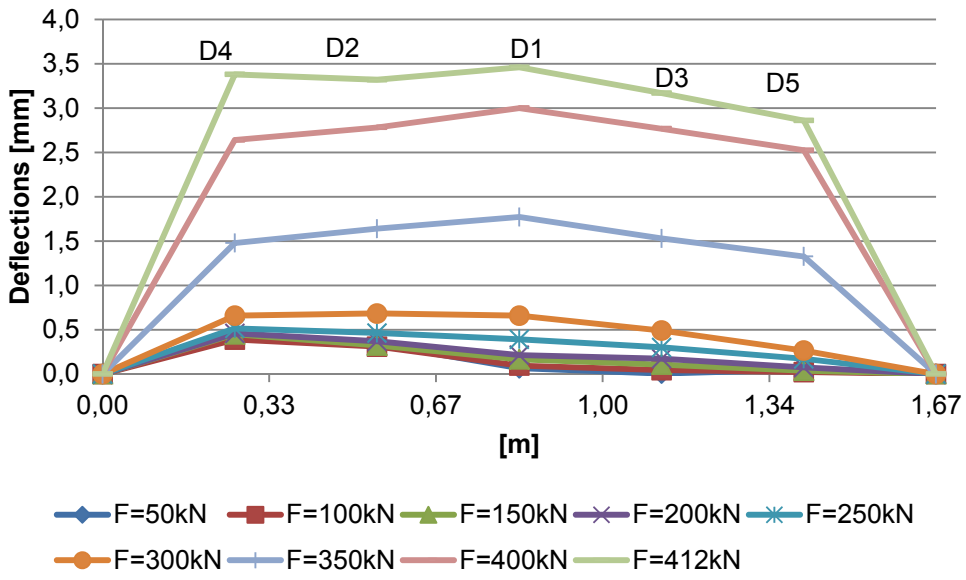

Figure 5.20: Specimen II.B – Evolution in deflections. Failure along the interface occurred in the left side of this graph

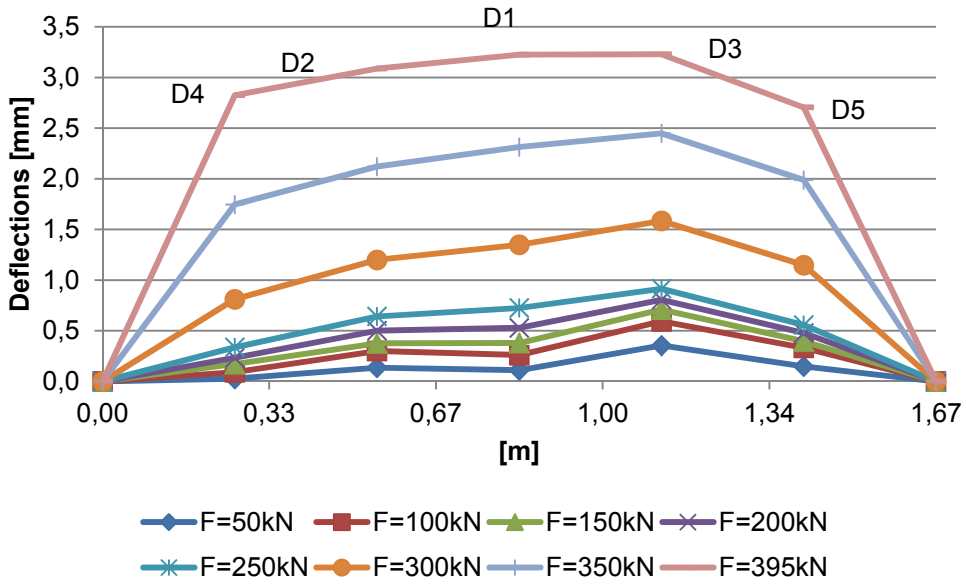

Figure 5.21: Specimen II.C – Evolution in deflections. Failure along the interface occurred in the left side of this graph

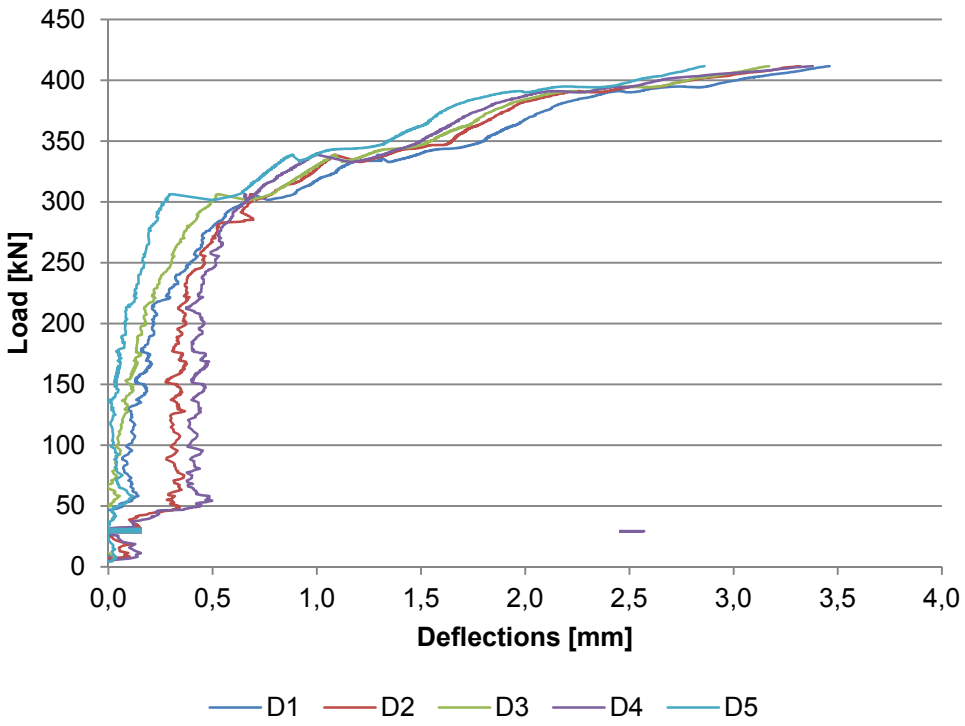

Figure 5.22: Specimen II.B – Load-deflection curve (F_{max} = 412kN)

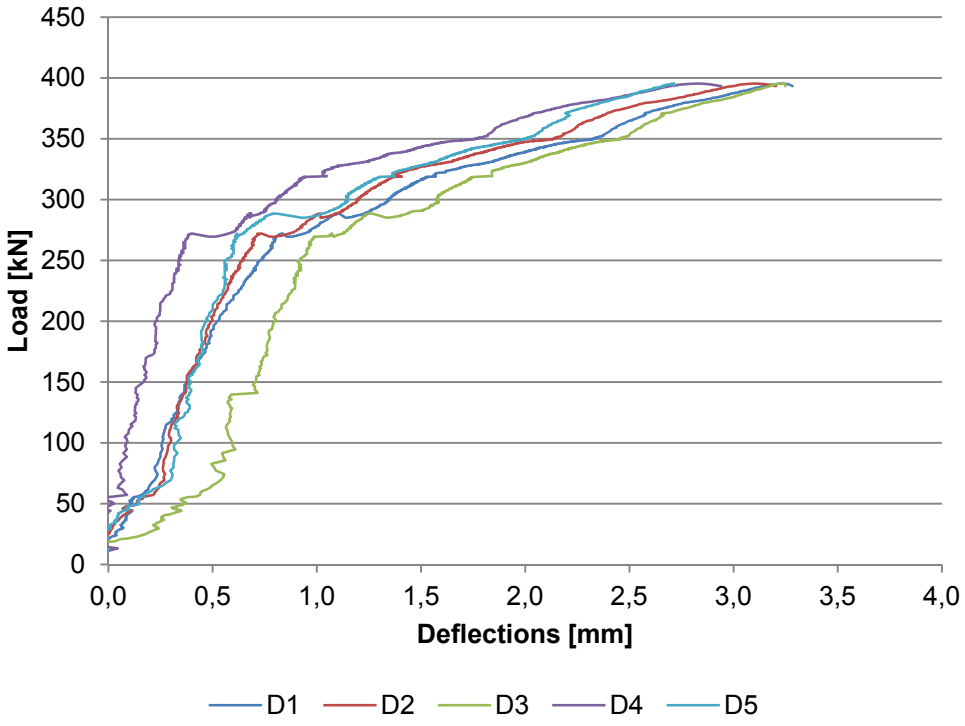

Figure 5.23: Specimen II.B – Load-deflection curve (F_{max} = 395kN)

5.2.3 Strengthening model III

5.2.3.1 Description of the failure modes

The three beams with the longitudinal reinforcement anchored in the substrate resisted to the higher load and exhibited more cracking and deflection before rupture, when compared to the previous strengthening solutions.

All three beams of strengthening model III exhibited relatively different failure modes. The differences in behavior of each beam might be associated to eccentricities related to the test setup, or, in the particular case of beam III.C, to difficulties in respecting the designed anchorage position, as to avoid drilling into a longitudinal bar or stirrup existent in the substrate (Figure 4.17).

Also, for beam III.C it was necessary to load the beam twice, as the hydraulic jack lost pressure before rupture occurred. After the first load cycle, the beam apparently returned to the initial position, and some cracks small cracks no longer were visible.

As mentioned, for this strengthening model, the goal was to study the effect of reinforcement crossing the interface localized near the edges of the new concrete layer, which coincides with the anchorage of the new longitudinal reinforcement in the substrate. It is difficult to predict the behavior of a monolithic beam with identical steel disposal; however, failure modes were clearly associated with the interface.

As it had been observed in the previous models, the initial crack corresponded to a flexural crack at midspan. In similarity with the observations during SMII tests, other flexural cracks were visible before a shear crack appeared neat the edges. At this point the behavior of each beam differed, as cracks in the overlay/interface did not evolve in the same way.

A partial crack along the interface was observed in beams III.A and III.B. These cracks started diagonally in the overlay and progressed along the interface. In beam III.C a crack along the interface was not visible.

In beam III.A, the interfacial crack was first formed in the overlay near the edge of the new RC layer, than approaching midspan, evolved into an interface crack, and then took the path of the first flexural crack (Figure 5.24 and Figure 5.25). Another shear crack near the edge of the overlay was also visible in the substrate, parallel to the interface.

In conclusion, in the region where reinforcement crossed the interface no crack along the interface was noticeable; however, in the region where reinforcement did not cross the interface, the interface crack became quite visible.

The failure mode for beam III.B (Figure 5.26 and Figure 5.27) is probably related to the fact that, at the opposite edges of the new RC layer, two consecutive reinforcement bars are not anchored, consequently, failure occurred diagonally. Although the failure load is superior to the one measured in beam III.A (Figure 5.1), less cracking was visible for this specimen. A crack along the interface, near the edges of the RC overlay was visible near the diagonal ends where the beam failed. Several cracks approximately parallel to the interface were visible near the edges that did not experience detachment of the new concrete layer.

Beam III.C (Figure 5.29) failed with crushing of concrete under the longitudinal reinforcement, in the interface area, and rupture in one of the reinforcement anchorages. Near the bent part of the reinforcement, large cracks in the concrete were visible, which indicates that steel was experiencing large deformations. These cracks progressed parallel to the interface, in a mixed overlay and substrate group of cracks,

until a point near midspan was reached, where they took the path of the initial flexural crack. At last, failure occurred with rupture of one longitudinal bar, at the anchorage, in the substrate (Figure 5.28).

Figure 5.24: Failure mode for beam III A

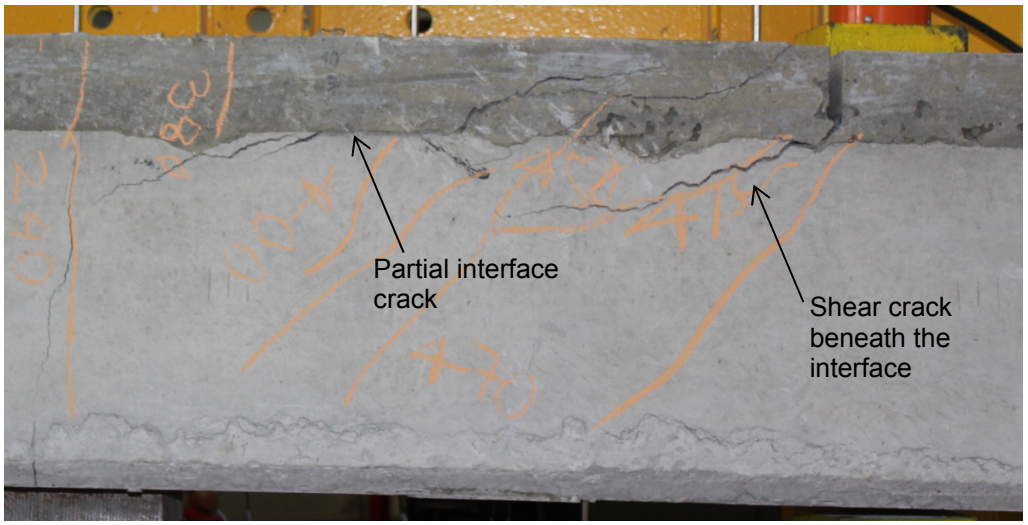

Figure 5.25: Shear cracks in the overlay and substrate and a partial crack along the interface (III.A)

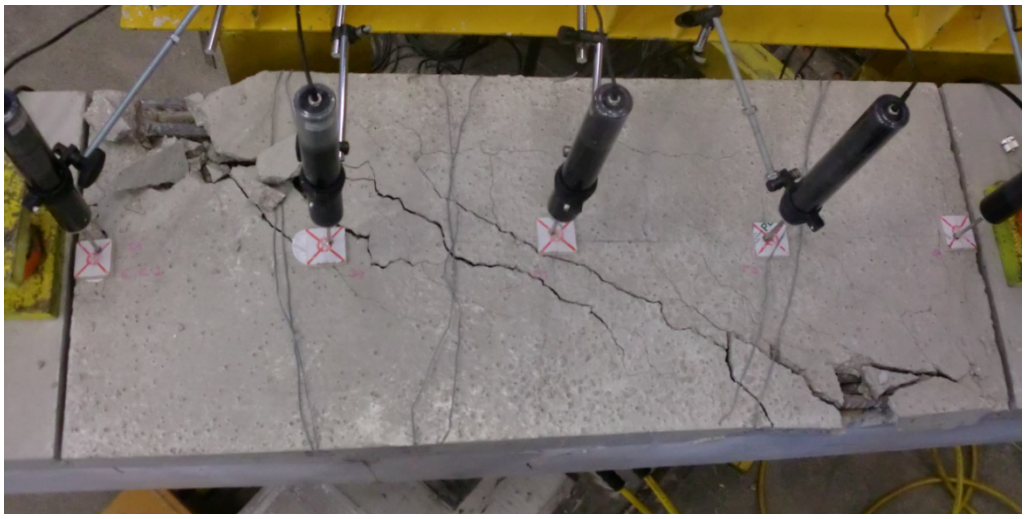

Figure 5.26: Failure mode for beam III B

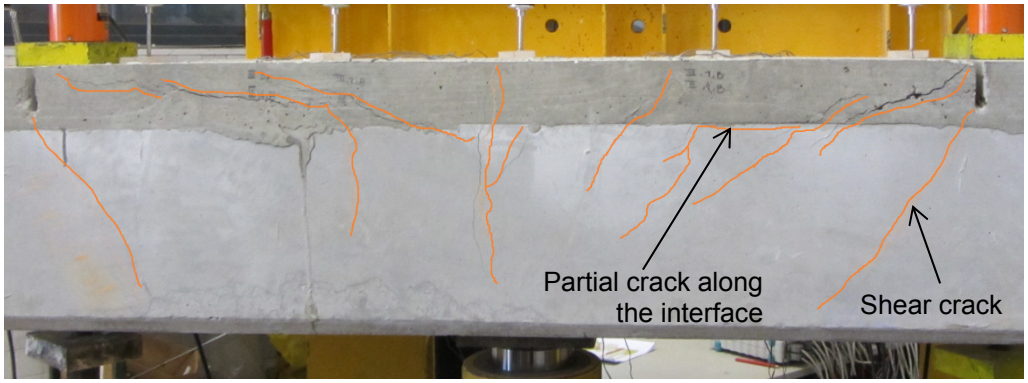

Figure 5.27: Partial crack along the interface (beam III.B)

Figure 5.28: Failure in overlay concrete progressing both in a crack along the interface and a crack under the interface (beam III.B)

Figure 5.29: Failure mode for beam III C

Figure 5.30: Rupture in the reinforcement (beam III.C)

5.2.3.2 Measured strains and deflections

Regarding the test on the beams of SMIII, the strain values are presented for each reinforcement bar, because, not only the measured strain values are quite different in each rebar, but also, the rebars were an anchorage on opposite sides. In Figure 5.31 there is a scheme with the location of the measured values.

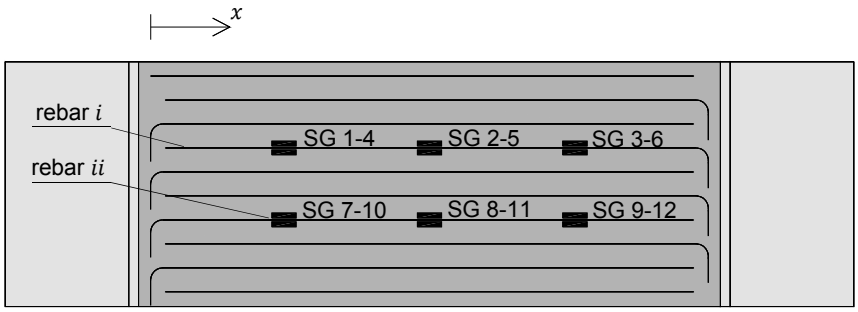

Figure 5.31: Map of the measured strain values

The measured results for strain and deflections in beam II.B are not demonstrated, as a human error occurred while monitoring the test.

In beam III.A, it is visible that the reinforcement bar "i" exhibits higher strain values than rebar "ii". This difference can be explained by the fact that rebar "i" is anchored in the side where the strengthening layer ultimately failed, and steel became increasingly stressed as cracks opened. The same amount of cracking did not occur in the side that did not experience failure. For $F = 506$ kN the measured strains in SG 3-6 (beam III.A) were higher than at midspan, highlighting the fact that, before failure, steel stress in the beam's anchored end was quite high.

Observing the strain distribution of reinforcement bar "ii" (Figure 5.33), it is visible that the highest slope is also in the failure side. A constant slope of the lines connecting the different known strain points is visible on the side that did not experience failure. However, in the failure side, the consideration of a constant rate for stress distribution is obviously not possible.

In Beam III.C first and second load cycles, it is also noticeable a slight increase in steel strains in the rebar anchored in the failure side ("ii"), in agreement with the previous observations.

In the load strain curves it can be seen that some strain gauges measured high extension values after the maximum load was achieved. From the observed results, failure can be considered somewhat ductile, due to some increase in extension, for an approximately constant load.

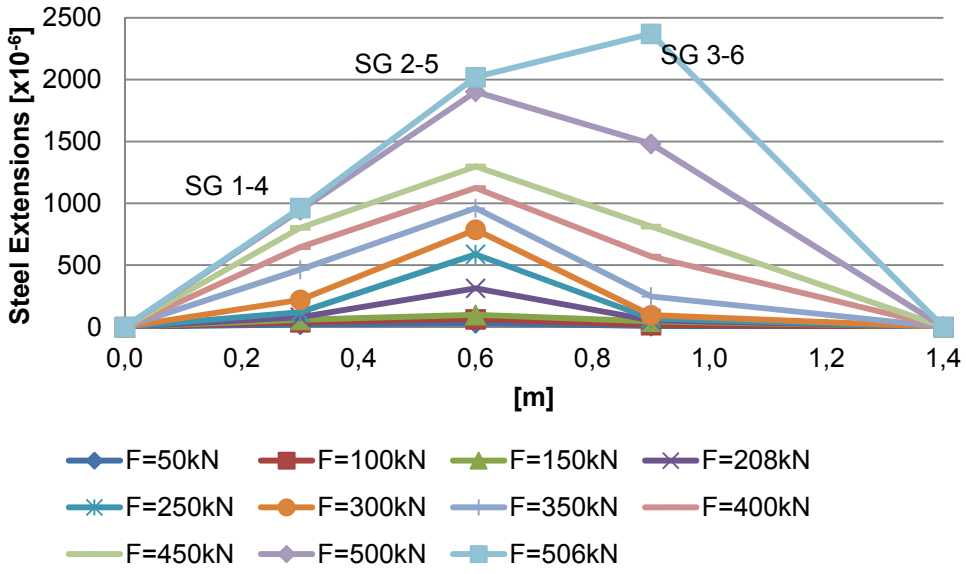

Figure 5.32: Specimen **III.A (rebar i)** – Evolution in steel strains. Failure along the interface occurred in the right side of this graph

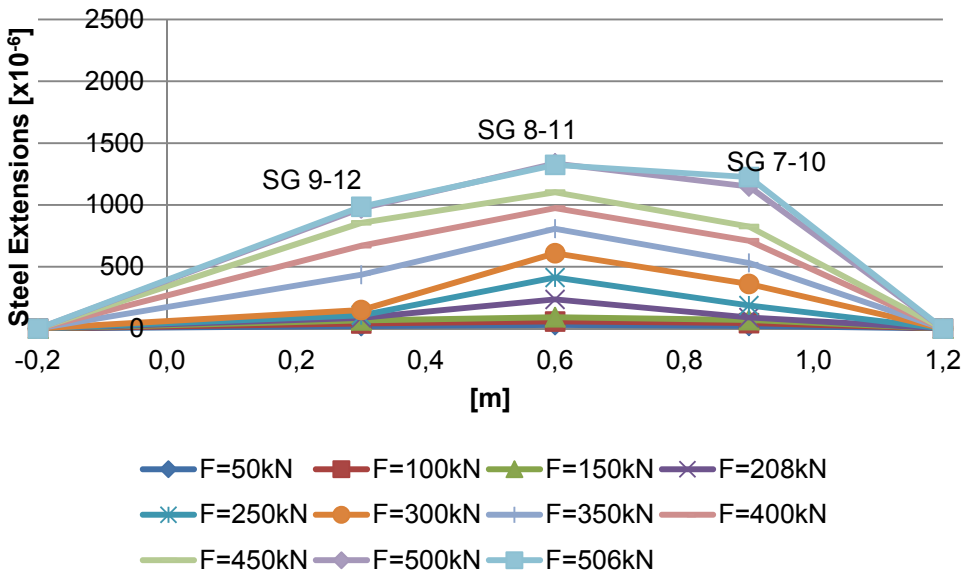

Figure 5.33: Specimen **III.A (rebar ii)** – Evolution in steel strains. Failure along the interface occurred in the right side of this graph

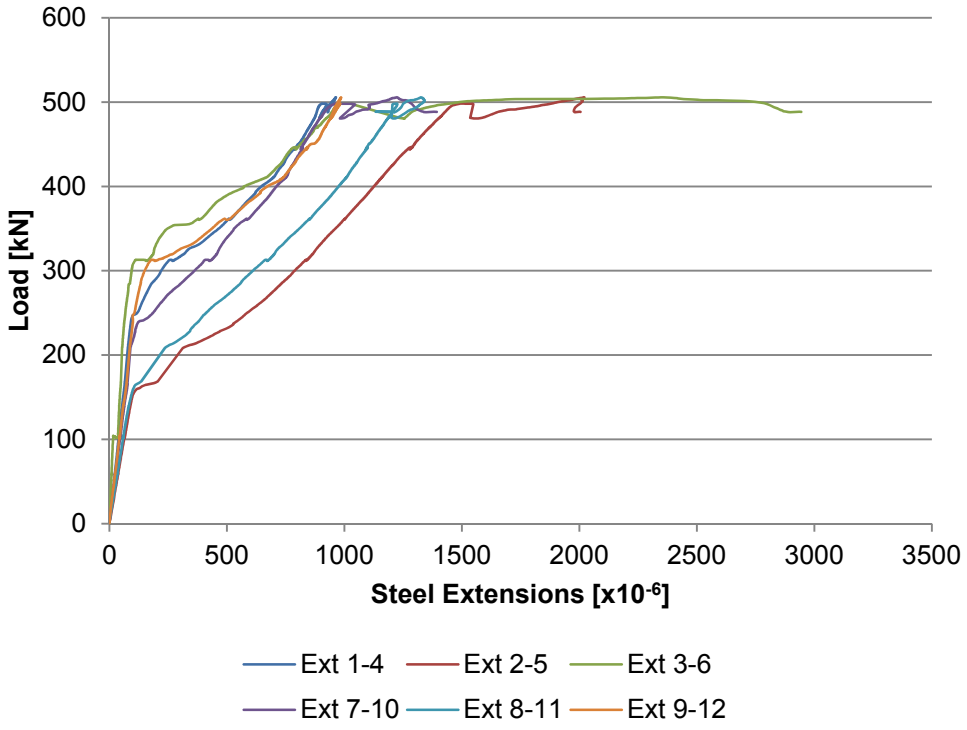

Figure 5.34: Specimen III.A – Load-steel strains curve (F_{max} = 506kN)

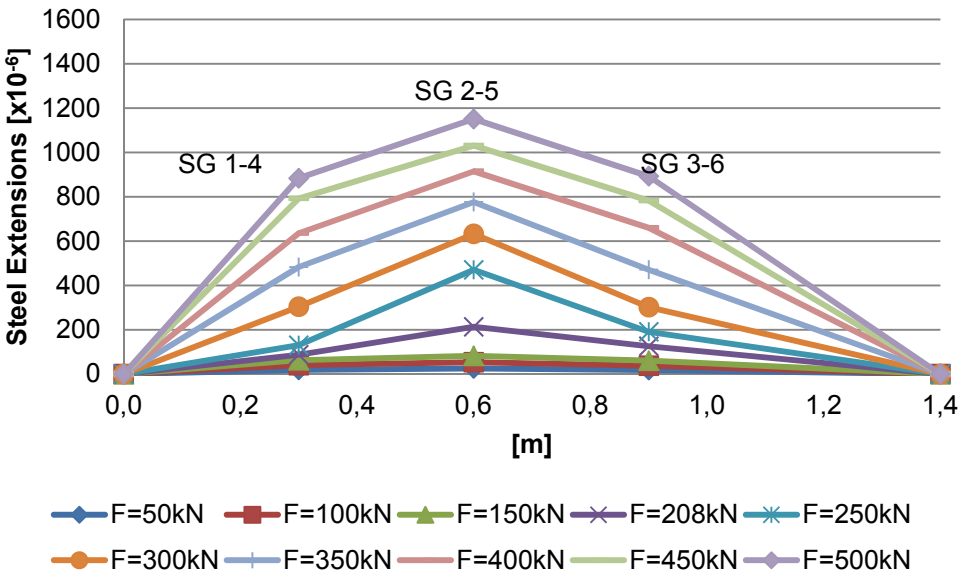

Figure 5.35: Specimen III.C (rebar i) – Evolution in steel strains **first** loading.

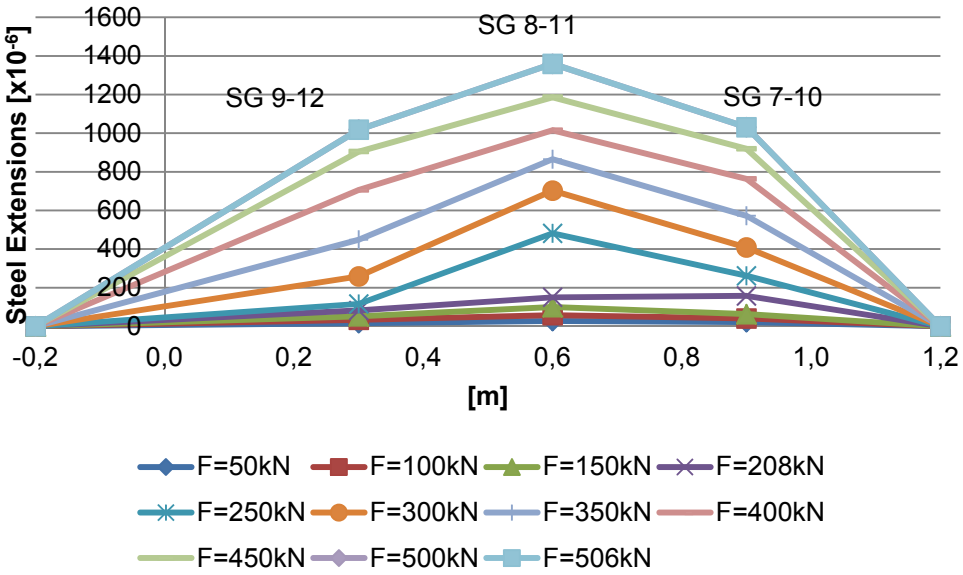

Figure 5.36: Specimen III.C (rebar ii) – Evolution in steel strains **first** loading.

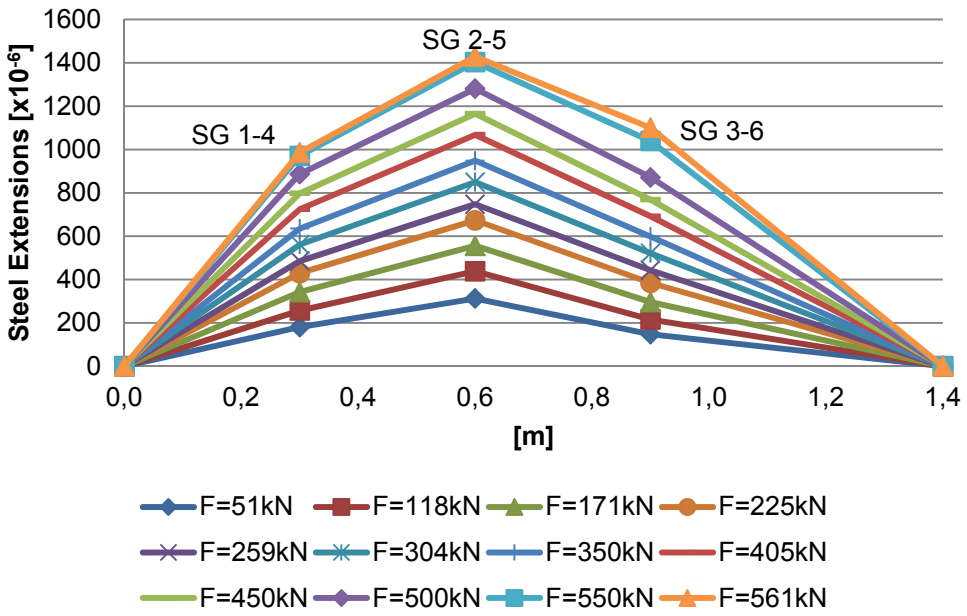

Figure 5.37: Specimen III.C (rebar i) – Evolution in steel strains **second** loading. Failure with concrete crushing under the interface's reinforcement occurred in the left side of this graph.

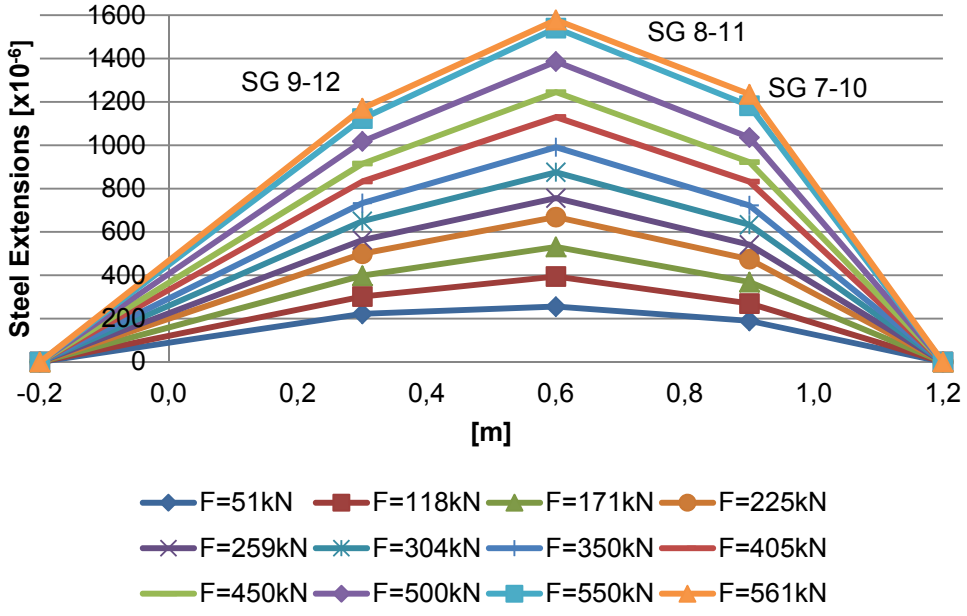

Figure 5.38: Specimen III.C (rebar ii) – Evolution in steel strains **second** loading. Failure with concrete crushing under the interface's reinforcement occurred in the left side of this graph.

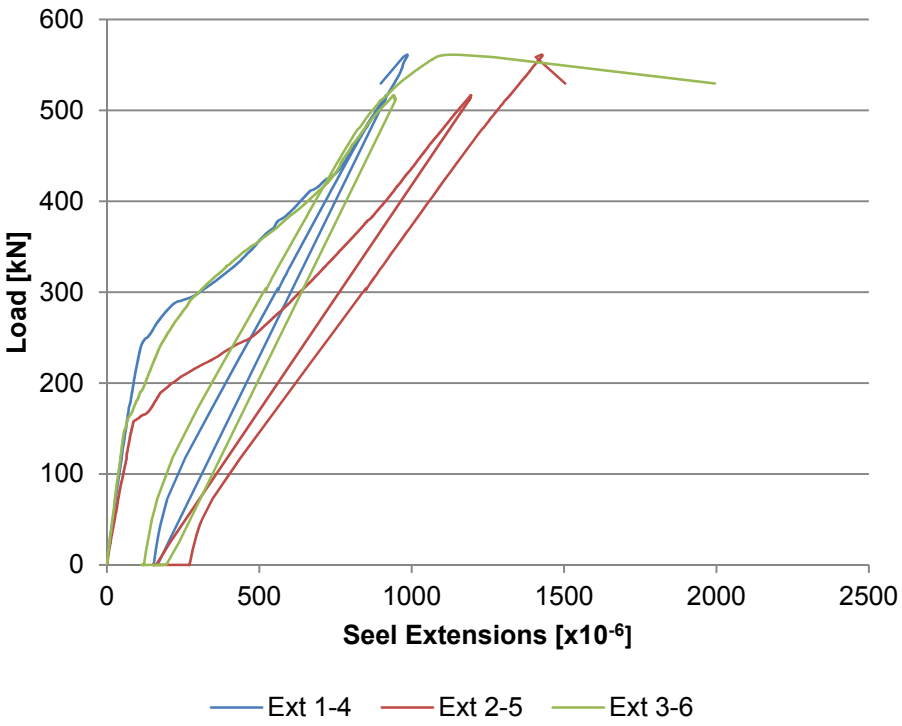

Figure 5.39: Specimen III.C – Load-steel strains curve (rebar i) (F_{max} = 561kN)

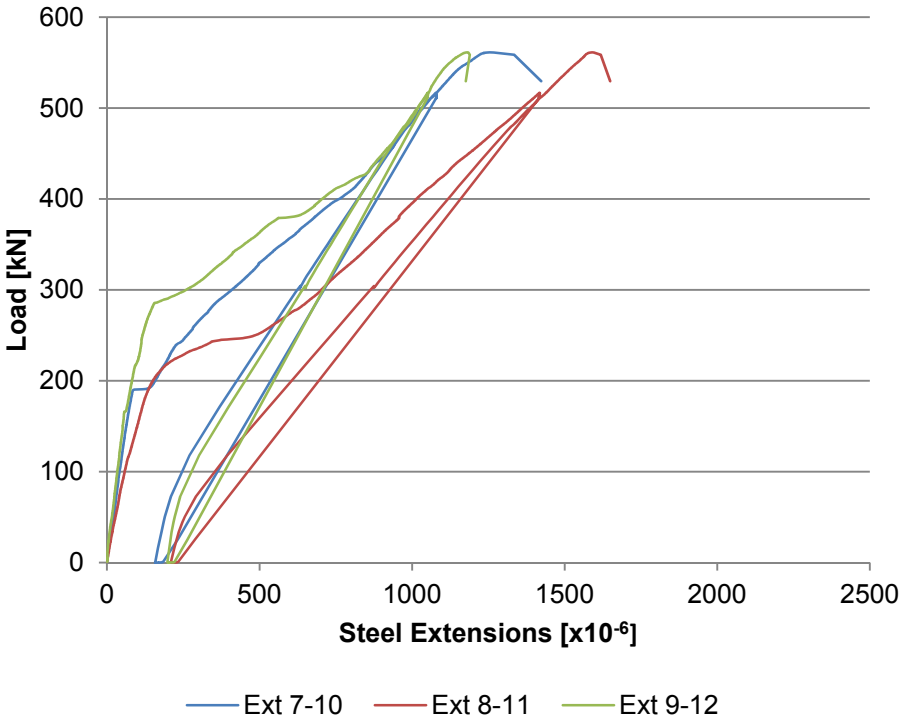

Figure 5.40: Specimen III.C – Load-steel strains curve (rebar ii) (F_{max} = 561kN)

Vertical deflections in relation to points D6 and D7 are in the same magnitude of the ones measured for strengthening model II (Figure 5.41 and Figure 5.42), however, the

evolution in steel strains shows that there are more variations in the overlay deflections, resulting probably in the fact that the deformation of the overlay accompanies more the deformation of the substrate. This was not the case with the previous model.

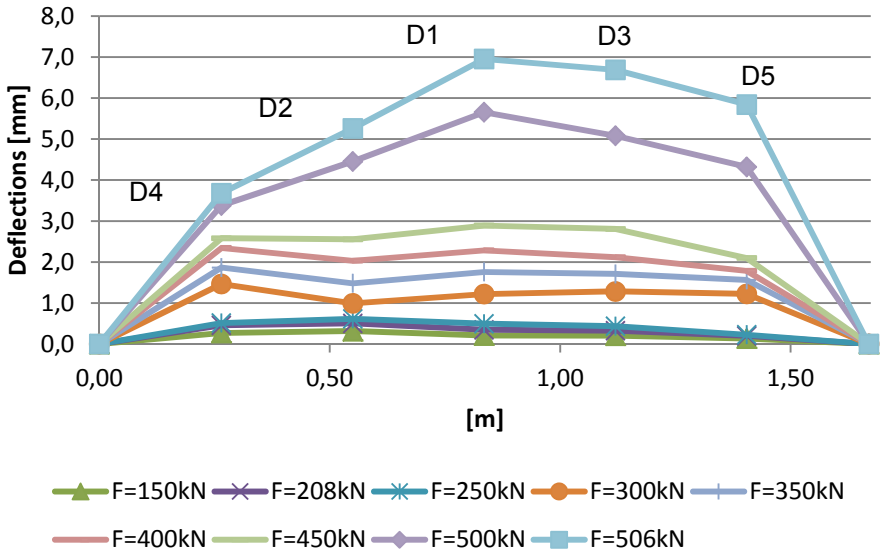

Figure 5.41: Specimen III.A – Evolution in steel strains. Failure along the interface occurred in the right side of this graph

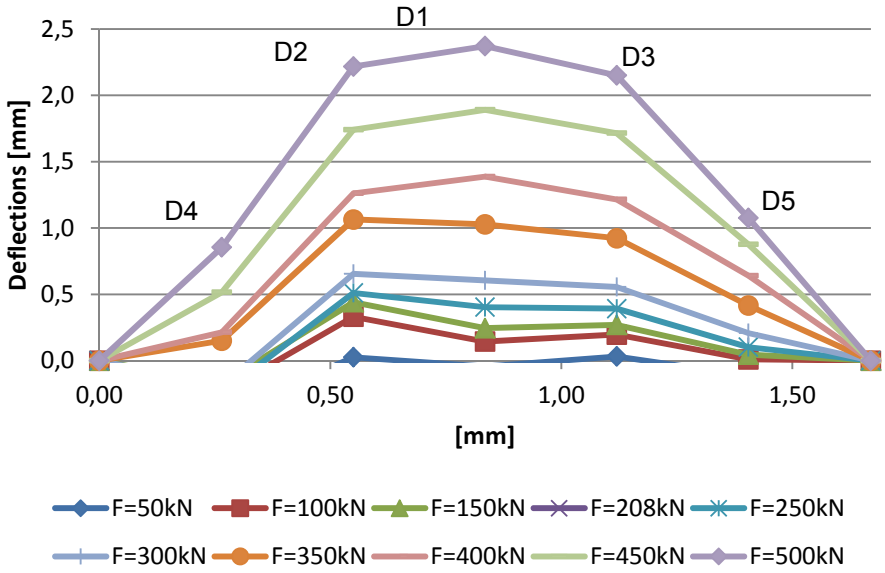

Figure 5.42: Specimen III.C – Evolution in deflections (**first** load cycle). Failure with concrete crushing under the interface's reinforcement occurred in the left side of this graph.

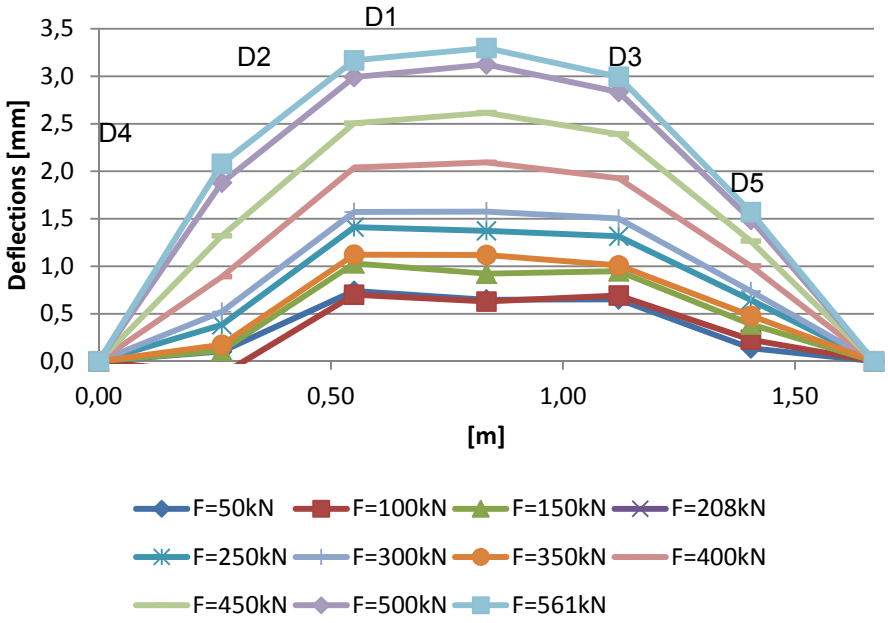

Figure 5.43: Specimen III.C – Evolution in deflections (**second** load cycle). Failure with concrete crushing under the interface's reinforcement occurred in the left side of this graph.

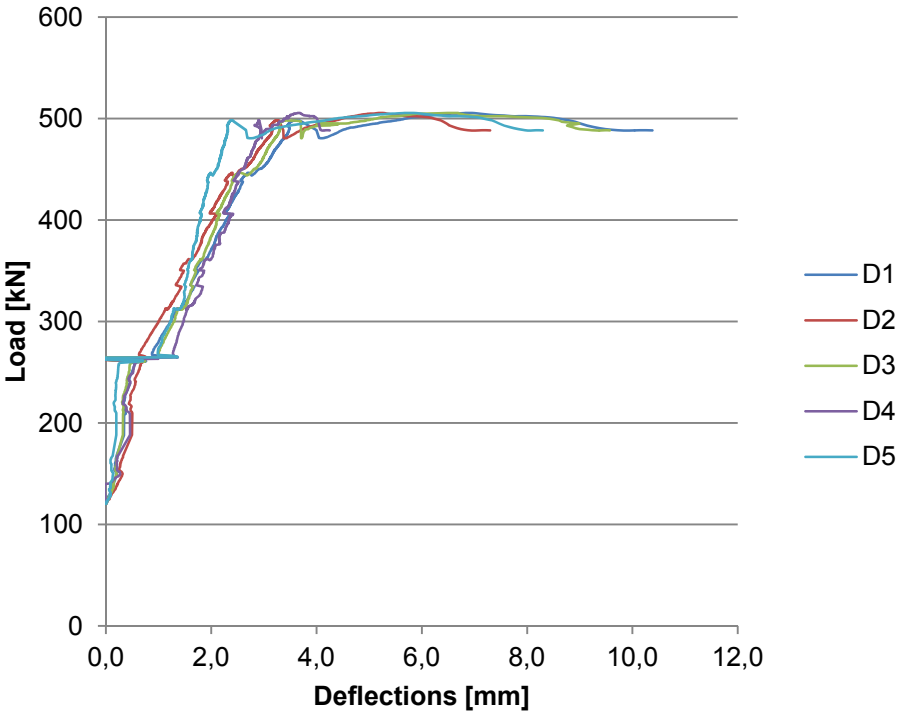

Figure 5.44: Specimen III.A – Load-deflection curve (F_{max} = 506kN)

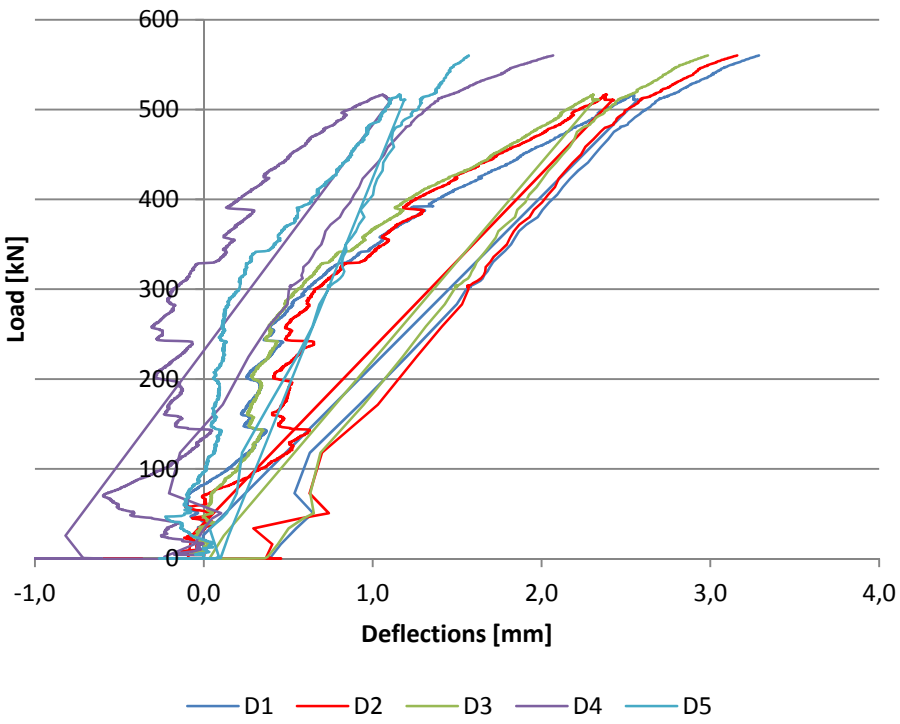

Figure 5.45: Specimen III.C – Load-deflection curve (F_{max} = 561kN)

5.3 Determination of the ultimate shear strength of the interface

5.3.1 Experimental resistance

Given the approximately linear distribution of steel strains in the reinforcement, the consideration of a constant rate for stress transmission along the interface seems appropriate for the beams of SMI and SMII.

The first approach to determine shear strength involves the equilibrium between steel forces and interface stress at midspan (see Figure 4.16 and Equation 4.5) is given by:

$$v_{i,exp1} = \frac{2\varepsilon_s E_s A_{s_o}}{l_i \cdot b_i} \tag{5.1}$$

Where,

ε_s is the average steel strains measured by SG 2-5-8-11

E_s is the steel's elasticity modulus

A_{s_o} is the overlay's reinforcement

l_i is the length of the interface

b_i is the width of the interface

The consideration of a constant shear stress along the interface might not be accurate for SMIII beams. Nevertheless, steel stress must be transmitted across the concrete

interface so $v_{i,exp1}$ was also calculated for SMIII, considering the premise of constant shear stress.

Since steel strains measured in rebar "i" are different from the ones measured in rebar "ii", and there is no information about the two non-anchored bars in the beams border, ε_s was determined through the following weighted average:

$$\varepsilon_s = \frac{4 \cdot max\{\varepsilon_{s,i}\,;\,\varepsilon_{s,ii}\} + 6 \cdot min\{\varepsilon_{s,i}\,;\,\varepsilon_{s,i\,i}\}}{10} \tag{5.2}$$

With $\varepsilon_{s,i}$ and $\varepsilon_{s,ii}$ being respectively, the midspan steel strains measured for the maximum load, in rebar "i" and "ii".

The determination of the interface resistance by the method proposed by EC2 and MC2010 is also possible:

$$v_{i,exp2} = \frac{V_{max}}{b \cdot z} \tag{5.3}$$

Where,

V_{max} is the average load measured in load cells LC1 and LC2

b is the width of the interface

z is the inner lever arm, determined by Equations 5.5-5.8

As the distribution of steel strains in a tensioned rebar embed in concrete is not constant, exhibiting peaks in the cracked regions, the consideration of the steel strains measured during the laboratory tests might introduce some error. Another approach might be to determine the steel force by solving the system of equation composed by Equations 5.4-5.7. This approach is similar to Equation 5.1, the difference resides in the determination of the steel force.

$$v_{i,exp3} = \frac{2F_s}{l_i \cdot b} \tag{5.4}$$

Where,

F_s is given by $\sigma_s \cdot A_s$

l_i is the length of the interface

b is the width of the interface

In Equations 5.3 and 5.4 linear behavior of compressed concrete before failure is assumed, as displayed in Figure 5.46. The height of the neutral axis, x, the inner lever arm, z, and the steel stress, σ_s are determined by solving the system of equations composed by Equations 5.5-5.8.

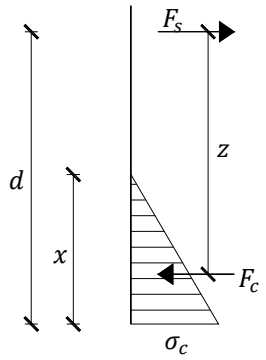

Figure 5.46: Equilibrium between steel and concrete forces

$$\sum F = 0 \Leftrightarrow F_c = F_s \Leftrightarrow \frac{bx}{2}\sigma_c = A_s\sigma_s \tag{5.5}$$

$$\sum M = 0 \Leftrightarrow F_c z = F_s z = M_{max} \Leftrightarrow A_s\sigma_s z = M_{max} \tag{5.6}$$

$$\frac{\varepsilon_s}{d-x} = \frac{\varepsilon_c}{x} \Leftrightarrow \frac{\sigma_s/E_s}{d-x} = \frac{\sigma_c/E_{c_{sub}}}{x} \tag{5.7}$$

$$z = d - \frac{x}{3} \tag{5.8}$$

Where x, z, σ_s, and σ_c are the unknowns of the system. The elasticity modulus of the substrate concrete, $E_{c_{sub}}$, in Equation 5.7, is related to the compressed zone, therefore, the substrate's elasticity modulus must be considered.

In Table 5.2 the system is solved, and the unknowns determined. As stress in concrete in the most distant fiber is inferior to the concrete's compressive resistance, the consideration of linear normal strain distribution in the cross-section is appropriate. In beams of SMIII, however, if this model were to be adopted, $\sigma_c \geq f_{cm}$.

Table 5.1: Determination of the height of the neutral axis, steel and concrete stress

Beam	I.A	I.B	I.C	II.A	II.B	II.C
b [m]	0,5					
d [m]	0,332					
A_s [cm^2]	20,11					
$E_{c_{sub}}$ [Gpa]	25,5	28,0	25,6	28,8	30,3	27,6
E_s [Gpa]	200					
M_{max} [kNm]	99,3	113,4	100,2	149,4	145,5	139,8
x [m]	0,117	0,112	0,116	0,111	0,109	0,113
z [m]	0,293	0,295	0,293	0,295	0,296	0,294
σ_s [Mpa]	167,9	190,8	169,6	251,2	245,5	236,5
σ_c [Mpa]	11,58	13,66	11,72	18,19	18,14	16,84

The values of the experimental ultimate shear stress of the interface, $v_{i,exp}$, , are displayed in Tables 5.2-5.4:

Table 5.2: Determination of experimental interface shear stress by Equation 5.1

Beam	I.A	I.B	I.C	II.A	II.B	II.C	III.A	III.C
A_s [cm^2]					20,11			
E_s [GPa]					200			
ε_s [μm]	710	803	813	-	1093	1094	1603	1518
l_i [m]					1,2			
b [m]				0,5				
$v_{i,exp1}$[MPa]	0,95	1,08	1,09	-	1,46	1,47	2,15	2,04

Table 5.3: Determination of $v_{i,exp2}$

Beam	I.A	I.B	I.C	II.A	II.B	II.C
V_{max} [kN]	140,4	160,4	141,7	211,2	205,8	197,7
b [m]				0,5		
z [m]	0,293	0,295	0,293	0,295	0,296	0,294
$v_{i,exp2}$ [MPa]	0,96	1,09	0,97	1,43	1,39	1,35

Table 5.4: Determination of $v_{i,exp3}$

Beam	I.A	I.B	I.C	II.A	II.B	II.C
A_s [cm^2]				20,11		
F_s [kN]	337,6	383,6	341,0	505,9	493,6	475,5
$v_{i,exp3}$ [MPa]	1,13	1,28	1,14	1,69	1,65	1,59

The obtained values for the ultimate stress in SMIII were the highest. SMII had obviously higher ultimate stress than SMI. The resistance provided by adhesion was approximately 1MPa. In SMII and SMIII the stress at the interface just before failure was about 1,4~1,7MPa and 2 MPa, respectively.

The ultimate shear stress of the interface is lower than the representative mean values provided in MC2010 (indicated in Table 3.1). The obtained experimental values are approximately 1~2MPa, whereas for rough and very rough interfaces, τ_c varies from 1,5 up to 3,5 MPa.

5.3.2 Provisions for shear resistance of the interface

The predicting models for shear resistance usually imply some kind of compressive load perpendicular to the interface, as a result of the tensioned reinforcement crossing the interface. However, for SMI the only contribution for shear resistance is adhesion. There was a concern that this expressions might present a low estimate when predicting the resistance provided by the single mechanism of adherence (as different mechanisms deliver maximum contribution at different stages of interface slip, they were not added at their maximum values).

Another issue is related to the fact that design expressions cannot be compared directly to experimental results. Adaptations to the design expressions were made, in order to proceed with comparisons. For the EC2 and MC2010 approach (Equations 3.21 and 3.23), interface resistance is given by

$$v_{ri} = cf_{ctm} + \rho_i f_{yk}\mu \leq 0{,}5\vartheta f_{cm} \quad (5.9)$$

The interface surface is considered indented by EC2 standards and very rough by the MC2010 approach (R_a ≥3mm). In both the code, the cohesion factor adopted is c = 0,5 and the friction coefficient is μ = 0,9.

MC2010 Equation 3.24, becomes:

$$v_{ri} = \gamma_c 0{,}09 k_c f_{ck}^{1/3} + \mu\kappa\rho_i f_{yk} + \alpha_F\sqrt{f_{yd} f_{cm}} \leq \beta_c f_{cm}\vartheta \quad (5.10)$$

Where the adhesion parcel is multiplied by the partial safety factor of concrete, γ_c.

The values for the concrete resistances used in the expressions were always the minimum between substrate and overlay, except in the influence of dowel action, where concrete strength of the substrate was used.

Since the surface roughness was determined by an average of profile heights instead of the sand patch test, in conformity with Table 3.5, the surface was considered very rough, so the adopted values for the coefficients in Equation 5.10 were k_c =2,3, κ =0,5, β_c =0,5 andμ =0,8 (although these values are recommended for water jetted surfaces).

The predicted shear resistance considering Walraven's approach (Equation 3.20) provides already experimental values.

Table 5.5: Predicted shear resistance (Walraven's sphere model)

$f_{c,cm}$ [MPa]	43,6	51,5	37,9	36,9	34,7	47,1
C_1	3,81	4,07	3,60	3,56	3,47	3,93
C_2	0,50	0,52	0,48	0,47	0,47	0,51
ρ_i	0,00201	0,00201	0,00201	0,00268	0,00268	0,00268
f_{yk} [MPa]	500	500	500	500	500	500
$v_{r,i}$ [MPa]	3,82	4,08	3,61	4,09	3,98	4,56

Table 5.6: Predicted shear resistance (EC2 Equation 3.21, MC2010 Equation 3.23)

Beam	I.A	I.B	I.C	II.A	II.B	II.C	III.A	III.B	III.C
c					0,5				
$f_{ctm,sub}$ [MPa]	1,85	2,48	1,88	2,69	3,10	2,38	2,32	2,19	2,87
$f_{ctm,o}$ [MPa]	1,86	1,86	1,86	3,31	3,31	3,31	3,31	3,31	3,31
ρ_i [%]	-	-	-	0,201	0,201	0,201	0,268	0,268	0,268
f_{yd} [MPa]	-	-	-	500	500	500	500	500	500
μ	-	-	-	0,9	0,9	0,9	0,9	0,9	0,9
"adhesion"	0,92	0,93	0,93	1,35	1,55	1,19	1,16	1,10	1,44
"friction+ dowel action"				0,90	0,90	0,90	1,21	1,21	1,21
$v_{r,i}$[MPa]	0,92	0,93	0,93	2,25	2,45	2,10	2,37	2,30	2,64

Regarding Equation 7.3-34 of MC2010 (Equation 3.24 of this dissertation), the interface resistance becomes:

Table 5.7: Predicted shear resistance (interfaces connected by dowels – MC2010)

Beam	I.A	I.B	I.C	II.A	II.B	II.C	III.A	III.B	III.C
k_c					2,3				
$f_{ck,min}$ [MPa]	15,3	15,4	15,3	26,9	33,2	22,4	21,6	19,8	29,6
μ	-	-	-	0,8	0,8	0,8	0,8	0,8	0,8
κ	-	-	-	0,5	0,5	0,5	0,5	0,5	0,5
ρ_i [%]	-	-	-	0,201	0,201	0,201	0,268	0,268	0,268
f_{yk} [MPa]	-	-	-	500	500	500	500	500	500
α_f	-	-	-	0,9	0,9	0,9	0,9	0,9	0,9
f_{cm} [MPa]	23,3	31,7	23,6	34,9	41,2	30,4	29,6	27,8	37,6
β_c	0,5	0,5	0,5	0,5	0,5	0,5	0,5	0,5	0,5
b	0,5	0,5	0,5	0,5	0,5	0,5	0,5	0,5	0,5
“adhesion”	0,77	0,77	0,77	0,93	1,00	0,87	0,86	0,84	0,96
“friction”	-	-	-	0,40	0,40	0,40	0,54	0,54	0,54
“dowel action”	-	-	-	0,24	0,26	0,22	0,29	0,28	0,33
v_{ri} [MPa]	0,77	0,77	0,77	1,57	1,66	1,50	1,69	1,66	1,83

When comparing the approaches to shear resistances MC2010 (Equation 3.23 and Equation 3.24), it is noticed that equation 3.24 is much more conservative.

Regarding the dowel action parcel in Table 5.7, it is noticeable that, for the considered roughness, the dowel action is about half (actually precisely 54%) of the total dowel action that would be obtained by Rasmunsen expression, which values are displayed in Table 4.11.

The same comparison could be made with the “friction” parcel and maximum tension values in Table 4.10, except the design of the post-installed reinforcement is not always characterized by failure in steel.

Again, shear resistance of the interface is lower than the representative mean values provided in MC2010 (indicated in Table 3.1). This situation could be solved by more reinforcement crossing the interface – however in this dissertation interfacial failure was intended.

5.3.3 Comparison between experimental resistances and expected values

The resistance values obtained through Walraven’s sphere model (Table 5.5) are higher than the resistances obtained in every other approach described above, because this expression is calibrated for push-off specimens. It can be concluded that Equation 3.20 is not appropriate to quantify shear stress for bonded concrete overlays in the tension zone.

To establish a comparison with the provisions for shear resistance in MC2010 and EC2 the values of $v_{i,exp1}$ and $v_{i,xp2}$are considered, as they provide similar results, and

a comparison with results of all models was intended. Also, shear stress $v_{i,exp3}$ is higher and when compared to predicted values, will produce a higher ratio $v_{i,exp}/v_r$.

The ratio between the experimental and predicted shear strength obtained for SMII demonstrates clearly the difference between these values. In SMIII the relation are closer to 1. This is also a result, of the differential distribution of shear reinforcement, as the predicted shear loads are quite similar in SMII and SMIII, due to a similar amount of reinforcement. This experimental program has shown that for similar amounts of reinforcement, the location of the same reinforcement crossing the interface contributes significantly for shear resistance.

Regarding the expected SMI, both design approaches present results which are close to the obtained resistance. EC2 and MC2010 (Equation 5.9) present a value very similar to the obtained experimentally.

Table 5.8: Comparisons between experimental and predicted values ($v_{i,exp1}$)

		I.A	I.B	I.C	II.B	II.C	III.A	III.C
$v_{i,exp1}$		0,95	1,08	1,09	1,46	1,47	2,15	2,04
EC2 and MC2010 (Eq. 5.9)	$v_{r,i}$	0,92	0,93	0,93	2,45	2,10	2,37	2,64
	$\boldsymbol{\frac{v_{i,exp1}}{v_{r,i}}}$	**1,03**	**1,16**	**1,17**	**0,6**	**0,7**	**0,91**	**0,77**
MC2010 (Eq. 5.10)	$v_{rd,i}$	0,77	0,77	0,77	1,66	1,50	1,69	1,83
	$\boldsymbol{\frac{v_{i,exp1}}{v_{r,i}}}$	**1,23**	**1,39**	**1,41**	**0,88**	**0,89**	**1,27**	**1,11**

Table 5.9: Comparisons between experimental and predicted values ($v_{i,exp2}$)

		I.A	I.B	I.C	II.A	II.B	II.C
$v_{i,exp2}$		0,95	1,08	0,96	1,42	1,38	1,34
EC2 and MC2010 (Eq. 5.9)	$v_{r,i}$	0,92	0,93	0,93	2,25	2,45	2,10
	$\boldsymbol{\frac{v_{i,exp2}}{v_{r,i}}}$	**1,04**	**1,17**	**1,04**	**0,64**	**0,57**	**0,64**
MC2010 (Eq. 5.10)	$v_{rd,i}$	0,77	0,77	0,77	1,57	1,66	1,50
	$\boldsymbol{\frac{v_{i,exp2}}{v_{r,i}}}$	**1,24**	**1,41**	**1,25**	**0,91**	**0,84**	**0,90**

5.3.4 Correlations between concrete resistance and adhesion

The predicting models available in literature, shear friction theory, the slant shear test, and the codes (MC2010 and EC2) usually relate adhesion with concrete compressive resistance, in such a way that:

$$v_{r,i} = a f_c^n \tag{5.11}$$

The values for the coefficient and the degree of the polynomial are identified in Table 5.10.

Table 5.10: Coefficient and degree of the polynomial

EC2 / MC2010 (Eq. 5.9)	$n = 2/3$	$f_c = f_{ck}$	$a = 0{,}14c$ $(0{,}14c = 0{,}07)$
MC2010 (Eq. 5.10)	$n = 1/3$	$f_c = f_{ck}$	$a = 0{,}09k_c$ $(0{,}09k_c = 0{,}207)$

In Table 5.1 it was visible that, in SMI, higher loads were resisted by the beams with higher concrete resistance in the overlay. Therefore it seems appropriate to relate the experimental resistance$v_{i,exp2}$, which is dependent on the maximum load applied. The relation is demonstrated in Figure 5.47.

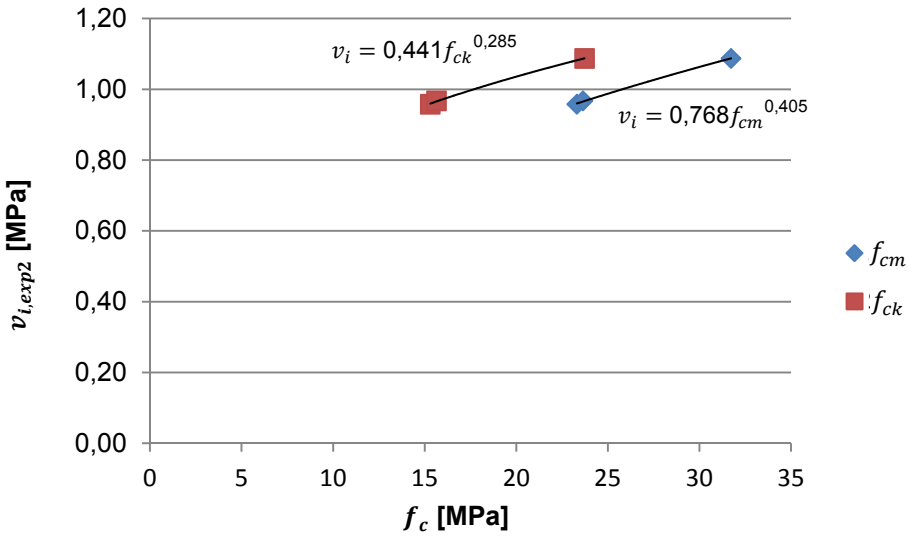

Figure 5.47: Influence of the compressive strength of the substrate in adhesion

The number of tested experiments is, however, limited to withdraw any definitive conclusion.

5.4 Tension perpendicular to the interface, near the edges of the new concrete layer

An explanation for the results in SMIII, and the creation of tension near the overlays border can be given by the example illustrated in Figure 5.48. The latter, represents the equilibrium of a concrete element at the border of the concrete layer, after concrete has cracked.

As it can be seen, to counteract the effect of the moment created by the steel force and the shear stress, tension perpendicular to the interface is created. Considering the distribution of tensions represented Figure 5.48, the distance between tension and compression forces perpendicular to the interface is $z = 2/3s$.

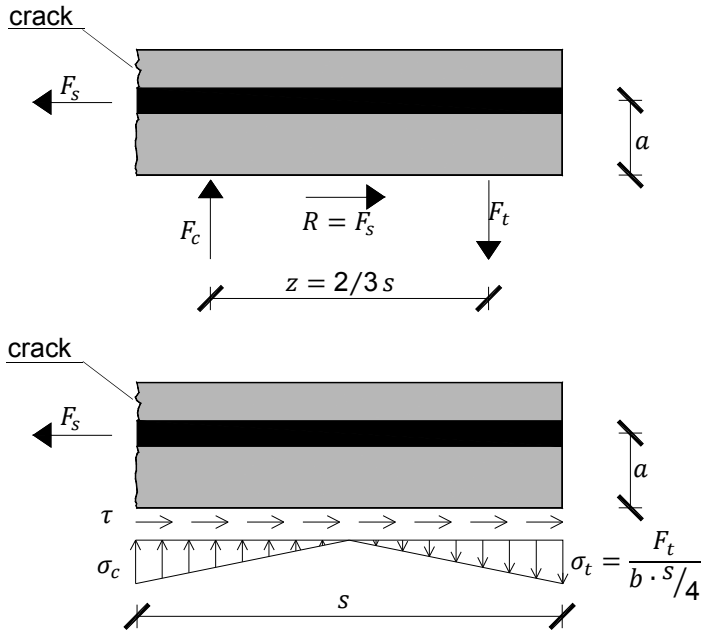

Figure 5.48: Tension in the interface, near the overlay's borders

The equilibrium between horizontal and vertical forces, and moments (Equations 5.12-5.14) lead to the consideration of tension and shear stresses described in Equations 5.15 and 5.16.

$$F_t = F_c \tag{5.12}$$

$$F_s = R \tag{5.13}$$

$$F_s = F_t \frac{2}{3} s \tag{5.14}$$

$$\tau = \frac{F_s}{b \cdot s} \tag{5.15}$$

$$\sigma_t = \frac{4a}{s} \tau \tag{5.16}$$

Where,

s is the length between the concrete border and a crack

5.5 Determination of the cracking load

The force that causes the first concrete fiber to crack is related to the cracking moment in the following relationship:

$$F_{cr_{midspan}} = \frac{4 \cdot M_{cr}}{l} \tag{5.17}$$

It would also be interesting to determine the force that causes concrete to crack where the other strain gauges are placed. Considering the bending moment distribution

(Figure 4.1), the force that would cause concrete to crack, at an arbitrary distance from midspan, x, is given by Equation 5.18.

$$F_{cr_x} = \frac{4M_{cr}}{l - 2x} \tag{5.18}$$

5.5.2 Experimental cracking load and moments

The load-strain graphs (displayed in section 5.2 of this dissertation) exhibited an initial linear behavior, until a certain point where the relation between steel strains and applied load followed a different direction, with higher steel deformation for the same increases in load. This linear elastic limit is related to stress in the concrete cross-section – it is the point when the tensile strength of concrete is reached and concrete cracks.

The same load-strain graphs were enlarged to try and observe the position where the load-strain development ceased being linear. This way, the cracking load was determined in the points where the strain gauges are located. As there are some differences between the cracking forces measured on SG1-4-7-10 and SG3-6-9-12, the lower value is assumed, because of the distribution of stress in reinforcement is not linear, and exhibits peaks where the concrete is cracked. The crack might coincide, or not, with the point where the strain gauges are placed.

For strengthening model III, only the midspan cracking force was determined, due to significant differences between the steel strains measured remaining strain gauges.

Relations between cracking loads and moments are established in Equation 5.17 and 5.18.

Table 5.11: Experimental cracking loads, F_{cr}^{exp} and moments F_{cr}^{exp},

Beam	I.A	I.B	I.C	II.B	II.C	III.A	III.C
$F_{cr_{midspan}}^{exp}$	90	105	100	135	165	155	160
$F_{cr_{x=0,3m}}^{exp}$	130	205	225	225	220	-	-
$M_{cr_{midspan}}^{exp}$	31,8	37,1	35,4	47,7	58,3	54,8	56,6
$M_{cr_{x=0,3m}}^{exp}$	27,6	43,5	47,7	47,7	46,7	-	-

5.5.3 Predicted cracking loads

When the concrete tensile resistance is exceeded, a crack opens and steel becomes relevant in the resisting mechanism. There are several approaches to the cracking moment. The most complex and complete involves the consideration of different elasticity modulus (both for substrate and overlay), and the effect of the reinforcement.

In this case, it is possible to consider an equivalent homogeneous section. By this approach, both the steel and the concrete overlay are replaced by an equivalent amount of substrate concrete.

The position of the neutral axis is given by:

$$y_G = \frac{A_{c_{sub}} y_{g_{sub}} + A_{eq,c_o} y_{g_o} + A_{eq,s_o} d + A_{eq,s_{sub}} a}{A_{c_{sub}} + A_{eq,c_o} + A_{eq,s_o} + A_{eq,s_{sub}}} \tag{5.19}$$

Where,

$A_{c_{sub}}$ is $b \cdot h_{sub}$

A_{eq,c_o} is $b \cdot \frac{E_{c_o}}{E_{c_{sub}}} \cdot h_o$

A_{eq,s_o} is $A_{s_o} \cdot \frac{E_s}{E_{c_{sub}}}$

$A_{eq,s_{sub}}$ is $A_{s_{sub}} \cdot \frac{E_s}{E_{c_{sub}}}$

E_{c_o} is the elasticity modulus of the concrete overlay

$E_{c_{sub}}$ is the elasticity modulus of the concrete substrate

E_s is the elasticity modulus of the reinforcement

d is the height of the tensioned steel reinforcement (0,332m)

d is the height of the compressed steel reinforcement (0,028m)

The uncracked moment of inertia can be determined by Equation 5.20.

$$I = \frac{bh_{sub}^3}{12} + A_{c_{sub}}\left(y_g - \frac{h_{sub}}{2}\right)^2 + \frac{b_{eq_o}h_o^3}{12} + A_{eq,c_o}\left(\frac{h_o}{2} + h_s - y_g\right)^2 + A_{eq,s_o}(d - y_g)^2 + A_{eq,s_{sub}}(y_g - a)^2 \quad (5.20)$$

Where,

b_{eq_o} is given by $b \cdot \frac{E_{c_o}}{E_{c_{sub}}}$

The relation above is based on the assumption that the moment of inertia of the reinforcement in relation to its own central axis is negligible.

The cracking moment causes tension at the top concrete fiber to reach concrete tensile resistance, f_{ctm}. As the substrate and overlay have different tensile resistances, it is necessary to calculate the values of the cracking moment both for the concretes tensile resistance at the extreme substrate and overlay reinforcement.

$$M_{cr_o}^{pred} = \frac{f_{ctm_{eq,o}} I}{h_s + h_o - y_G} \quad (5.21)$$

$$M_{cr_{sub}}^{pred} = \frac{f_{ctm_s} I}{h_s - y_G} \quad (5.22)$$

The discontinuity in tension is considered negligible, because it is admitted that the cracking moment occurs at very small slips, before adhesion is lost, and the difference in strains caused by the eventual loads the substrate was submitted before the strengthening action is also considered negligible, because it was only submitted to the concrete's own weight.

In the overlay, the values for tensile resistance must also be corrected, to correspond with homogenized section:

$$f_{ctm_{eq,o}} = f_{ctm_o} \frac{E_{c_o}}{E_{c_{sub}}} \quad (5.23)$$

It is important to confirm if using a simplified method to determine the cracking moment can provide a realistic approach to concrete cracking. In that case, equation 5.24 may be used.

$$M_{cr_{simp}}^{pred} = f_{ctm_o} \frac{bh^2}{6} \quad (5.24)$$

The concrete tensile resistance is considered the one of the overlay, because, for low values of slip, it corresponds to the most tensioned zone.

The expected values for the cracking moment, and the simplified cracking moment are displayed in Table 5.12 and Table 5.13.

Table 5.12: Predicted cracking moments and forces

Specimen	I.A	I.B	I.C	II.A	II.B	II.C	III.A	III.B	III.C
$M_{cr_o}^{pred}$ [kNm]	26,2	22,6	26,0	50,1	46,3	53,6	54,3	56,0	48,3
$M_{cr_s}^{pred}$[kNm]	39,9	50,2	40,4	58,3	64,8	53,1	52,1	49,9	61,3
$M_{cr_{simp}}^{pred}$ [kNm]	20,08	20,08	20,08	35,69	35,69	35,69	35,69	35,69	35,69

The simplified cracking moment, $M_{cr_{simp}}^{pred}$, was used to calculate the simplified cracking forces $F_{cr_{simp,midsp}}^{pred}$ and $F_{cr_{simp,x=0,3m}}^{pred}$. The lower value between the cracking moment $M_{cr_{sub}}^{pred}$ and $M_{cr_o}^{pred}$ was adopted to obtain the values of the cracking forces$F_{cr_{midsp}}^{pred}$ and $F_{cr_{x=0,3m}}^{pred}$.

Table 5.13: Predicted cracking forces

Specimen	I.A	I.B	I.C	II.A	II.B	II.C	III.A	III.B	III.C
$F_{cr_{midsp}}^{pred}$ [kN]	74,1	63,9	73,6	141,8	130,9	150,2	147,4	141,0	136,7
$F_{cr_{simp,midsp}}^{pred}$ [kN]	56,8	56,8	56,8	101,0	101,0	101,0	101,0	101,0	101,0
$F_{cr_{x=0,3m}}^{pred}$ [kN]	128,7	111,0	127,8	246,4	227,4	260,9	256,1	244,9	237,4
$F_{cr_{simp,x=0,3m}}^{pred}$ [kN]	98,6	98,6	98,6	175,4	175,4	175,4	175,4	175,4	175,4

The obtained simplified cracking loads/moments are inferior to the cracking loads/moments obtained with the homogenized concrete cross-section. Although the consideration of an inferior cracking load might induce that there is certain margin of safety, it might also lead to the consideration of a lower amount of reinforcement in order to avoid brittle failure.

5.5.4 Comparisons between the expected cracking moments and the predicted cracking moments

It is interesting to observe that the predicted cracking moments were quite similar to the obtained ones at midspan. However, at one-fourth of the span, the distance between the expected and the obtained cracking increased. This might be related to

an additional reinforcement layer. In relation to the simplified cracking moment, higher differences were observed between expected cracking and obtained cracking.

The differences may also be due to the assumption of continuous stress in the interface. In reality stress distribution is not continuous, however, in this dissertation; no method for determining interfacial slip is addressed.

Table 5.14: Comparison between experimental and predicted cracking loads

Beam	I.A	I.B	I.C	II.B	II.C	III.A	III.C
$\frac{M_{cr_{midspan}}^{exp}}{M_{cr}^{pred}}$	1,2	1,6	1,4	1,0	1,3	1,0	1,1
$\frac{M_{cr_{x=0,3m}}^{exp}}{M_{cr}^{pred}}$	1,0	1,8	1,8	0,9	1,0	-	-
$\frac{M_{cr_{midspan}}^{exp}}{M_{cr,simp}^{pred}}$	1,6	1,8	1,8	1,3	1,6	1,5	1,6
$\frac{M_{cr_{x=0,3m}}^{exp}}{M_{cr,simp}^{pred}}$	1,3	2,1	2,3	1,3	1,3	-	-

5.6 Comparisons between the different models

5.6.1 Determination of a homogeneity coefficient

5.6.1.1 Resisting bending moment of a concrete cross-section with similar geometry

The equilibrium in a concrete cross-section with $b = 0{,}5\text{m}$,$d = 0{,}332\text{m}$ and $A_s = 20{,}11\text{cm}^2$ can be given by Equations 5.25 and 5.26.

$$\sum F = 0 \Leftrightarrow A_s \cdot f_{yk} = \frac{17}{21} \cdot x \cdot b \cdot f_{cm} \tag{5.25}$$

$$\sum M = 0 \Leftrightarrow M_r = \frac{17}{21} \cdot x \cdot b \cdot f_{cm} \cdot z \tag{5.26}$$

Where,

x is the height of the compression zone

z is assumed to be equal to $0{,}9d$

f_{cm} is the resistance of the compressed concrete (substrate concrete)

The compatibility equation is given in Equation 5.27. If $\varepsilon_s > \varepsilon_y$, the initial assumption that stress in steel corresponds to the yield stress is verified.

$$\frac{\varepsilon_s}{d - x} = \frac{\varepsilon_c}{x} \tag{5.27}$$

The values for the homogeneity coefficient are displayed in Table 5.15.

Table 5.15: Homogeinity coefficients

Beam	I.A	I.B	I.C	II.A	II.B	II.C	III.A	III.B	III.C
f_{cm}	23,3	31,7	23,6	34,9	41,2	30,4	29,6	27,8	37,6
x	0,11	0,08	0,11	0,07	0,06	0,08	0,08	0,09	0,07
M_r	290,9	302,3	291,5	305,1	309,5	300,9	300,0	297,8	307,2
ε_s	7,4	11,3	7,6	12,8	15,8	10,7	10,3	9,5	14,1
F_{max}	280,7	320,8	283,4	422,5	411,6	395,4	505,6	521,1	561,4
M_{max}	99,3	113,4	100,2	149,4	145,5	139,8	178,8	184,2	198,5
γ_m	0,34	0,38	0,34	0,49	0,47	0,46	0,60	0,62	0,65
$\overline{\gamma_m}$		0,35			0,47			0,62	

When compared to the design approach developed by Gomes and Appleton (1997), it can be seen that the homogeneity coefficient obtained for the experimental beams is inferior to the proposed by the authors (which is based on EC80). Failure modes associated with the interface may reduce the value of the homogeneity coefficient.

5.6.2 Increase in flexural resistance, provided by reinforcement crossing the interface, in relation to adhesion

The increase in flexural resistance provided by reinforcement crossing the interface, in relation to SMI, is given by:

$$\%IFR = \frac{F_{max} - \overline{F}_{SMI}}{\overline{F}_{SMI}} \cdot 100 \tag{5.28}$$

Where,

F_{max} is the maximum load resisted by each beam
$\overline{F}_{SMI}$ Is the average load resisted by the beams of SMI ($\overline{F}_{SMI}$ =295kN)

In Table 5.16 the average increases in flexural resistance provided by the different types of reinforcement crossing the interface are displayed. SMII exceeded the adhesion resistance in 39%. Specimen C of SMIII surpassed adhesion in 90% and in average this strengthening solution provided an increase in flexural resistance of 79%.

Table 5.16: Average increase in flexural resistance, provided by reinforcement crossing the interface

Beam	$\%IFR,A$	Average
II.A	43%	
II.B	40%	39%
II.C	34%	
III.A	71%	
III.B	77%	79%
III.C	90%	

Chapter 6

Conclusions and further research

6.1 General considerations

The use of RC overlays in the tension zone, with the intent of increasing flexural resistance, is always susceptible to failure modes related to the interface. These failure modes should be included in the strengthening design.

Stress is transmitted across concrete interfaces through adhesion, mechanical interlock, friction and dowel action. Each of these mechanisms has its maximum contribution to shear strength at different times and is dependent on the slip between concrete layers. In the present dissertation, an experimental study was developed in order to compare the effectiveness of different strengthening solutions.

The differences between the overall load bearing behavior of strengthened RC beams with reinforcement crossing the interface was studied. The reinforcement was either uniformly distributed or placed only near the edges of the RC overlay. The influence of adhesion is also analyzed.

Chapter 6 presents a synopsis of the experimental research and obtained results.

At last, further research related to bonded concrete layers is suggested.

6.2 Resistance of strengthened beams and of the interface

Reinforced concrete overlays can significantly improve flexural resistance in horizontal concrete elements such as concrete beams or slabs. In this dissertation the effects of adhesion and reinforcement crossing the interface are analyzed, based on experimental tests performed on nine composite beams.

The RC beams had similar geometry, and were strengthened with the same amount of longitudinal reinforcement. Three different strengthening solutions, consisting of three specimens each, were adopted.

The amount of longitudinal reinforcement was kept constant in all strengthening layers. The main difference between solutions is related to the way stress is transferred across the interface.

In the first strengthening solution (SMI), stress was transmitted between concrete layers through adhesion. In the beams of this model, no reinforcement crossing the interface was placed. The other two strengthening solutions had either evenly distributed connectors crossing the interface, (SMII) or longitudinal reinforcement bent into an “*L*” shape, which were anchored in the substrate near the borders of the new concrete layer (SMIII).

The knowledge of the interface strength in tension was also a goal for this dissertation. However, due to difficulties while drilling cores for the pull-off test, it was not possible to obtain acceptable values for bond strength.

6.2.1 Maximum loads and failure modes

A clean rupture along the interface, in one of the beam's sides was only obtained in SMI. Failure along the interface occurred shortly after a shear crack was formed near the supports, coinciding with the borders of the overlay.

The other strengthening solutions (with the exception of beam III.C) all experienced initially, a visible partial midspan crack. However, failure was not characterized by rupture in the reinforcement crossing the interface, but began between the concrete and steel in the . Ruptures began in the overlay and evolved into the existing midspan crack. This indicates that, although failure modes are related to the interface, interfacial failure was probably not the main reason why the system failed. More cracking and deformation were visible in SMII, when compared to SMI, and also in SMIII when compared to SMII.

Due to difficulties while drilling the holes for the post-installed reinforcement, specimen III.C had a slight difference regarding the anchorage of the bent longitudinal bars. Also, during the laboratory tests, the hydraulic jack lost pressure before failure, so the beam had to be re-loaded. This beam (III.C) resisted the most load and exhibited both concrete crushing and rupture in one of the longitudinal rebars that was anchored in the substrate.

In average there was an improvement in the load bearing capacity from SMII and SMIII in relation to SMI of 39 and 79%, respectively.

6.2.2 Steel strains

Obviously, in agreement with the maximum loads, the beams of SMI had lower steel extensions than SMII beams. SMIII experienced the highest values in flexural resistance.

In SMI and II the highest steel strains were measured at midspan. Steel strains measured at one fourth of the rebar were about half this value, which imposed an approximately constant stress transfer rate between concrete and steel.

For strengthening model III this constant stress rate was no longer visible. Generally midspan strains were also higher. In the particular case of specimen III.A – rebar i – the maximum value for steel extension was not measured at midspan, but on the strain gauge closer to where the rebar was anchored.

Regarding the evolution of steel strains with increasing load, it is clearly visible that failure is quite brittle in SMI. SM III shows more steel deformation before rupture than SMII. The measured steel strains in beam III.A exhibit a virtually increase in strain for approximate the same load, which characterizes ductile behavior.

6.2.3 Vertical displacements

Since the beams are very stiff, the measured deflections before failure are rather small. All beams of SMI failed with vertical displacements smaller than 2mm.

As to SMII and SMIII, although the measured vertical deflections were about the same range, SMIII exhibited a more continuous evolution in steel deflections in relation to the substrate. The evolution in vertical displacements measured in SMII (Figure 5.20 and Figure 5.21) shows that vertical deflections in the overlay did not accompany the

substrate deformation, indicating less composite action. This can be related to tension in the reinforcement at the edges of the new concrete layer; since in SMIII more steel was tensioned near the edges of the concrete layer, the opening of the interfacial crack was prevented, and deformations are more continuous.

6.2.4 Ultimate shear stress and provisions for shear resistance at the interface

The shear resistance of the interface due to adhesion is approximately 1MPa. The values for shear stress in SMII and SMIII are not representative of the actual shear resistance of the interface, because failure was not characterized by the reinforcement crossing the interface. However, the ultimate shear stress endured by the interface was considered.

Shear distribution in SMIII was not constant along the interface length, however, as a simplification a constant stress transference rate between concrete and steel was considered.

In SMII the ultimate shear stress was about 1,4MPa. For SMIII a value of approximately 2MPa was calculated.

The provisions for the adhesion shear resistance described in MC2010 and EC2 presented good estimations of the experimental resistance.

Since the steel ratio in SMII was similar to SMIII, design code expressions estimated similar shear resistances for both models. However, the ultimate shear stress the interface was subjected during the test was, in the case of SMII, considerably inferior to the predictions for shear strength in MC2010 and EC2.

6.2.5 Cracking moment

The experimental cracking moments were determined by enlargement of the load-steel strain curves, in the locations were strain gauges were placed (at one fourth of the reinforcement bars and at midspan). It was visible that in both locations, the cracking moment did not have the same value.

In most cases, the expected values calculated with an equivalent concrete cross-section, and a simplified approach presented acceptable results.

The adoption of a simplified method for the determination of the cracking moment, such as the suggested in the present dissertation leads, generally, to higher differences from the experimental cracking moment. However, although in this paper the cracking moments were similar, this method might not very accurate, especially if concretes have different strengths (and elasticity modulus).

6.3 Influence of concrete compressive strength on adhesion

In design code expressions, adhesion between concrete layers cast at different times has been related to the concrete compressive strength and roughness. The relation between adhesion and the concrete compressive strength of the substrate was clearly visible for the specimens of SMI, as this was the only parameter that varied between the specimens.

Although a relation can be made between these values (which is indicated in Figure 5.47), it would have been necessary to carry on with more tests.

6.4 Consideration of homogeneity coefficients

EC8 and the design approach suggested by Gomes and Appleton (1997) consider a homogeneity coefficient for the purpose of evaluating flexural strength in beams equal to 0,9, and full composite action between materials.

Full composite action between substrate and overlay was not achieved during the experimental program, neither was it the scope for this dissertation. The ratios between the experimental moments and the resisting bending moment, considering a monolithic cross-section with the same steel and concrete properties, and the equal geometry, were 0,35, 0,47 and 0,62, for strengthening models I II and III, respectively.

6.5 Final Remarks

In the present research, it is quite visible the increase in flexural resistance provided by the addition of a reinforced concrete layer in the tension zone to an existing RC beam with a deficit in flexural resistance.

It was concluded, in agreement with the design code expressions in MC2010 and EC2, that the resistance provided by adhesion was dependent on the concrete compressive strength. However, experimental results are not sufficient to withdraw a valid relation. Shear resistance provided by adhesion can be considered uniform along the length of the interface.

The premise of uniform distribution of shear load along the length of the interface might lead to a regular distribution of reinforcement across the area of the interface, A_i. Therefore, if shear transmission is uniform, there would be no need for a stepped distribution of reinforcement. MC2010 already alerts for the fact that near the edges of the new concrete layer, stress due to restraint forces near the perimeter of the overlay create tension in this region. Edge reinforcement can positively contributes for the elimination of a debonding failure mode.

The addition of steel crossing the interface is important, not only for the increase in shear strength, but also for the overall load bearing behavior. The experimental models with reinforcement exhibited more cracking and deformation prior to ruin. A higher concentration of reinforcement near the edges also enhanced significantly composite behavior, as vertical deflections in the overlay accompanied more the substrate deflection.

SM II and SMIII did not exhibit pure interfacial failures. Although these beams (with exception of III.C) exhibited a partial interfacial failure, rupture began between longitudinal steel and concrete, near the edges.

It was possible to estimate the ultimate shear strength at the interface, assuming constant shear stress. Again, SMIII exhibited higher ultimate shear stress values than SMII. However, since the amount of reinforcement is very similar, design code expressions predicted approximately the same resistance for both models.

In conclusion, the best solution was to increase the anchorage of the rebars, and have more reinforcement crossing the interface near the edge of the new concrete layer. This solution exhibited not only the best composite action, with vertical displacements in the overlay accompanying more the substrate deformations (in relation to SMII), but also the best load bearing capacity.

The relation between shear and bond strength was not possible, because of difficulties related to the pull-off test.

6.6 Further research

With this research, it was intended to contribute to the development of the strengthening technique of bonded concrete overlays in the tension zone.

Regarding shear resistance provided by the adhesion mechanism, it would be interesting to continue with other flexural tests and compare the shear resistances provided adhesion with results of pull-off tests.

The analysis elaborated in this dissertation could be used as an indicator of expected values for interfacial strength, namely provided by adhesion. More experimental models with different solutions should be developed and compared, for instance, a strengthening solution with reinforcement crossing all the interface area, and also more concentrated near the interface perimeter. Tests on unidirectional and bidirectional slabs should also be executed.

It would be also interesting to recreate the strengthening modes present in this dissertation using structural analysis software, and investigate the stress state of the interface.

References

Abbasnia, R., Khanzadi, M., & Ahmadi, J. (2009). Mortar mix proportions and free shrinkage effect on bond strength between substrate and repair concrete. In: Alexander et al (eds.). *Concrete Repair, Rehabilitation and Retrofitting II*. 2009 Taylor and Francis Group. London.

Abu-Tair, A., Lavery, D., Nadjai, A., Rigden, S., & Ahmed, T. (2000). A new method for evaluating the surface roughness of concrete cut for repair or strengthening. *Construction and Building Materials*. **14**: 171-176.

Bakhsh, K. N. (2010). *Evaluation of bond strength between overlay and substrate in concrete repairs*. Master degree thesis. KTH Architecture and the Built Environment.

Banu, D., & Taranu, N. (2010). Traditional solutions for strengthening reinforced concrete slabs. *Bouletin of the Polytechnic Institute of Jassy, Constructions, Architechture Section*. **LVI (LX)**: 53-62

Beushausen, H., & Alexander, M. (200. 7). Localized strain and stress in bonded concrete overlays subjected to differential shrinkage. *Materials and structures*. **40**:189-199.

Bianchi, P. (2007) *Bridge Rehabilitation with concrete overlay*. Hilti.

Borges, A. M. (2008). *Análise do comportamento de juntas de betonagem. Instituto Superior Técnico*.– Dissertação de Mestrado em Engenharia Civil. Universidade Técnica de Lisboa. 92 pp.

CEB FIB (2010). Model Code 2010: First complete draft.

Clímaco, J. & Regan, P. E. (2001). Evaluation of bond strength between old and new concrete in structural repairs. *Magazine of Concrete Research*. **53**: 1-14.

Comité Euro-International du béton (1998). CEB-FIB Model Code 1990. Thomas Telford Services.

Courard, L. Michel, F. Schwall, D. Wielen, A. V., Piotrowski, T., Garbacz, A., Perez, F., & Bissonnette, B. (2006). Surfology: concrete surface evaluation prior to repair.

Datta, A., & Seraj, S. (2003). Effect of overlay on punching shear capacity of slabs. *Journal of Civil Engineering. The institution of Engineers, Bangladesh*. 31: 67-82.

Dritsos, S., Pilakoutas, K. & Kotsira, E. (1995). Effectiveness of flexural strengthening of RC members. *Construction and Building Materials*. **9**: 165-171.

EN 1504-3 (2005) European standard: Products and systems for the protection and repair of concrete structures – *Definitions, requirements, quality control and evaluation of conformity – Part 3: Structural and non-structural repair*. European Committee for Standardization.

EN 1998-3 (2003) European standard: *Eurocode 2: Design of structures for earthquake resistance – Part 3: Strengthening and repair of buildings*. European Committee for Standardization.

Garbacz, A. Górka, M., & Courard, L. (2004) Effect of concrete surface treatment on adhesion in repair systems. *Magazine of Concrete Research*. **56**:1-12.

Garcia, S. R. A. & Clímaco, J. C. T. S. (2001). Eficiência da aderência de materiais de reparo para estruturas de concreto. *Actas do 43º Congresso Brasileiro do Instituto Brasileiro do Concreto – IBRACON*. Foz do Iguaçu, Agosto 2001.

Gomes, A. & Appleton, J. (1997): Strengthening of reinforced concrete structures by use of jacketing. *Revista Portuguesa de Engenharia de Estruturas*. **42**:7-14.

Gonçalves, A. (2007). Betões Autocompactáveis. Slides do Seminário Materiais em Ambiente Marítimo. Funchal.

Issa, M.A., Issa, M.A. Islam, M.S. & Chudnovsky, A. (2003). Fractal dimension – a measure of facture roughness and toughness of concrete. *Engineering Fracture Mechanics* **70**:125-137.

Júlio, E.N.B.S., Branco, F.A.B., Silva, V.D., & Lourenço, J.F. (2006). Influence of added concrete compressive strength on adhesion to an existing concrete substrate. *Building and Environment*. **41**:1934-1939.

Júlio, E. N. B. S., Dias-da-Costa, D., Branco, F.A.B., Alfaiate, J.M.V. (2010). Accuracy of design code expressions for estimating longitudinal shear strength of strengthening concrete overlays. *Engineering Structures*. **32**: 2387-2393.

Keesom, R. W., Bouwmeester-van den Bos, W. J., van Kaam, M., & van der Horst, A. Q. C. (2008) Strengthening of Prestressed viaducts by means of a reinforced concrete overlay. *Tailor Made Concrete Structures*. 2008 Taylor & Francis Group. London.

Lenz, P., & Zilch, K. (2011). Concrete shear joints – suggestions for optimized design of concrete to concrete bond. *Proceedings of the Design of concrete structures and bridges using eurocodes*, Bratislava, 12-13 September 2011. pp. 61-64.

Leonardt, F., & Monning E., (1979). Calcolo di progetto & techniche costruttive, Vol. II Casi speciali di dimensionamento nelle costruzioni in c. a. e c.a.p. Edizione di Scienza e Tecnica.

Lúcio, V.J.G., & Marreiros, R.P.C. (2005). Estado do conhecimento em aderência de varões nervurados de aço ao betão em elementos de betão armado. UNIC.

Miltenberger, M. (2001). Capacity design of grouted anchors. *16th International Conference on Structural Mechanics in Reactor Technology*. Washington, DC, USA, 2001.

Moyamez, A., Ramezanianpour, A. A., Rajaie, H. & Ehsani, M. R. (2002) Experimental investigation of the methods of evaluating the bond strength between concrete substrate and repair materials. *IJE Transactions B: Applications*. **15**:319-332.

Munger, F., Wike, M., & Randl, N. (1997). Design of shear transfer in concrete-concrete composite structures. *Proceedings of the IABSE Conference*, Innsbruk, 1997. pp. 163-168.

NP EN 1992-1-1 (2010) *Norma Portuguesa: Eurocódigo 2: Projecto de Estruturas de Betão – Parte 1-1: Regras Gerais e Regras para Edifícios*. Instituto Português da Qualidade.

NP EN 206-1 (2007) *Norma Portuguesa: Betão Parte 1: Especificação, Produção, Desempenho e Conformidade.* Instituto Português da Qualidade.

Omar, B. (2010). Influence of the roughness and moisture of the substrate surface on the bond between old and new concrete. *Contemporary Engineering Sciences*. **3**: 139-147

Patel, N. B. (2010). *Factors affecting the interface shear strength of pavement layers.* Master degree thesis. Department of Civil and Environmental Engineering, Louisiana State University and Agricultural and Mechanical College. 147 pp.

Pereira, N. B., Barros, J. A. O., & Camões, A. (2004). Betão Autocompactável Reforçado com Fibras de Aço. *Técnica*. pp. 25-31.

Perez, F., Morency, M. Bissonnette, B., & Courard, L. (2009). Correlation between the roughness of the substrate surface and the debonding risk. In: Alexander et al (eds.), *Concrete Repair, Rehabilitation and Retrofitting II*. 2009 Taylor and Francis Group. London.

Pires, E. F. (2003). *Comportamento e Desempenho do Reforço à Flexão de Lajes de Concreto Armado através do Aumento da Seção na Região Comprimida*. Tese de Mestrado em Engenharia de Estruturas. Departamento de Engenharia de Estruturas, Escola de Engenharia, Universidade Federal de Minas Gerais. 99 pp.

Pistolesi, C., Maltese, C., & Bovassi, M. (2009). Low shrinking self-compacting concretes for concrete repair. In: Alexander et al (eds.). *Concrete Repair, Rehabilitation and Retrofitting II*. 2009 Taylor and Francis Group. London.

Ramezanianpour, A., Shahhosseini, V., & Nilforoushan, A. (2007). Bond characterization between concrete substrate and repairing materials. *Journal of Technology & Education*. **1**: 38-43.

Randl, N. (2011). Experiences with the MC2010 concrete-to-concrete provisions in Austria. *Proceedings of the fib Symposium*. Prague 2011. pp. 99-102.

Randl, N., & Zilch, K. (2009). Strengthening of structures with concrete overlays: current research, regulations and practice. *Proceedings of the International fib Symposium*, June 2009, London.

Reguengo, R. (2010). *Comportamento da ligação pilar-fundação em estruturas pré-fabricadas com armaduras salientes do pilar ensaios monotónicos e cíclicos*. Dissertação de Mestrado em Engenharia Civil – Ramo de Estruturas e Geotecnia. Faculdade de Ciências e Tecnologias. Universidade Nova de Lisboa. 87pp.

Rilem State of the Art Reports (2011). *Bonded cement based material overlays for the repair, the lining or the strengthening of slabs or pavements*. Springer.

Rodrigues, C. C., (2005). *Reparação e reforço de estruturas de betão armado com sistemas compósitos de FRP*. Publicação UNIC – DTC6. Lisboa.

Santos, E. W. F., Shehata, I. A. E. M., & Shehata, L. C.D. (2007). Reforço de Vigas de Concreto Armado à Flexão por Encamisamento Parcial. *Actas dos Anais do 49º Congresso Brasileiro do Concreto CBC2007*. pp. 1-16.

Santos, P. M. D., & Júlio, E. B. S. (2010). Recommended improvements to current shear-friction provisions of model code. *Proceedings of the 3rd fib International Congress*, 2010.

Santos, P. M. D., Júlio, E. N. B. S., & Silva, V. D. (2007). Correlation between concrete-to-concrete bond strength and the roughness of the substrate surface. *Construction and Building Materials*. **21**: 1688-1695.

Sika® Grout (2011): http://pt01.webdms.sika.com/fileshow.do?documentID=137

Silfwerbrand, J. (2003). Shear bond strength in repaired concrete structures. *Materials and Structures*. **36**:419-424

Simmons, I. (2004). Behavior and design of post-installed rebar connections. Fib task group 4.5 – 6th meeting. October 2004.

Smoak, G. (2004). *Guide to Concrete Repair*. United States Department of the Interior, Bureau of Reclamation. Technical Service Center

The Concrete Society (1984). *Repair of concrete damaged by reinforcement corrosion. Report of a working party*. Author's Edition.

Walraven, J. C. (2007). Strengthening and bond between new and old concrete. Overlay design concept. T. U. Delft.

Walraven, J., Frénay, J., Pruijssers, A. (1987). Influence of concrete strength and load history on the shear friction capacity of concrete members. *PCI Structures*. **32**: 66-84

Yao, J., & Teng, J. C. (2007). Plate end debonding in FRP-plated RC beams – I: Experiments. *Engineering Structures* **29**: 2457-2471.

Appendix A

Roughness Parameters

The 100x50mm grid where the profile heights of the interface were measured is displayed in Figure A.1. In Tables A.1-A.9 the average roughness, R_a of each profile is presented.

If in the measuring position coincides with the location of a hole for the post installed reinforcement, the letter H is marked.

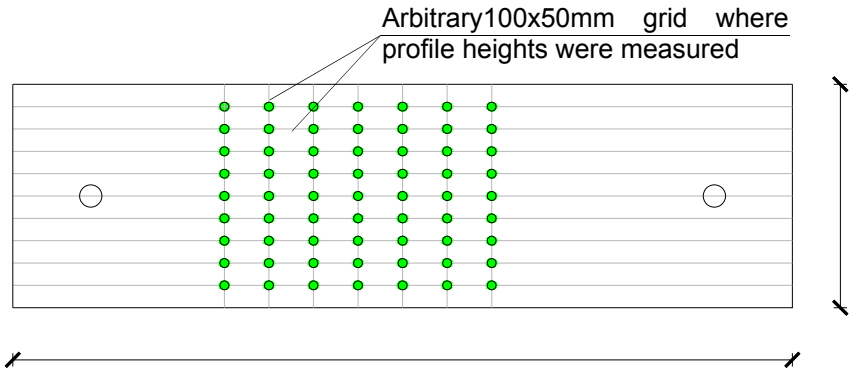

Figure A.1: Arbitrary grid where profile heights were measured

Table A.1: Average roughness (Beam I.A)

	Beam I.A [mm]									R_a
	5,2	9,2	11,4	8,0	6,6	10,4	4,5	0,0	3,0	2,5
	1,4	5,0	1,4	7,5	2,3	10,2	6,8	11,4	1,5	2,9
	3,0	6,2	7,5	6,1	2,0	7,1	8,8	6,9	0,8	1,8
	8,7	9,6	13,2	14,3	10,8	8,4	9,3	7,1	2,7	1,6
	0,8	6,4	4,2	2,5	3,8	6,4	7,5	5,8	8,1	1,6
	1,7	3,1	2,0	2,5	7,2	9,5	8,6	11,7	6,6	3,1
R_a	2,5	1,6	3,9	2,9	2,8	1,5	1,4	3,1	3,1	

Table A.2: Average roughness (Beam I.B)

	Beam I.B [mm]									R_a
	6,4	5,3	1,14	7,5	5,1	11,4	7,7	8,2	8,7	1,7
	8,3	3,7	9,7	9,4	1,4	5,3	1,8	4,0	3,6	2,4
	5,0	1,0	3,2	6,8	2,7	1,8	2,5	3,3	9,7	1,5
	6,2	4,7	3,0	10,8	11,4	3,4	12,0	8,1	11,3	2,8
	1,0	7,3	6,0	0,8	0,8	2,5	4,7	10,1	12,4	2,6
	5,7	5,9	8,0	8,6	1,6	5,1	7,7	4,7	10,1	1,6
R_a	1,7	1,9	2,6	2,4	3,2	1,8	2,8	2,1	2,1	

Table A.3: Average roughness (Beam I.C)

	Beam I.C [mm]									R_a
	11,8	8,9	9,5	5,2	4,8	11,3	8,3	7,5	9,5	1,7
	6,4	11,3	9,8	11,3	5,5	9,0	5,0	9,5	6,4	1,9
	6,1	9,2	9,3	9,5	4,3	7,5	13,0	15,7	8,6	2,3
	12,5	4,5	10,6	7,7	9,2	6,4	7,7	4,1	9,3	2,0
	5,5	5,2	7,5	1,0	6,0	7,9	8,7	9,0	10,6	1,7
	5,5	7,6	9,2	7,0	10,6	12,5	5,6	6,2	12,2	1,9
R_a	2,8	2,0	0,9	2,7	2,3	2,1	2,0	2,6	1,6	

Table A.4: Average roughness (Beam II.A)

	Beam II.A [mm]									R_a
	5,5	1,6	4,0	3,5	6,3	3,8	7,4	12,4	7,2	2,1
	3,9	1,5	17,8	11,3	12,5	8,7	8,9	6,1	4,5	3,4
	2,2	9,3	4,3	9,6	H	15,4	7,2	13,9	4,5	3,3
	6,0	5,3	18,1	13,3	3,7	6,6	6,8	7,4	12,2	3,4
	0,0	14,0	4,1	5,6	11,9	18,0	5,7	6,5	10,4	4,3
	1,8	10,9	5,3	10,5	4,1	6,6	13,0	14,4	9,1	3,4
R_a	1,9	3,6	5,3	2,1	3,9	3,6	2,4	4,6	3,1	

Table A.5: Average roughness (Beam II.B)

	Beam II.B [mm]									R_a
	5,8	5,7	9,7	9,7	14,3	7,6	18,3	14,3	1,43	3,4
	8,6	8,3	12,0	7,4	8,9	9,9	21,3	11,5	13,5	2,7
	5,0	H	9,9	14,9	H	4,3	H	10,0	13,6	2,7
	10,1	16,3	H	14,6	14,0	6,6	11,4	13,1	14,8	2,1
	13,4	7,2	06,8	18,1	5,2	7,4	9,2	9,0	12,3	2,9
	8,4	6,9	6,2	9,4	6,1	7,2	H	6,8	13,6	1,1
R_a	2,1	2,8	3,1	4,1	4,9	1,8	1,7	3,4	2,3	

Table A.6: Average roughness (Beam II.C)

	Beam II.C [mm]									R_a
	10,1	12,8	15,8	25,5	7,5	12,3	12,4	11,8	18,0	3,4
	7,9	3,6	27,0	7,6	1,5	1,8	11,2	11,2	9,5	5,0
	2,8	5,2	0,5	2,8	8,4	23,1	20,4	14,6	8,5	6,4
	9,2	10,8	10,6	26,2	26,0	11,8	13,4	11,1	20,6	5,3
	12,8	14,0	13,3	12,0	3,2	12,9	13,6	6,1	16,8	2,5
	8,7	11,5	10,4	2,7	16,0	4,7	9,9	26,8	16,0	4,7
R_a	3,1	4,6	7,4	10,3	7,2	6,5	3,7	5,9	5,9	

Table A.7: Average roughness (Beam III.A)

	Beam III.A [mm]									R_a
	9,6	15,9	9,5	11,4	21,6	21,5	4,2	15,9	10,4	4,5
	12,9	7,3	9,1	17,7	20,8	9,1	8,9	8,0	17,1	3,9
	10,6	20,1	3,7	3,4	12,4	1,4	7,0	8,7	16,8	4,0
	16,6	16,8	9,8	8,7	13,8	13,3	13,4	20,9	13,3	2,5
	11,5	11,9	6,6	9,4	6,2	4,7	2,7	11,5	12,9	2,7
	19,8	16,4	17,9	17,2	8,6	9,4	19,0	19,1	18,7	3,2
R_a	3,0	4,8	3,5	5,0	6,2	5,6	4,2	5,9	2,6	

Table A.8: Average roughness (Beam III.B)

	Beam III.B [mm]									R_a
	1,5	9,2	15,1	8,8	3,3	2,2	22,8	12,5	9,2	2,3
	17,4	19,4	14,0	10,8	17,8	19,3	18,7	22,2	18,6	1,6
	17,3	10,2	25,1	5,4	20,1	3,0	7,0	3,3	0,0	3,7
	21,4	20,2	13,5	9,1	22,0	10,4	6,2	6,7	11,2	3,9
	21,4	25,1	8,8	10,8	19,2	20,0	5,8	16,7	9,3	2,8
	13,5	18,6	5,0	15,0	11,2	12,5	7,0	4,0	4,3	2,1
R_a	4,4	4,4	3,1	4,4	3,4	2,8	3,2	2,8	3,5	

Table A9: Average roughness (Beam III.C)

	Beam III.C [mm]									R_a
	5,0	11,4	5,2	3,9	5,2	0,0	3,0	8,9	1,2	5,2
	2,7	5,1	3,8	5,0	6,8	8,1	8,7	3,5	1,8	2,3
	9,6	4,8	8,3	19,1	12,7	13,3	1,9	6,7	6,0	6,0
	15,9	3,2	9,1	2,2	16,7	9,9	5,6	5,2	5,2	5,0
	3,3	16,1	15,8	9,2	11,8	15,9	13,0	11,3	9,1	5,7
	0,8	9,7	4,2	4,0	5,4	5,9	8,6	1,6	3,8	4,2
R_a	3,7	4,1	5,7	2,4	4,0	5,2	7,2	7,0	4,8	

Appendix B

Pull-off test results

Test results of the pull-off tests in beams I.A and I.B are presented in Table B.1 and B.2 respectively.

Table B.1: Pull-off test results for beam I.A

Core	1	2	3	4	5	6
Tensile stress [MPa]	0,05	0,12	0,37	0,53	0,63	1,12

Table B.2: Pull-off test result for beam I.B

Core	1	2	3	4	5	6
Tensile stress [MPa]	0,35	0,37	0,72	0,74	0,47	0,32